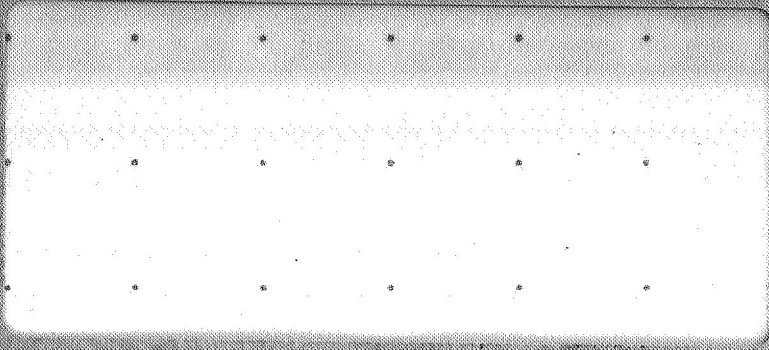


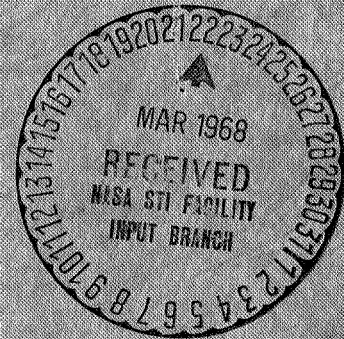
822818778
 (ACCESSION NUMBER)
 171
 (PAGES)
 NASA-CR-616-22
 (NASA CR OR TAX OR AD NUMBER)
 (THRU)
 (CODE)
 (CATEGORY)

FACILITY FORM 602



GPO PRICE \$ _____
 CFSTI PRICE(S) \$ _____
 Hard copy (HC) 3.00
 Microfiche (MF) .65

ff 653 July 65



Fluid Power Controls Laboratory
School of Mechanical Engineering
OKLAHOMA STATE UNIVERSITY
 Stillwater, Oklahoma

INTERIM REPORT NO. 65-4

STUDY OF FLUID TRANSIENTS IN
CLOSED CONDUITS

Contract: NAS 8 11302

INTERIM REPORT NO. 65-4

Contractor: Oklahoma State University, Stillwater, Oklahoma

Segment Generating Report: School of Mechanical Engineering
Fluid Power and Controls Laboratory

STUDY OF FLUID TRANSIENTS IN CLOSED CONDUITS

CONTRACT: NAS 8 11302

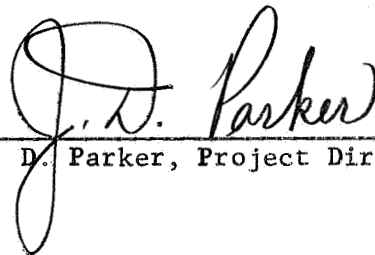
CONTROL NUMBER: DCN-1-4-50-01153-01(IF)
CPB 02-1209-64

Date: 27 June 1966

Prepared for: George C. Marshall Space Flight Center, Huntsville, Alabama

Prepared by: C. R. Gerlach

Approved:

A handwritten signature in cursive script that reads "J. D. Parker". The signature is written in black ink and is positioned above a horizontal line.

J. D. Parker, Project Director

PREFACE

The author would like to express his appreciation to the George C. Marshall Space Flight Center for partial financial support during this study and for allowing it to be submitted to the Graduate College of Oklahoma State University in partial fulfillment of the requirements for the degree of Doctor of Philosophy.

ABSTRACT

The dynamics of viscous fluid transmission lines have been investigated with emphasis being placed upon topics of interest in both fluid systems engineering and acoustic fields.

An exact solution of the first-order Navier-Stokes equation was obtained to describe the dynamics of a viscous, compressible liquid in closed conduits. This solution demonstrated the existence of an infinite set of viscous modes of propagation. Calculations were made of the spatial attenuation factor and phase velocity for several modes for both rigid and elastic flexible conduit walls. Also calculated were the velocity profiles near an oscillating piston and subsequently the state of shear stress near the piston.

Engineering models, based upon approximations of the zeroth mode, were developed and experimental studies were made of the frequency response and transient response of a viscous fluid transmission line.

In a viscous fluid transmission line, there exists an infinite set of higher order viscous modes of propagation. These modes are generated at the line ends or at points of discontinuity and exist at all frequencies. Each higher mode possesses a relative cutoff frequency below which the attenuation is very great. An experimental study, using a flow visualization technique to observe the state of shear stress, verified the existence of these modes.

The transfer equation model discussed in this work has been experimentally verified over the range of parameters

$$0.00001 < \frac{\nu L}{c_0 r_0^2} < 0.02$$

$$0.5 < \frac{\omega L}{c_0} < 10.0.$$

The tapered-lumped model developed was found to be of good utility in modeling a transmission line when part of a complex system.

TABLE OF CONTENTS

Chapter	Page
I. INTRODUCTION TO THE PROBLEM	1
Introduction	1
Lumped and Distributed Systems	2
Mathematical Description of the Problem	3
Scope of Treatise	7
Computer Program Listings	8
II. STATE OF THE ART	9
Introduction	9
Distributed Parameter Models	9
Fluid Transmission Line Concept	18
Lumped Models	23
Conduit Wall Effects	32
III. EXACT SOLUTION OF FIRST-ORDER NAVIER-STOKES EQUATIONS	36
Introduction	36
Mathematical Formulation of the Problem	36
Solution	38
IV. APPLICATION OF THE EXACT SOLUTION TO THE CASE OF A RIGID FLUID CONDUIT	45
Introduction	45
Characteristic Equations for Eigenvalues	45
Approximate Form of Zeroth Mode Equations	47
Derivation of Zeroth Mode Transfer Equations	54
Zeroth Mode Frequency Response	61
Zeroth Mode Transient Response	64
V. EXPERIMENTAL VERIFICATION OF ZEROth MODE TRANSFER EQUATIONS	72
Introduction	72
Experimental Frequency Response	72
Experimental Transient Response	74

Chapter	Page
VI. THE HIGHER MODES OF VISCOUS PROPAGATION	80
Introduction	80
Higher Mode Eigenvalues for Rigid Conduit	80
Velocity Profiles	86
Series Expansion	87
Experimental Investigation of Viscous Modes	95
Discussion	99
VII. NON-RIGID WALL EFFECTS	103
Introduction	103
Elastic Flexible Walls	104
Elastic Stiff Walls	111
VIII. DEVELOPMENT OF TAPERED-LUMPED MODEL	114
Introduction	114
Development of Model	115
Comparison of Exact and Approximate Models	116
Application of Model in Problem Solution	128
Discussion	136
IX. SUMMARY, CONCLUSIONS, AND RECOMMENDATIONS	137
Summary	137
Conclusions	138
Recommendations for Future Study	139
SELECTED BIBLIOGRAPHY	140
APPENDIX A - CALCULATION OF EIGENVALUES	143
APPENDIX B - INVERSE LAPLACE TRANSFORMATION FOR VISCOUS WATER HAMMER PROBLEM	148
APPENDIX C - COMPUTER PROGRAM LISTINGS	152

LIST OF TABLES

Table	Page
I. Electrical Analogs	29
II. Values of Φ 's and Ψ 's	31
III. Tabulation of the First Six Coefficients of the Series Expansion for a Piston Oscillating in a Rigid Conduit ($F_{nr} = 0.2,$ $D_{nr} = 0.01$)	95
IV. Valve Area Data for Example Problem 1	129

LIST OF FIGURES

Figure	Page
2.1 Suddenly Closed Valve - Classical Water Hammer Problem	11
2.2 Actual Pressure Versus Time Plot for Suddenly Closed Valve	13
2.3 Pressure for Suddenly Closed Valve From Linear Friction Model	16
2.4 Four-Terminal Representation of Fluid Conduit	19
2.5 Series Arrangement of Two Fluid Components	20
2.6 Combined Series Elements	22
2.7 Lumped Model Inertance Element	24
2.8 Lumped Model Capacitance Element	25
2.9 Lumped Model Resistive Element	26
2.10 Fundamental Representation of Lumped Line	27
2.11 Electrical Analogy for Fundamental Lumped Conduit With Friction	29
2.12 Variations of Electric Analogs	29
2.13 Analog for n-Segmented Lumped Conduit With Friction	30
2.14 Tapered Lossless Analog	31
2.15 Propagation Velocity Versus Frequency for Nonviscous Fluid	35
3.1 Coordinate System	36
4.1 Ratio of Real Part of Propagation Operator From Equation (4.7) to Exact Value Versus Radial Frequency Number	50

Figure	Page
4.2	Ratio of Dimensionless Phase Velocity From Equation (4.7) to Exact Value Versus Radial Frequency Number 51
4.3	Typical Zeroth Mode Velocity Profiles Due to a Sinusoidal Axial Pressure Gradient 53
4.4	Diagram of Fluid Conduit for Zeroth Mode Transfer Equations 56
4.5	Diagram of Fluid Conduit With Averaged Quantities at Each End 57
4.6	Variation of the Zeroth Mode Spatial Attenuation Factor With Axial Frequency Number 59
4.7	Dimensionless Phase Velocity, c/c_0 , Versus Axial Frequency Number for the Zeroth Mode 60
4.8	Amplitude of the Zeroth Mode Characteristic Impedance Versus Axial Frequency Number 62
4.9	Phase of the Zeroth Mode Characteristic Impedance Versus Axial Frequency Number 63
4.10	Amplitude of \bar{Z}_1 From Equation (4.25) for the Case of Zero Termination Impedance 65
4.11	Water Hammer Pressure History From Equation (4.33), Axial Damping Number 0.001 69
4.12	Water Hammer Pressure History From Equation (4.33), Axial Damping Number 0.02 70
4.13	Water Hammer Pressure History From Equation (4.33), Axial Damping Number 0.1 71
5.1	Experimental Model for Studying the Frequency Response of a Fluid Line 73
5.2	Experimental Amplitude, $[P/\rho_0 c_0 V_0]$, Obtained From the Frequency Analysis of an 80 Foot Line With Water as the Working Fluid 75
5.3	Experimental Amplitude, $[P/\rho_0 c_0 V_0]$, Obtained From the Frequency Analysis of an 80 Foot Line With MIL 5606 as the Working Fluid 76
5.4	Experimental Model for Studying the Transient Response 77

Figure	Page
5.5 Typical Pressure History Traces Obtained From the Model of Figure 5.4	78
6.1 Plot of the Spatial Attenuation Factor Versus Radial Frequency Number for Three Modes	82
6.2 Plot of the Dimensionless Phase Velocity Versus Radial Frequency Number for Three Modes	83
6.3 Spatial Attenuation Factor γ_{r0} Versus Radial Frequency Number for the First Mode	84
6.4 Dimensionless Phase Velocity c/c_0 Versus Radial Frequency Number for the First Mode	85
6.5 Axial Velocity Profile Function, $F_{zn}(r)$, for Four Modes ($F_{nr} = 0.2$, $D_{nr} = 0.001$)	88
6.6 Axial Velocity Profile Function, $F_{zn}(r)$, for Four Modes ($F_{nr} = 0.2$, $D_{nr} = 0.01$)	89
6.7 Axial Velocity Profile Function, $F_{zn}(r)$, for Four Modes ($F_{nr} = 1.0$, $D_{nr} = 0.01$)	90
6.8 Near Piston Velocity Profile (r Dependent Part Only) Calculated From Six Terms of Equation (6.3) With $F_{nr} = 0.2$, $D_{nr} = 0.01$	94
6.9 Schematic of Experimental Apparatus Used to Visually Observe the State of Shear Stress Near an Oscillating Piston	96
6.10 Photographs of Experimentally Observed State of Shear Stress	98
6.11 Lines of Constant Axial Velocity Gradient Obtained From Figure 6.8	100
7.1 Zeroth Mode Spatial Attenuation Versus F_{nr} for a Rigid and an Elastic Flexible Wall	107
7.2 Dimensionless Phase Velocity, c/c_0 , Versus F_{nr} for a Rigid and an Elastic Flexible Wall	108
7.3 First Mode Spatial Attenuation Versus F_{nr} for a Rigid and an Elastic Flexible Wall	109
7.4 Dimensionless Phase Velocity, c/c_0 , Versus F_{nr} for a Rigid and an Elastic Flexible Wall	110

Figure	Page
8.1 Variation of the Approximate Model Parameter F_{cn} With Axial Damping Number	117
8.2 Variation of the Approximate Model Parameter C_{cn} With Axial Damping Number	118
8.3 Variation of the Approximate Model Parameter F_{sn} With Axial Damping Number	119
8.4 Variation of the Approximate Model Parameter C_{sn} With Axial Damping Number	120
8.5 Comparison of One-Term Approximation of Cosh $\Gamma(i\omega)$ With Exact Value (Amplitude and Phase), $D_{nz} = 0.01$	122
8.6 Comparison of One-Term Approximation of Cosh $\Gamma(i\omega)$ With Exact Value (Amplitude and Phase), $D_{nz} = 0.0001$	123
8.7 Comparison of Two-Term Approximation of Cosh $\Gamma(i\omega)$ With Exact Value (Amplitude and Phase), $D_{nz} = 0.01$	124
8.8 Comparison of Two-Term Approximation of Cosh $\Gamma(i\omega)$ With Exact Value (Amplitude and Phase), $D_{nz} = 0.0001$	125
8.9 Comparison of Exact Solution (Zeroth Mode) and One Term of the Tapered-Lumped Model for the Water Hammer Problem	127
8.10 Schematic of Physical Layout for Example Problem 1	129
8.11 Comparison of Analytical Prediction Using One Term of Model With Experimental Results Obtained by NASA	131
8.12 Schematic of Physical Layout for Example Problem 2	132
8.13 Amplitude and Phase of $X(i\omega)/Y(i\omega)$ Versus Frequency With and Without Line Effects for Example Problem 2	134

CHAPTER I

INTRODUCTION TO THE PROBLEM

Introduction

The increased sophistication of present-day and proposed fluid systems has demanded that the engineer employ increasingly complex methods of analysis for studying these systems. This is indeed true for the case of non-steady flows in fluid conduits. To the practicing engineer, the presently available procedures for analyzing fluid transmission lines may present one of the following problems:

1. Perplexing mathematical detail when dealing with "exact" or distributed parameter models.
2. All problems, except the most elementary, demand extensive use of the digital computer for both distributed model and graphical methods.
3. Oversimplified lumped parameter models lead to inadequate answers for many typical problems.

The analyst thus finds that, except for a few simple and specialized problems, it is very difficult to approach "exact answers". These problems do not, in any case, lessen the need for adequate transmission line models useful for the study of everyday fluid systems.

A typical system may contain many components such as pumps, valves, actuators, reservoirs, motors, etc., generally connected

together in some manner by fluid lines. A complete analysis of such a system must involve not only the components but also the fluid lines. This is particularly true for unsteady conditions where the effects of the fluid lines have, in some cases, caused otherwise well-designed systems to be inoperable.

In general, the area of study associated with the flow of fluids through conduits is called "Conduit Dynamics". A rigorous application of Conduit Dynamics to the study of a fluid line involves a complete study of the fluid itself plus a study of the effect which the pipe or conduit has upon the fluid. For example, in making computations involving the effect of fluid compressibility, large errors may occur if the compressibility effect due to the elasticity of the pipe walls is not included.

Lumped and Distributed Systems

The physical properties of all real systems are distributed with respect to time and space. The extent or influence of this distributive effect varies greatly, depending on the particular system being studied. For the case of the fluid systems which will be of concern, this distributive effect may or may not need be considered. In general, those physical systems which are described by relations involving distributed parameters are called distributed parameter systems. The dynamical equations for distributed systems are generally partial differential equations. Those systems which do not involve distributed parameters are called lumped parameter systems. The dynamical equations for lumped systems are generally ordinary differential equations. If one

takes a distributed parameter system, averages the effect of the distributed parameter(s), and concentrates this average at some point, then one has "lumped" the system. The validity of approximating a distributed system by a lumped system or systems depends upon the operating conditions of the system and also upon the manner in which the lumping is performed.

Mathematical Description of the Problem

The exact description of the motion of a fluid for any type of fluid mechanics problem necessarily involves the simultaneous solution of the equations of change for the fluid. In mathematical terms, this description includes: (a) a continuity equation expressing the conservation of mass, (b) an equation of motion expressing the conservation of momentum, (c) an energy equation expressing the conservation of energy, and (d) one or more equations which relate the response of the fluid to thermal and mechanical stresses (equations of state). In addition, it is necessary to prescribe the motion at the fluid boundary which, for the problem dealt with here, means one needs a description of the motion of the conduit walls. This may involve an additional set of equations of change for the conduit itself.

An exact description, i.e., an exact solution of the governing equations, is nearly impossible. However, by means of various simplifying assumptions, it is possible to arrive at solutions which yield rather good quantitative descriptions of the system being analyzed. In many cases, these simplifying assumptions are questionable. By means of the discussions which follow, an effort will be made to present, in an organized manner, the work which has been accomplished by previous

investigators. Indications will be made, where possible, of the application and limitation of the ideas.

If one adopts an Eulerian point of view, that is, if one defines the fluid motion relative to a fixed spatial coordinate system, then the fluid equations of change may be written as follows (1).

(a) Continuity Equation

A mathematical statement of the conservation of mass for a fluid is

$$\frac{\partial \rho}{\partial t} + \nabla \cdot (\rho \bar{v}) = 0 \quad (1.1)$$

where ρ and \bar{v} are, respectively, the instantaneous fluid density and vector velocity in terms of the spatial coordinate location and time.

(b) Equation of Motion

The conservation of momentum for the fluid is expressed by the force equation

$$\begin{aligned} \rho \left\{ \frac{\partial \bar{v}}{\partial t} + (\bar{v} \cdot \nabla) \bar{v} \right\} &= \rho \bar{F} - \nabla p + (\mu_B + \frac{4}{3}\mu) \nabla (\nabla \cdot \bar{v}) \\ &- \mu \nabla \times (\nabla \times \bar{v}) + (\nabla \cdot \bar{v}) \nabla \mu' + 2 (\nabla \mu \cdot \nabla) \bar{v} \\ &+ \nabla \mu \times (\nabla \times \bar{v}). \end{aligned} \quad (1.2)$$

In this equation,

$\bar{F} \equiv$ vector body force per unit mass

$p \equiv$ total fluid pressure

$\mu \equiv$ shear viscosity

$\mu' \equiv$ dilatational viscosity

$\mu_B \equiv$ bulk viscosity

where each is generally a function of the spatial coordinate position and time.

(c) The Energy Equation

The energy equation may be written in the form

$$\rho g c_v \frac{DT}{Dt} - \frac{Dp}{Dt} = \mu \Phi - \nabla \cdot \bar{q}$$

where Φ is the dissipation function (2,3) and \bar{q} is the vector heat flux.

(d) Equation of State of Fluid

The equation of state of a fluid is the functional relationship between its pressure, density and temperature (i.e., its state variables). For a liquid, it is often written as

$$dp = \kappa \frac{d\rho}{\rho}$$

where κ is the bulk modulus of elasticity of the liquid.

Simplifying the Equations of Change

The problem of simplifying a set of equations of change is sometimes rather difficult from the standpoint that one needs to know something about the answer before the significance of various terms or variables being simplified or eliminated can be judged. Often one can neglect what seem to be minor terms and completely eliminate the possibility of mathematically predicting some physical phenomena in the process.

Previous studies of the dynamics of fluids in conduits have shown

the following trends:

1. Thermal effects appear negligible for liquids in many cases but not for gases.
2. Except for extremely high frequencies, the bulk viscosity may be neglected; however, it may be necessary to account for time dependent shear viscosity effects (viscoelastic effects).
3. Nonlinear effects for acoustic type disturbances in liquids appear small or negligible.

With these trends in mind, the mathematical description will now be simplified to a somewhat more tractable form, keeping in mind that, principally, liquids are being dealt with in this study. The stipulation of negligible thermal effects for a liquid eliminates the energy equation as one of the describing relations, thus leaving the equation of motion, the continuity equation and the state equation. If further, it is assumed that the bulk viscosity is zero and that the shear and dilatational viscosities are spatially independent, then the equation of motion becomes

$$\rho \left\{ \frac{\partial \bar{v}}{\partial t} + (\bar{v} \cdot \nabla) \bar{v} \right\} = \rho F - \nabla p + \mu \left\{ \frac{4}{3} \nabla (\nabla \cdot \bar{v}) - \nabla \times \nabla \times \bar{v} \right\} \quad (1.3)$$

which is the Navier-Stokes equation. The equations of change contain nonlinearities; however, it has been indicated that such effects are probably minor or negligible so the equations will now be linearized.

Assume

$$\bar{v} = \bar{v}_0 + \bar{v}_1$$

$$P = P_0 + P_1$$

$$P = P_0 + P_1 \quad (1.4)$$

where sub-0 denotes steady-state or time independent quantities (or at least slowly varying with respect to sub-1 quantities) and sub-1 denotes the first-order acoustic or disturbance quantities. Introducing Equations (1.4) into the continuity, motion and state equations, the desired linearized or first-order equations of change (assuming no body force) become

$$\rho_0 \frac{\partial \bar{v}_i}{\partial t} = -\nabla P_1 + \mu \left\{ \frac{4}{3} \nabla (\nabla \cdot \bar{v}_i) - \nabla \times \nabla \times \bar{v}_i \right\} \quad (1.5)$$

which will be called the first-order Navier-Stokes equation,

$$\frac{\partial P_1}{\partial t} + \rho_0 \nabla \cdot \bar{v}_i = 0 \quad (1.6)$$

for the first-order continuity equation, and

$$dA = \kappa \frac{d\rho_1}{\rho_0} \quad (1.7)$$

for the liquid state equation.

Equations (1.5), (1.6), and (1.7) are the first-order equations of change for a compressible liquid (neglecting thermal effects) and will be the basis of discussion for this treatise.

Scope of Treatise

The scope of this treatise on the dynamics of fluid transmission lines may be summarized as follows:

1. Comprehensively examine and review all literature

pertinent to the dynamics of fluid flow in closed conduits.

2. Obtain an exact solution of the first-order equations of change to describe the dynamics of a viscous, compressible liquid in a closed conduit.
3. Experimentally determine the validity of the exact solution.
4. Develop a practical and accurate approximate model of a fluid transmission line which should be suitable for use by the practicing engineer.

One of the objectives of the writer in this work is to bridge some of the gaps between the areas of fluid systems engineering and acoustics which have recently been growing more closely allied, primarily due to the rapidly developing area of fluidics.

Computer Program Listings

For the convenience of the reader, all pertinent computer programs used in performing the calculations for this work have been listed in Appendix C.

CHAPTER II

STATE OF THE ART

Introduction

Literature related to the subject of this treatise cuts across the boundaries of many fascinating disciplines. These include electrical transmission line theory, electromagnetic waveguides, acoustic waveguides, loudspeaker theory and the wave mechanics of elastic solids. To attempt a complete discussion of material from all of these areas would be completely beyond the scope of this work. However, some of the more significant results which pertain to the description of liquids as the working medium will be discussed.

Distributed Parameter Models

In Chapter I, it was stated that the exact description of a fluid conduit involves the simultaneous solution of the equations of change for the fluid. Studies of some previous investigators which are based upon solutions of some reduced form of Equations (1.5), (1.6), and (1.7) will now be given.

Frictionless Model

The starting point for studies of conduit dynamics is the one-dimensional wave equation which was first derived by d'Alembert in about

1750 in connection with his studies of vibrating strings. Joukowsky (4) and Allievi (5) are generally credited as first associating wave phenomena with water hammer problems in order that studies of the wave equation could be used in explaining pressure transients in conduits. The wave equation for a compressible liquid is derivable from Equations (1.5), (1.6), and (1.7) if one assumes that the viscous effects are negligible. The result is

$$\frac{\partial^2 v}{\partial t^2} = c_0^2 \nabla^2 v \quad (2.1)$$

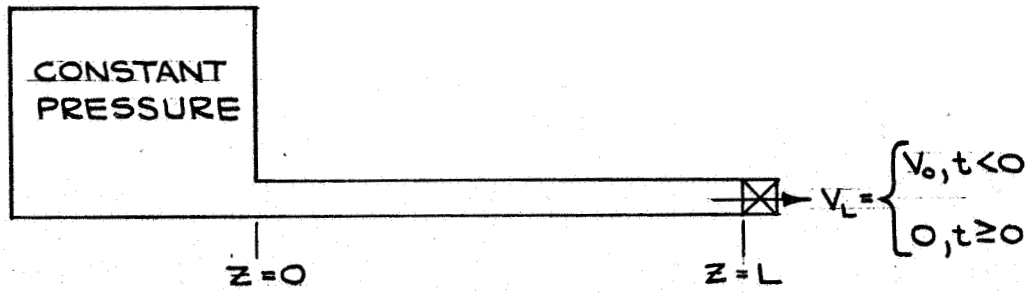
where c_0 is the isentropic speed of sound in the fluid and is given, for a fluid, by

$$c_0 = \sqrt{\frac{K}{\rho_0}} \quad (2.2)$$

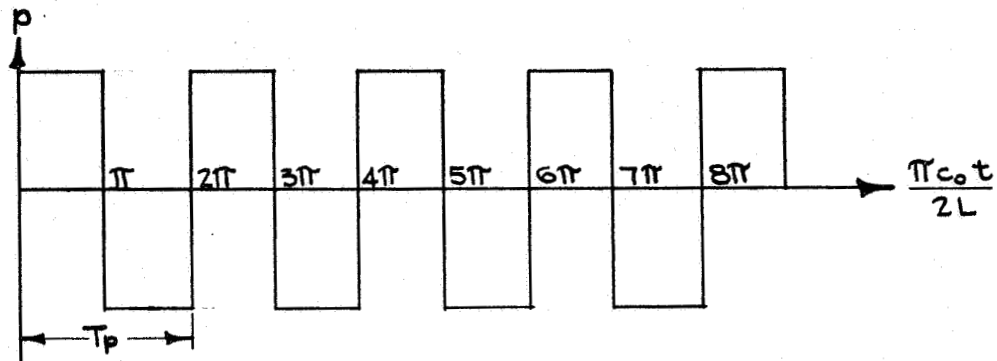
v represents the fluid disturbance velocity in the direction of propagation. Solutions to Equation (2.1) predict sinusoidal pressure and velocity disturbances propagating unattenuated with respect to space and time with a velocity c_0 . If Equation (2.1) is solved for the case of a suddenly closed valve on one end of a line with a constant pressure reservoir at the other end, Figure 2.1a, then the disturbance pressure will be of the form

$$P(t) = \rho_0 c_0 v_0 \left(\frac{4}{\pi} \right) \sum_{n=1}^{\infty} \left(\frac{1}{2n-1} \right) \sin \left\{ \frac{\pi c_0}{2L} (2n-1)t \right\} \quad (2.3)$$

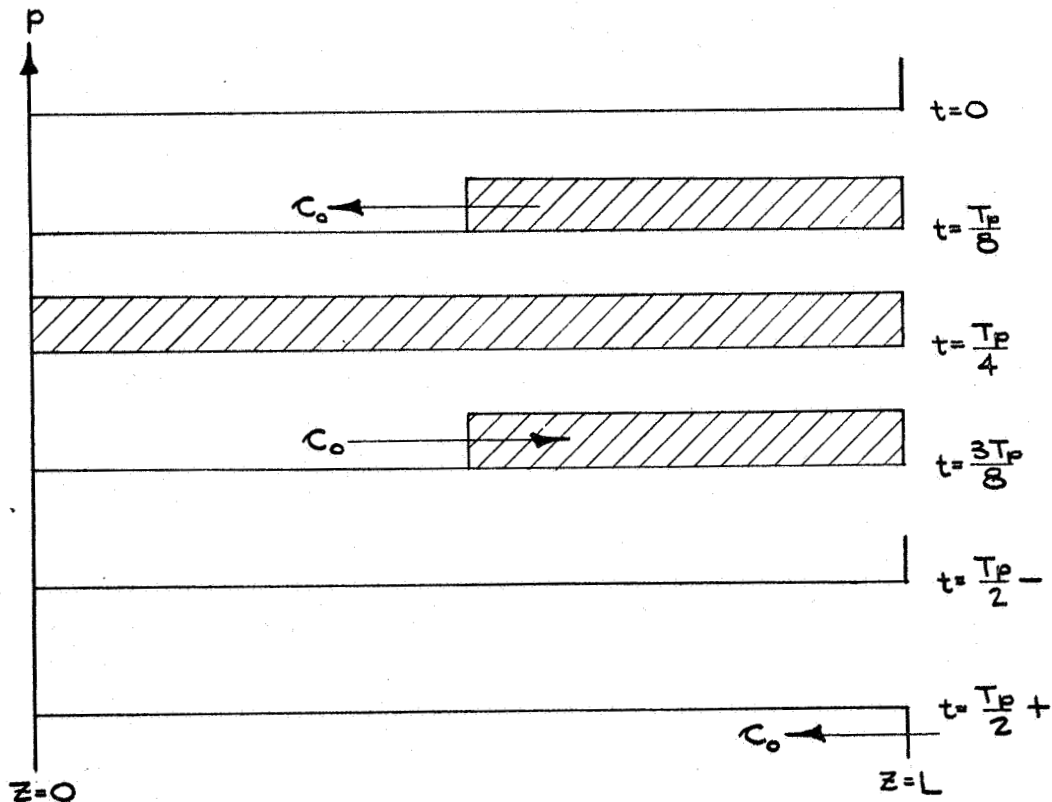
where v_0 is the initial mean velocity in the pipe before flow stoppage. Equation (2.3) is the mathematical expression for a square wave with period $(4L/c_0)$, see Figure 2.1b. Now examine the physical chain of events which result in this pressure square wave. At the instant of



(a) Conduit With Suddenly Closed Valve at One End, Reservoir Other End



(b) Square Wave Pressure Variation at Suddenly Closed Valve



(c) Pressure History of Waves in Conduit for One-Half Period

Figure 2.1. Suddenly Closed Valve - Classical Water Hammer Problem

valve closure, the fluid at $z = L$ is instantly stopped and the kinetic energy of the fluid is converted instantaneously (no friction) to potential energy (pressure). This positive pressure wave propagates toward $z = 0$ with velocity c_0 and reflects back to $z = L$ with zero pressure, see Figure 2.1c. The pressure wave then becomes negative and propagates again to $z = 0$ where it reflects with zero pressure back again to $z = L$, thus completing one cycle of the pressure wave.

It is evident from this discussion that the conduit of Figure 2.1 has a characteristic "natural" frequency of oscillation $fc = c_0/4L$. A critical analysis of Equation (2.3), however, shows that this particular disturbance actually consists of an infinite number of discrete characteristic frequencies $fc = c_0(2n-1)/4L$. In general, one may say that a conduit will have an infinite number of characteristic frequencies, whose values depend not only upon c_0 and L , but also upon the end conditions for the conduit. When one excites this system with some form of time variant non-sinusoidal disturbance, the system response will be the sum of the response of each characteristic frequency. The extent to which a given characteristic frequency will be "excited" depends on the type of disturbance. In general, the "sharper" the disturbance, the greater will be the extent to which the high frequency terms are excited. It is important to realize that the above results are very idealized and include neither the effects of friction or of pipe wall elasticity (these topics will be discussed later on). The results, however, indicate the upper limit of amplitude for a given disturbance. Extensive treatments of the application of this simple theory to practical problems may be found in references (6, 7, 8). These

applications, in general, involve a graphical or numerical solution of the wave equation.

Friction Effects

When researchers (e.g., 9) performed experiments on models demonstrating water hammer they found considerable discrepancy between the simple plane wave theory and actual results. They found that when sudden flow changes were effected, the resulting pressure transients changed shape with time similar to the diagram in Figure 2.2.

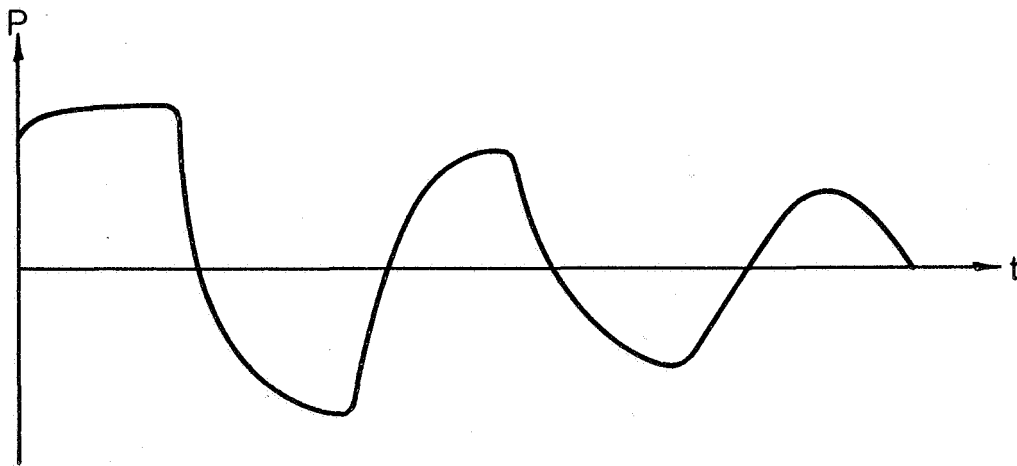


Figure 2.2. Actual Pressure Versus Time Plot for Suddenly Closed Valve

It may be seen that, in the actual case, the sharp corners of the pressure trace are being "rounded off" and the amplitude is decaying with time. This phenomena results from dispersive and dissipative effects which are a consequence of viscosity, pipe wall effects, etc.

In general, they result from friction effects. It is interesting to note that the greatest dispersion and dissipation occur on the high frequency terms which are those terms responsible for the sharp corners of the pressure trace. To account for all dispersive and dissipative effects would require an exact solution of the governing equations. However, past researchers have obtained useful results by means of approximate solutions.

Plane Wave Viscous Model

It was demonstrated by Stokes that plane or unbounded waves do not satisfy the simple one-dimensional wave equation, but rather, due to viscosity, must satisfy

$$\frac{\partial^2 v}{\partial t^2} = c_0 \frac{\partial^2 v}{\partial z^2} + \frac{4}{3} \nu \frac{\partial^3 v}{\partial z^2 \partial t} . \quad (2.4)$$

Equation (2.4) may be obtained from Equations (1.5), (1.6), and (1.7) by assuming one-dimensional effects only. Solutions to Equation (2.4) may be represented by

$$v = v_0 e^{\pm \gamma z + i \omega t} \quad (2.5)$$

where γ is a complex constant called the propagation constant or propagation factor and is given, in general by

$$\gamma = \gamma_r + i \gamma_c . \quad (2.6)$$

The quantity γ_r is the spatial attenuation factor since the term $e^{\pm \gamma_r z}$ represents the spatial decay or attenuation of the wave. The quantity

ω/γ_c is called the phase velocity and is the actual velocity of propagation of the disturbance. In general, the phase velocity does not equal c_0 . The value of γ for the solution given in Equation (2.5) is

$$\gamma = \frac{i\omega}{c_0 \sqrt{1 + \frac{4}{3} \frac{i\omega\nu}{c_0^2}}} \quad (2.7)$$

ω represents the angular frequency of the disturbance.

Solutions to Equation (2.4) have been obtained by some researchers in an effort to account for dispersion and dissipation effects in water hammer (10). These solutions, however, greatly underestimate the viscous effect because Equation (2.4) accounts for shear only in the direction of propagation (the z direction). Much greater viscous effects are acting in the radial direction due to the fact that the fluid velocity must go to zero at the pipe wall. One must conclude then that solutions to Equation (2.4) will not adequately describe the viscous effects in conduit dynamics.

Linear Resistance Model

The approach that a great number of researchers have used is to modify Equation (1.5) by substituting in place of the viscosity dependent terms a friction term which is proportional to the velocity (6, 7, 9, 11, 12, 13, 14, 15). The resulting equation of motion is

$$\frac{\partial v}{\partial t} = -\frac{1}{\rho_0} \frac{\partial p}{\partial z} - R_1 v \quad (2.8)$$

R_1 is a resistance or friction coefficient often given by the laminar flow resistance value, or

$$R_1 = \frac{8\gamma}{r_0^2} ; \quad (2.9)$$

r_0 being the pipe radius. When Equation (2.8) is solved simultaneously with the continuity equation and the equation of state, the same solution as in Equation (2.5) is obtained, except γ now has the value

$$\gamma = \frac{i\omega}{\kappa_0} \sqrt{\frac{R_1}{i\omega} + 1} . \quad (2.10)$$

If the solution to Equation (2.8) is obtained for the case of a suddenly closed valve, the pressure versus time plot at the valve will look similar to Figure 2.3.

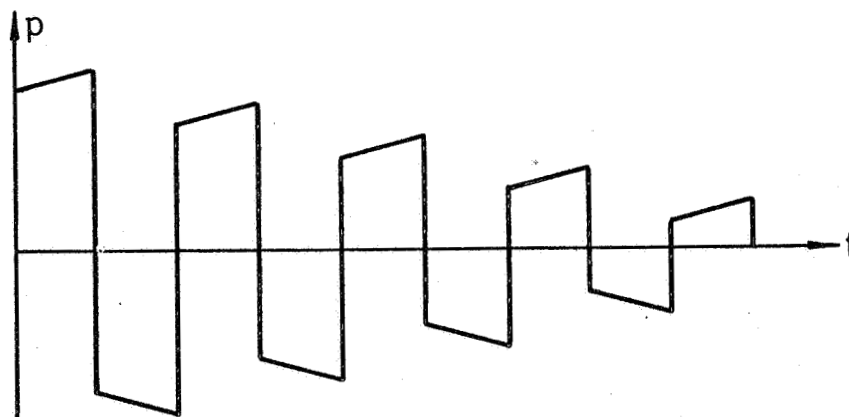


Figure 2.3. Pressure for Suddenly Closed Valve From Linear Friction Model

Although this linear friction model does not give the exact answer, especially over a wide frequency range, it has good utility when

experimental values of R_1 may be determined and when the frequency range is limited.

Two-Dimensional Viscous Model-Longitudinal Mode Only

A model reported in the literature (16, 17) which more exactly describes the first-order viscous effects for the longitudinal mode of vibration only is a result of the solution of the following reduced form of the equation of motion

$$\rho_0 \frac{\partial v}{\partial t} = - \frac{\partial p}{\partial z} + \mu \left\{ \frac{\partial^2 v}{\partial r^2} + \frac{1}{r} \frac{\partial v}{\partial r} \right\}. \quad (2.11)$$

The resulting propagation factor is

$$\eta = \frac{\left(\frac{i\omega}{c_0} \right)}{\left\{ 1 - \frac{2 J_1(\xi r_0)}{\xi r_0 J_0(\xi r_0)} \right\}^{1/2}} \quad (2.12)$$

where

$$\xi^2 = - \frac{i\omega}{\nu} \quad (2.13)$$

and where $J_1(\xi r_0)$ and $J_0(\xi r_0)$ are, respectively, the first and zeroth order Bessel functions (18) of the argument ξr_0 . Brown (16) has obtained the pressure history for the case of a suddenly closed valve using the solution to Equation (2.11). His results have much the same general shape as that of the experimental results of other authors, but the results are inconclusive since no supporting experimental results were included with the theoretical predictions. It can be concluded, however, that Equation (2.11) is a better representation of the true physical situation than the models previously discussed. From the

standpoint of frequency response characteristics as reported by Oldenberger and Goodson (12), this theory follows very closely the experimental results. Brown (16) and two other authors (19, 20) have solved Equation (2.11) for a fluid in which the heat transfer may not be neglected, thus it must be solved simultaneously with the energy, continuity and state equations. This results in a propagation factor

$$\gamma = \frac{i\omega}{\kappa_0} \left\{ \frac{1 + (\gamma^* - 1) \frac{2 J_1(\xi r_0)}{\xi r_0 J_0(\xi r_0)}}{1 - \frac{2 J_1(\xi r_0)}{\xi r_0 J_0(\xi r_0)}} \right\}^{1/2} \quad (2.14)$$

where now

$$\xi^2 = - \frac{i\omega}{\nu} \sigma_0 \quad (2.15)$$

and σ_0 is the Prandtl number (2) and γ^* is the ratio of specific heats for the fluid. This model has not been experimentally verified by researchers so its validity must be regarded, at this time, as undetermined.

Fluid Transmission Line Concept

So far, only the discussion of time domain solutions of the equations have been given. If one were to begin the exact study of a fluid system in which several components were involved, then the time domain approach would be exceedingly difficult. A useful and simple approach when dealing with the frequency analysis of fluid conduits (or any fluid component) is that of the fluid transmission line (7, 12, 21). Consider the fluid line to be representable as shown in Figure 2.4 as a four-terminal system. If one solves the system equations for a conduit

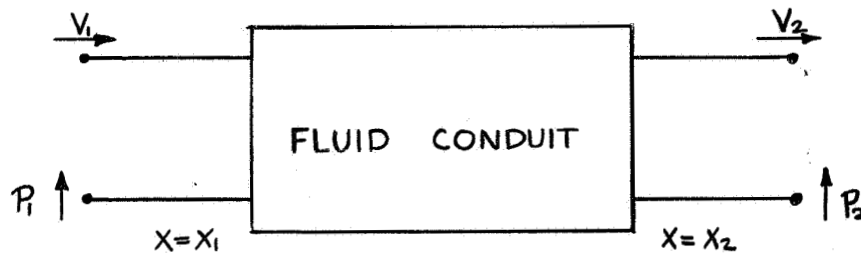


Figure 2.4. Four-Terminal Representation of Fluid Conduit

in the Laplace transform domain, then a rather simple set of equations relating the four transformed variables is obtained, thus

$$P_2(s) = P_1(s) \cosh \gamma L - Z_c V_1(s) \sinh \gamma L \quad (2.16)$$

and

$$V_2(s) = V_1(s) \cosh \gamma L - \frac{P_1(s)}{Z_c} \sinh \gamma L. \quad (2.17)$$

In Equations (2.16) and (2.17), $V_1(s)$, $V_2(s)$, $P_1(s)$, and $P_2(s)$ represent the Laplace transform of the respective time functions and s is the Laplace variable. Also,

$$L = X_2 - X_1 \quad (2.18)$$

and

$$Z_c = \frac{\rho_0 c_0^2 \gamma}{s}. \quad (2.19)$$

Z_c is called the characteristic impedance of the conduit. The γ which appears in Equations (2.16), (2.17), and (2.19) is identical with previous γ 's except that here $i\omega = s$, the Laplace variable. The value of

Y , of course, depends upon the model. It is important to note that this form of the transfer equations is the same for all of the previous models discussed, only the value of Y varies. The transfer equations for the four-terminal representation of Figure 2.4 will change, in general, when there is motion of the pipe wall and when we include the higher modes of propagation. Note also that the fluid velocities represented here are average values; that is, they have been integrated over the cross-section; thus, they are only dependent on time and the axial coordinate.

The utility of valid transfer equations in the frequency analysis of a conduit system cannot be over-emphasized. If four-terminal transfer equations can be written for each element of a fluid system, then the total system performance may be analyzed by combining the equations into a new set of transfer equations which represent the entire system. Suppose, for example, that two components of a fluid system are arranged in series as shown in Figure 2.5.

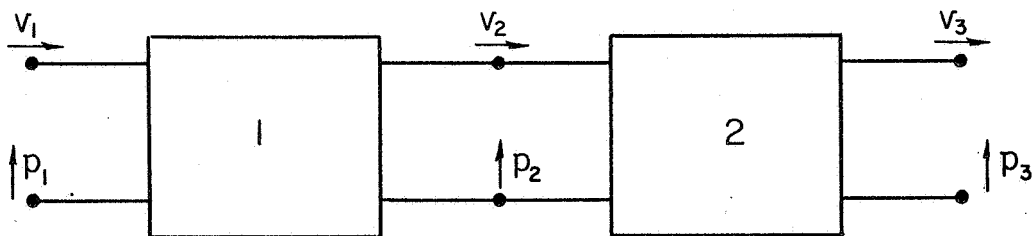


Figure 2.5. Series Arrangement of Two Fluid Components

Suppose that the transfer equations for element 1 may be expressed in the form

$$P_2(s) = A_1(s) P(s) + B_1(s) V_1(s) \quad (2.20)$$

and

$$V_2(s) = C_1(s) P(s) + D_1(s) V_1(s). \quad (2.21)$$

Writing these equations in matrix form gives

$$\begin{bmatrix} P_2 \\ V_2 \end{bmatrix} = \begin{bmatrix} A_1 & B_1 \\ C_1 & D_1 \end{bmatrix} \begin{bmatrix} P_1 \\ V_1 \end{bmatrix} \quad (2.22)$$

In a similar manner, one may write for element 2,

$$\begin{bmatrix} P_3 \\ V_3 \end{bmatrix} = \begin{bmatrix} A_2 & B_2 \\ C_2 & D_2 \end{bmatrix} \begin{bmatrix} P_2 \\ V_2 \end{bmatrix} \quad (2.23)$$

Substitution of Equation (2.22) into (2.23) yields

$$\begin{bmatrix} P_3 \\ V_3 \end{bmatrix} = \begin{bmatrix} A_2 & B_2 \\ C_2 & D_2 \end{bmatrix} \begin{bmatrix} A_1 & B_1 \\ C_1 & D_1 \end{bmatrix} \begin{bmatrix} P_1 \\ V_1 \end{bmatrix} \quad (2.24)$$

or, by matrix multiplication,

$$\begin{bmatrix} P_3 \\ V_3 \end{bmatrix} = \begin{bmatrix} (A_1 A_2 + B_2 C_1) & (A_2 B_1 + B_2 D_1) \\ (A_1 C_2 + C_1 D_2) & (B_1 C_2 + D_1 D_2) \end{bmatrix} \begin{bmatrix} P_1 \\ V_1 \end{bmatrix} \quad (2.25)$$

One might, for convenience, write

$$\begin{bmatrix} P_3 \\ V_3 \end{bmatrix} = \begin{bmatrix} A_3 & B_3 \\ C_3 & D_3 \end{bmatrix} \begin{bmatrix} P_1 \\ V_1 \end{bmatrix} \quad (2.26)$$

so that, effectively, elements 1 and 2 have been combined into a new element 3. The new element may be represented as shown in Figure 2.6.

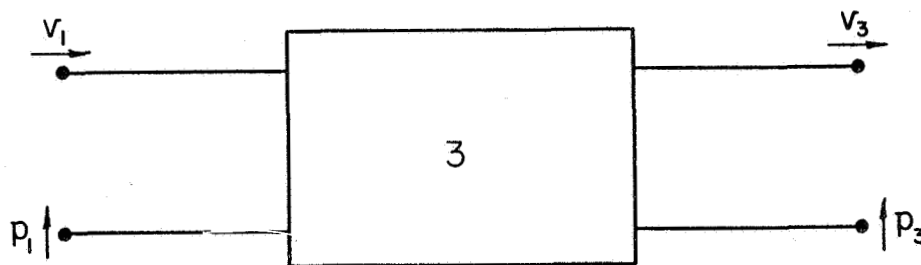


Figure 2.6. Combined Series Elements

Methods similar to this have been employed to great advantage in the analysis of noise transmission in complex fluid system which involve series and parallel elements (22). The matrix theory for four-terminal elements has been worked out by Pipes (23) for various types of arrangements of the elements.

In general, the matrix method approach is ideally suited to frequency analysis studies of a conduit system. It allows very complex systems to be analyzed easily with a digital computer.

Lumped Models

Up to now, only distributed parameter models of conduit systems have been discussed. Such models were found to be expressible in terms of transfer relations which lend themselves well to frequency analysis. In general, these distributed models are difficult to deal with in the time domain. This is a major handicap for many technically interesting problems such as problems involving conduit systems which contain valves closing or opening arbitrarily with time. In cases such as this, one may want only the time response of the system. In terms of the distributed parameter models, this means that the transfer relations for the system of interest must be transformed from the Laplace domain back into the time domain, or that some numerical or graphical procedure must be used to solve the system describing equations. The transformation of the transfer relations is very formidable; on the other hand, the graphical or numerical procedures are rather simple ways to analyze a system but lack the degree of generality usually desired in system analysis. Due to these drawbacks in the application of the distributed parameter models, lumped parameter approximations are often used in conduit system analysis. These models also have drawbacks which must be kept in mind. The major restriction which must be imposed on the lumped model of a distributed system is that it is valid only at low frequency. The method has been found to be valid, in most instances, only if the frequencies involved are not greater than about one-eighth of the first critical frequency of the lumped element. The exception to this restriction would be a system which has sufficient damping so that compressibility may be neglected. Now, examine some typical ways in

which conduit systems are lumped; first, consider the basic lumped elements, i.e., inertance, capacitance and resistance (7, 21, 24).

Fluid Inertance

Consider the fluid line shown in Figure 2.7. Assume that only the pressure and inertia forces are important and that compressibility may be neglected.

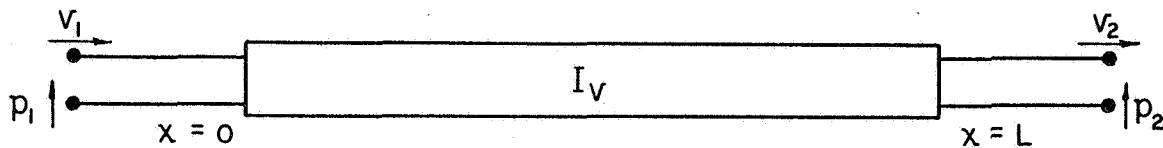


Figure 2.7. Lumped Model Inertance Element

Writing the equation of motion for this case gives

$$p_1 - p_2 = \rho_0 L \frac{dv}{dt} = I_v \frac{dv}{dt} \quad (2.27)$$

where $v_1 = v_2 = v$ since the flow is incompressible. The quantity $\rho_0 L$ represents a fluid inertance. Before proceeding, it should be noted that Equation (2.27) is often found in various other forms in the literature. It may be found also as

$$p_1 - p_2 = \frac{\rho_0 L}{A} \frac{dq}{dt} = I_q \frac{dq}{dt}$$

where q is the flow rate and A is the cross-sectional area. For this

case, the fluid inertance is $\rho_0 L/A$. Another form of Equation (2.27) is

$$P_1 - P_2 = \frac{L}{Ag} \frac{dw}{dt} = I_w \frac{dw}{dt}$$

where w is the weight flow rate. Notice that the inertance, I , is not the same in each case. Notice also that these equations are valid only for constant area lines.

Fluid Capacitance

Now consider a fluid line in which only compressibility effects are important, i.e., inertia or inertance effects and resistance effects are unimportant. With respect to Figure 2.8, applying the continuity and state equations, one has, since $p_1 = p_2 = p$,

$$v_1 - v_2 = \frac{L}{K} \frac{dp}{dt} = C_v \frac{dp}{dt}. \quad (2.28)$$

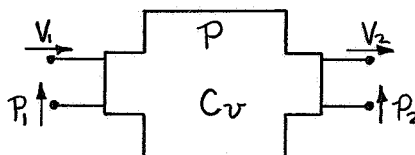


Figure 2.8. Lumped Model Capacitance Element

Again, as was true for Equation (2.27), one could just as well have written Equation (2.28) in terms of q or w , but the value of C would also have been different; thus,

$$q_1 - q_2 = \frac{AL}{\kappa} \frac{dP}{dt} = C_q \frac{dP}{dt}$$

and also

$$w_1 - w_2 = \frac{\rho_0 g AL}{\kappa} \frac{dP}{dt} = C_w \frac{dP}{dt}.$$

Fluid Resistance

Because of the large number of parameters which may affect the fluid resistance, it becomes more difficult in this case to write a valid theoretical relationship which holds for a wide range of flow and pressure variations. The usual approach, therefore, is to treat fluid resistance semi-empirically by defining the pressure drop due to resistance between points 1 and 2 of a lumped resistive element as where

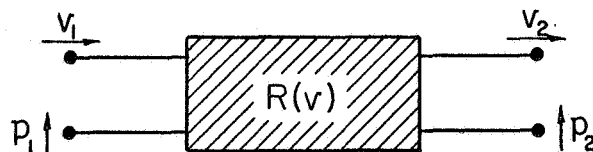


Figure 2.9. Lumped Model Resistive Element

$v_1 = v_2 = v$ and $R(v)$ is an experimentally determined function of velocity. Of course, if the pressure and velocity are steady, then $R(v)$ is well known from information contained in standard fluid mechanics textbooks. For the case of oscillating flow only (no net flow), one can

get a good value for the resistance coefficient by considering a low frequency approximation of the two-dimensional viscous distributed parameter model.

Fundamental Lumped Model

Combining the three basic elements yields the fundamental representation of a lumped line. Combining Equations (2.27) and (2.28) and

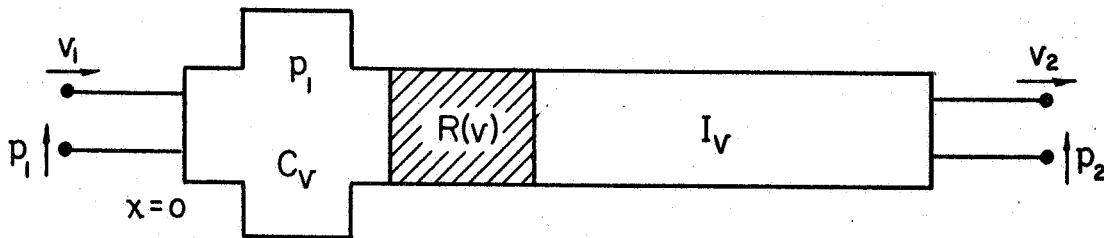


Figure 2.10. Fundamental Representation of Lumped Line

considering also Equation (2.29), then one may write for the fundamental representation

$$p_1 - p_2 = I_v \frac{dv_2}{dt} + R(v) v_2 \quad (2.30)$$

and

$$v_1 - v_2 = C_v \frac{dp_1}{dt} \quad (2.31)$$

Now, take the Laplace transformation of Equations (2.30) and (2.31),

thus

$$P_1(s) - P_2(s) = sI_v V_2(s) + R(v) V_2(s) \quad (2.32)$$

and

$$V_1(s) - V_2(s) = sC_v P_1(s). \quad (2.33)$$

Writing these last two equations in the standard transfer form gives,

$$P_2(s) = P_1(s) \{1 + sC_v [sI_v + R(v)]\} - V_1(s) \{sI_v + R(v)\}$$

and

$$V_2(s) = V_1(s) - sC_v P_1(s).$$

There are many possible ways of representing a conduit with lumped elements other than the representation of Figure 2.10.

Equivalent Electrical Circuits

One motivation for using lumped models, other than simplicity, is that they readily yield to simulation on an analog computer. Using a pressure-voltage analogy, the electrical equivalent of the fundamental lumped model becomes that shown in Figure 2.11. The values of R_e , L_e , and C_e depend upon what is made to be the analog of electrical current. Table I shows the analogous quantities for three possible analogs. Other circuits which are often used in an effort to improve the accuracy of representation are shown in Figure 2.12.

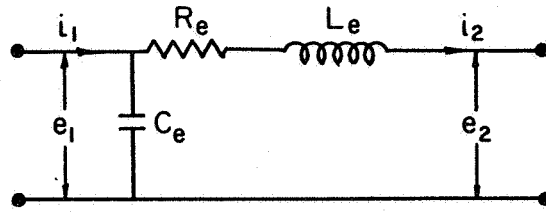
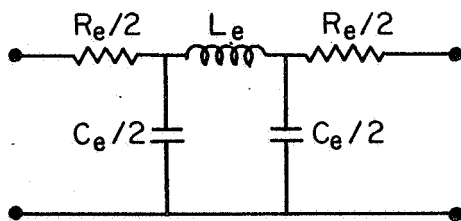


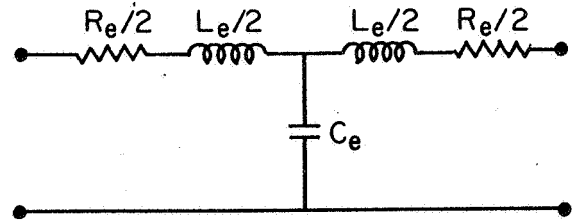
Figure 2.11. Electrical Analogy for Fundamental Lumped Conduit With Friction

TABLE I
ELECTRICAL ANALOGS

Electrical Quantity	Voltage e	Current i	Resistance R_e	Inductance L_e	Capacitance C_e
Analogous	p	v	$R(v)$	$\rho_o L$	L/κ
Conduit System	p	q	$\frac{R(v)}{A}$	$\frac{\rho_o L}{A}$	AL/κ
Quantity	p	w	$\frac{R(v)}{\rho_o Ag}$	$\frac{L}{Ag}$	$\frac{\rho_o gAL}{\kappa}$



PI REPRESENTATION



T REPRESENTATION

Figure 2.12. Variations of Electrical Analogs

Method for Improving Lumped Model

It was stated previously that a lumped model generally is valid only if the frequencies involved are not greater than about one-eighth of the first critical frequency of the lumped element.

This restriction can be eliminated by using several "lumps" to simulate a conduit. Suppose, for example, that the highest frequency encountered is about ten times too high for valid lumping; then, if ten electrically equivalent circuits are used in series (after reducing R_e , L_e , and C_e by a factor of ten), one is able to circumvent the original restriction. Figure 2.13 shows the electrical analog for an n-segmented lumped model.

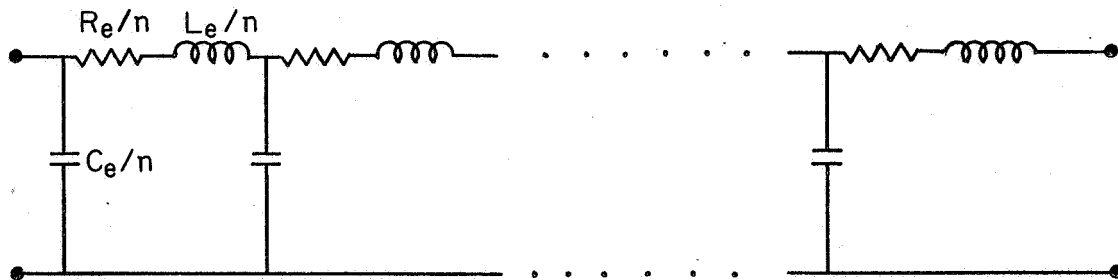


Figure 2.13. Analog for n-Segmented Lumped Conduit With Friction

In practice, it has been found that this model does lead to greater accuracy, but that the number of segments required becomes very great when the frequencies involved go beyond about the second critical value. Another method of lumping, invented to overcome this difficulty, is discussed below.

Tapered Models

The representation of lossless fluid lines by a tapered lumped model is the subject of a patent by Paynter (25). The analog of an n-segmented tapered representation as presented in the patent is shown in Figure 2.14. The values of the Ψ 's and Φ 's is dependent on the value of n and are given in Table II for values of n up to 5.



Figure 2.14. Tapered Lossless Analog

TABLE II

VALUES OF Φ 'S AND Ψ 'S

n→	0	1	2	3	4	5
Φ_0	1.000	.250	.142	.099	.075	.061
Ψ_1		.541	.289	.199	.152	.122
Φ_1		.750	.311	.205	.154	.124
Ψ_2			.367	.218	.159	.127
Φ_2			.547	.244	.168	.131
Ψ_3				.295	.182	.137
Φ_3				.452	.209	.146
Ψ_4					.257	.160
Φ_4					.394	.185
Ψ_5						.229

It has been found that this tapered representation gives good results for any number of critical frequencies and the number of "lumps" or segments needed for an accurate representation up to a given frequency is equal to

$$N_c + 1$$

where N_c is the number of critical frequencies below the desired cutoff frequency.

Conduit Wall Effects

Thus far in the developments, the effects which the conduit wall may have upon the fluid dynamics have been neglected. Depending upon the operating parameters of the system being analyzed, accounting for the effects of the wall may be very simply achieved or, on the other hand, may require an extensive mathematic treatment in order to get reasonable answers. Fortunately, most problems which are of concern can be handled with the simple treatment. Problems demanding a complex analysis usually occur only when dealing with extremely high operating frequencies.

Simplified Analysis

Korteweg in 1878 showed that wave propagation was dependent upon both the elasticity of the fluid and of the conduit wall and that the resultant propagation velocity must be equal to or less than c_0 . It has been shown (see, for example, Reference 7) that the actual sound velocity is

$$\kappa = \frac{\kappa_0}{\sqrt{1 + \kappa f / E_t}} \quad (2.34)$$

where E_t is Young's modulus for the tube material and f is given by

$$f = \begin{cases} D_o/h & \text{thin-walled tube} \\ 2 \left(\frac{D_o^2 + D_i^2}{D_o^2 - D_i^2} \right) & \text{thick-walled tube} \end{cases} \quad (2.35)$$

In Equation (2.35), D_o represents the conduit outside diameter and D_i represents the inside diameter. All that is required in the simplified analysis is that one replace c_o with the c of Equation (2.34) in the analysis.

More Exact Analysis

There have been a large number of papers written pertaining to the effect of conduit wall elasticity on the transmission characteristics of fluid within the conduit. Basically, conduits may be divided into two types with regard to the elastic characteristics of their walls: elastic flexible and elastic stiff. For a conduit with elastic flexible walls, it is assumed that pressure variations within the conduit can cause radial deformations which do not cause corresponding axial disturbances in the conduit wall, i.e., all disturbances in the wall are localized and cannot propagate axially along the conduit wall. For elastic stiff walls, on the other hand, disturbances can propagate axially along the pipe wall. Some of the authors who have made contributions on the effects of conduit elasticity are Lamb (26), Jacobi (27), Morgan (28), Lin and Morgan (29), and Skalak (30). None of these authors have treated exactly a viscous fluid in this connection. An

exact treatment of both flexible and stiff walls for a viscous fluid is outlined in Chapter VII.

In general, the relations expressing the propagation velocity variation with frequency have trends as shown sketched in Figure 2.15. Notice that only one mode transmits for all frequencies for the case of an elastic flexible wall, whereas two modes transmit at all frequencies for an elastic stiff wall. Note also that the limiting value for small frequency in both cases approaches the same value, c/c_0 . This is the same value as predicted by the simplified analysis from Equation (2.34). One can see then that the simplified analysis is exact for low frequencies for the zeroth mode (nonviscous fluid only).

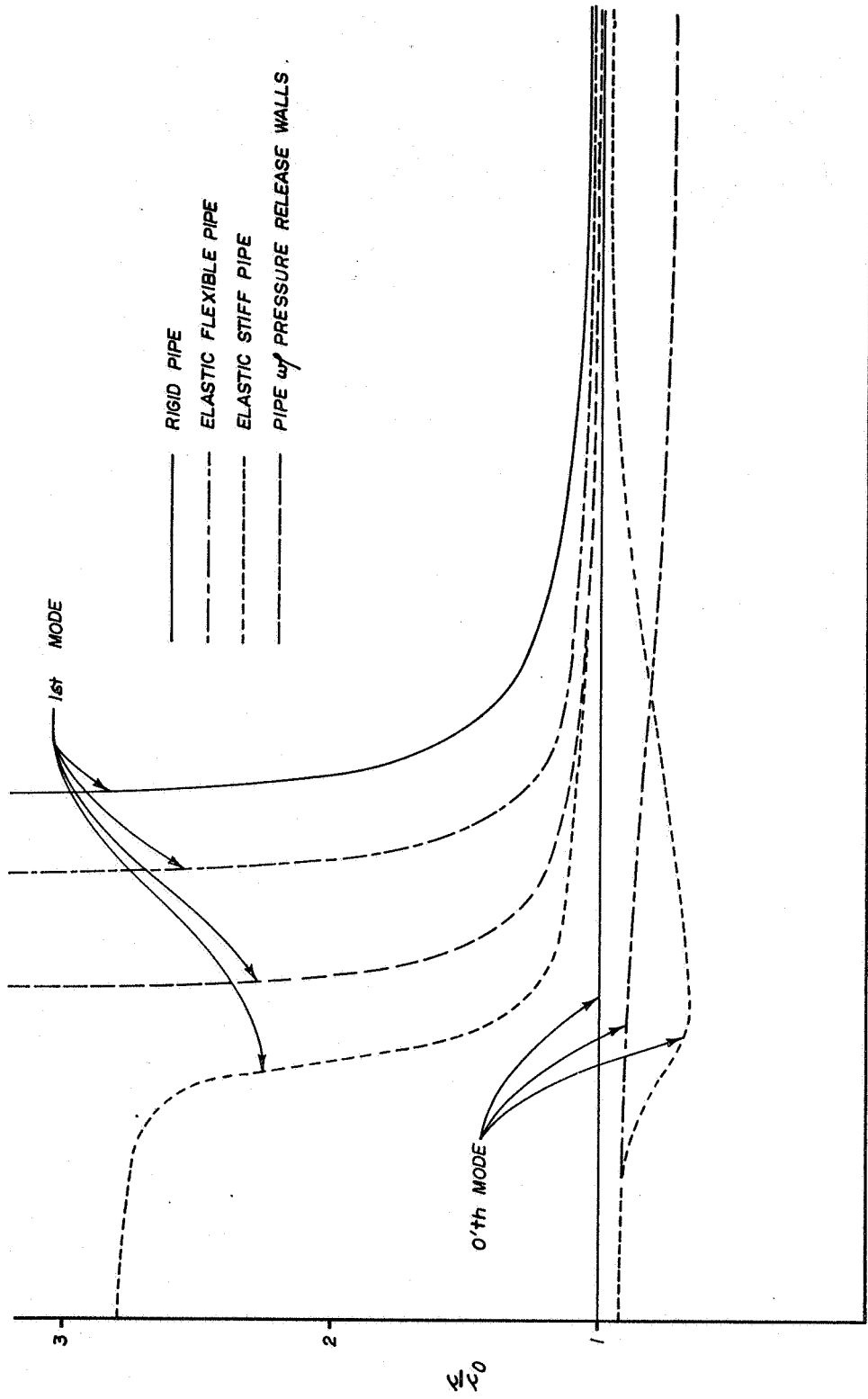


Figure 2.15. Propagation Velocity Versus Frequency for Nonviscous Fluid

CHAPTER III

EXACT SOLUTION OF FIRST-ORDER NAVIER-STOKES EQUATIONS

Introduction

In this chapter, a solution of the first-order Navier-Stokes equations, as developed in Chapter II, is given for a cylindrical, axisymmetric coordinate system. This solution will be the mathematical foundation for the remainder of this treatise.

Mathematical Formulation of the Problem

For the purposes of this discussion, consider a fluid conduit to be describable in terms of a cylindrical coordinate system as shown in Figure 3.1.

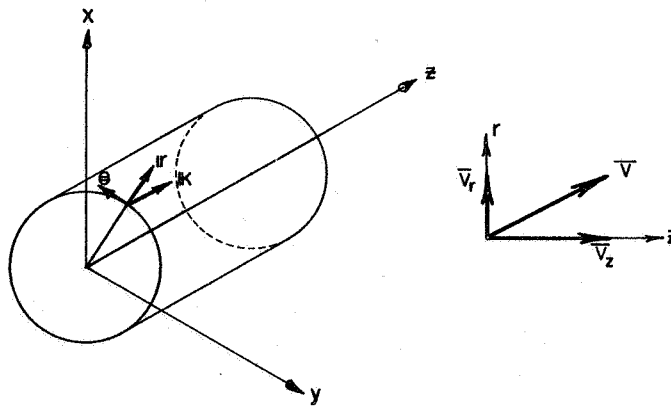


Figure 3.1. Coordinate System

Assuming that thermal effects are not important, the first-order equations of change for a liquid are

$$\rho_0 \frac{\partial \bar{v}_i}{\partial t} = -\nabla p + \mu \left\{ \frac{4}{3} \nabla (\nabla \cdot \bar{v}_i) - \nabla \times (\nabla \times \bar{v}_i) \right\} \quad (3.1)$$

which is the first-order Navier-Stokes equation,

$$\frac{\partial p_1}{\partial t} + \rho_0 \nabla \cdot \bar{v}_i = 0 \quad (3.2)$$

for the first-order continuity equation, and

$$dp_1 = \kappa \frac{d\rho_1}{\rho_0} \quad (3.3)$$

which is a liquid equation of state. Combining Equations (3.2) and (3.3) gives

$$\frac{\partial p_1}{\partial t} + \rho_0 c_0^2 \nabla \cdot \bar{v}_i = 0 \quad (3.4)$$

where $c_0 = \sqrt{\kappa/\rho_0}$ is the isentropic speed of sound for the fluid under consideration. The Equations (3.1) and (3.4) are the equations of change in terms of the first-order variables \bar{v}_i and p_1 . It may be recalled from Chapter I that \bar{v}_i and p_1 represent small perturbations from the zero-order conditions \bar{v}_0 and p_0 . The restrictions on these equations are:

1. The fluid velocity ($\bar{v} = \bar{v}_0 + \bar{v}_i$) at any point and time is much less than the velocity of sound in the fluid, thus justifying omission of the nonlinear terms.
2. Perturbations in the density are negligible compared to the average density; that is, $|\rho_1| \ll \rho_0$.

3. Temperature effects are negligible.
4. Fluid viscosity is spatially independent.
5. The flow field is axi-symmetric.

Solution

To facilitate the solution of Equations (3.1) and (3.4), define a scalar potential φ and a vector potential $\bar{\Psi}$ such that

$$\bar{v}_1 = \nabla\varphi + \nabla \times \bar{\Psi}. \quad (3.5)$$

This means it is being postulated that the vector velocity is composed of the gradient of the scalar potential φ plus the curl of the vector potential $\bar{\Psi}$. Taking the divergence of (3.5) gives

$$\nabla \cdot \bar{v}_1 = \nabla^2 \varphi \quad (3.6)$$

and also taking the curl of (3.5) yields

$$\nabla \times \bar{v}_1 = \nabla \times (\nabla \times \bar{\Psi}) = \nabla(\nabla \cdot \bar{\Psi}) - \nabla^2 \bar{\Psi}. \quad (3.7)$$

The vorticity vector $\bar{\zeta}$ associated with the perturbation velocity \bar{v}_1 may be written as

$$\bar{\zeta} = \nabla \times \bar{v}_1 \quad (3.8)$$

and that $\bar{\zeta}$ and $\bar{\Psi}$ are related by

$$\bar{\zeta} = \nabla(\nabla \cdot \bar{\Psi}) - \nabla^2 \bar{\Psi}. \quad (3.9)$$

For axi-symmetric flow, $\bar{\zeta}$ has only a component in the direction perpendicular to r and k , thus in the \ominus direction, by virtue of Equation (3.8). It is necessary that $\bar{\Psi}$ have only a \ominus component also, as may be seen from

the relationship between $\bar{\zeta}$ and $\bar{\Psi}$ given in Equation (3.9). Therefore,

$$\bar{\Psi} = \Theta \psi. \quad (3.10)$$

Since the operator ∇ has only r and k components for axi-symmetric conditions, $\nabla \cdot \bar{\Psi} = 0$, which leads to

$$\nabla \times \bar{v}_i = \bar{\zeta} = -\nabla^2 \bar{\Psi}. \quad (3.11)$$

In summary, then, the divergence of the perturbation velocity vector is related to the scalar field φ by Equation (3.6); for axi-symmetric flow, the curl of the perturbation velocity vector, also referred to as the vorticity, is related to the vector field $\bar{\Psi}$ by Equation (3.11).

Taking the divergence of Equation (3.1), the vorticity is eliminated since the divergence of a curl is zero, and thus

$$\frac{\partial \nabla \cdot \bar{v}_i}{\partial t} = -\frac{1}{\rho_0} \nabla \cdot (\nabla p_1) + \frac{4}{3} \nu \nabla \cdot [\nabla (\nabla \cdot \bar{v}_i)]. \quad (3.12)$$

Substitution of (3.6) into (3.12) yields

$$\frac{\partial \nabla^2 \varphi}{\partial t} = -\frac{1}{\rho_0} \nabla^2 p_1 + \frac{4}{3} \nu \nabla^2 (\nabla^2 \varphi)$$

or

$$\frac{\partial \varphi}{\partial t} = -\frac{p_1}{\rho_0} + \frac{4}{3} \nu \nabla^2 \varphi. \quad (3.13)$$

From Equations (3.4) and (3.6)

$$\frac{\partial p_1}{\partial t} = -\rho_0 c_0^2 \nabla^2 \varphi. \quad (3.14)$$

Taking the partial derivative of (3.13) with respect to t and

substituting $\partial p_1 / \partial t$ from (3.14) gives

$$\frac{\partial^2 \varphi}{\partial t^2} = c_0^2 \nabla^2 \varphi + \frac{4}{3} \nu \frac{\partial}{\partial t} \nabla^2 \varphi. \quad (3.15)$$

Taking the curl of Equation (3.1), the result is

$$\frac{\partial (\nabla \times \bar{v}_1)}{\partial t} = -\nu \left\{ \nabla \times [\nabla \times (\nabla \times \bar{v}_1)] \right\} \quad (3.16)$$

or

$$\frac{\partial \nabla^2 \bar{\psi}}{\partial t} = -\nu \left\{ \nabla \times [\nabla \times (\nabla^2 \bar{\psi})] \right\}. \quad (3.17)$$

By virtue of the vector identity

$$\nabla \times (\nabla \times \bar{v}_1) = \nabla (\nabla \cdot \bar{v}_1) - \nabla^2 \bar{v}_1$$

and the fact that $\bar{\xi}$ and $\bar{\Psi}$ have only Θ components, Equations (3.16) and (3.17) reduce to

$$\frac{\partial \bar{\xi}}{\partial t} = \nu \nabla^2 \bar{\xi} \quad (3.18)$$

and

$$\frac{\partial \bar{\Psi}}{\partial t} = \nu \nabla^2 \bar{\Psi}. \quad (3.19)$$

Physically, Equation (3.15) is a viscous wave equation for plane or one-dimensional waves; thus, φ is a viscous plane-wave potential function. Equation (3.18) is a vorticity diffusion equation and (3.19) is a diffusion equation for the function $\bar{\Psi}$. By means of the substitution $\bar{v}_1 = \nabla \varphi + \nabla \times \bar{\Psi}$ the two coupled partial differential equations, (3.1) and

(3.4), which appear to be difficult to solve in original form have been transformed into two independent partial differential equations (3.15) and (3.19) of known solvable form. Equations (3.15) and (3.19) will now be solved. The solutions will be obtained in the Laplace domain for convenience.

Applying the Laplace transformation to Equations (3.15) and (3.19) yields (assuming initial conditions zero)

$$s^2 \hat{\varphi} = \rho_0^2 \nabla^2 \hat{\varphi} + \frac{4}{3} \nu s \nabla^2 \hat{\varphi} \quad (3.20)$$

and

$$s \hat{\psi} = \nu \nabla^2 \hat{\psi} \quad (3.21)$$

where $\hat{\varphi}$ and $\hat{\psi}$ are the transformed quantities.

Solving Equations (3.20) and (3.21) by the method of separation of variables yields

$$\hat{\psi} = A J_1(kr) e^{\gamma z} \quad (3.22)$$

and

$$\hat{\varphi} = B J_0(\beta r) e^{\gamma z} \quad (3.23)$$

where A and B are constants of integration and γ is the separation constant. $J_0(\beta r)$ and $J_1(kr)$ denote the zero and first-order Bessel functions of the first kind with arguments βr and kr , respectively. Also, the equations

$$k^2 = \gamma^2 - s/\nu \quad (3.24)$$

and

$$\beta^2 = \gamma^2 - \frac{S^2}{C_0^2 + \frac{4}{3}\nu S} \quad (3.25)$$

relate the parameters, k , γ , and β . It should be noted that the separation constant γ must be the same in Equation (3.22) and (3.23) since Ψ and Φ must both contribute to the perturbation velocity. Now that Φ and Ψ are known, \bar{v}_1 can be found since

$$\bar{v}_1 = \nabla \hat{\Phi} + \nabla \times \hat{\Psi} \quad (3.26)$$

where \bar{v}_1 is the Laplace transform of \bar{v}_1 . Since

$$\nabla \hat{\Phi} = r \frac{\partial \hat{\Phi}}{\partial r} + k \frac{\partial \hat{\Phi}}{\partial z} \quad (3.27)$$

and

$$\nabla \times \hat{\Psi} = -r \frac{\partial \hat{\Psi}}{\partial z} + k \frac{1}{r} \frac{\partial}{\partial r} (r \hat{\Psi}), \quad (3.28)$$

equation (3.26) becomes

$$\bar{v}_1 = r \left\{ \frac{\partial \hat{\Phi}}{\partial r} - \frac{\partial \hat{\Psi}}{\partial z} \right\} + k \left\{ \frac{\partial \hat{\Phi}}{\partial z} + \frac{1}{r} \frac{\partial}{\partial r} (r \hat{\Psi}) \right\}. \quad (3.29)$$

The Laplace transformed velocity components may now be written as

$$V_{1r} = \frac{\partial \hat{\Phi}}{\partial r} - \frac{\partial \hat{\Psi}}{\partial z} = - \left\{ B \beta J_1(\beta r) + A \gamma J_1(kr) \right\} e^{\gamma z} \quad (3.30)$$

and

$$V_{1z} = \frac{\partial \hat{\Phi}}{\partial z} + \frac{\partial \hat{\Psi}}{\partial r} + \frac{\hat{\Psi}}{r} = \left\{ B \gamma J_0(\beta r) + A k J_0(kr) \right\} e^{\gamma z}. \quad (3.31)$$

From the equality of the γ 's in Equations (3.24) and (3.25)

$$\gamma^2 = k^2 + \frac{S}{\nu} = \beta^2 + \frac{S^2}{\rho_0^2 + \frac{4}{3} S \nu} \quad (3.32)$$

It now remains to calculate the transformed pressure, thus from Equations (3.4), (3.6), and (3.23)

$$sP_1 = -\rho_0 \rho_0^2 \nabla^2 \hat{\varphi} = -\rho_0 \rho_0^2 B (\gamma^2 - \beta^2) J_0(\beta r) e^{\gamma z/2}$$

or

$$P_1 = -\frac{\rho_0 \rho_0^2}{s} B (\gamma^2 - \beta^2) J_0(\beta r) e^{\gamma z/2} \quad (3.33)$$

Equations (3.30), (3.31), and (3.33) are the exact general simultaneous solution of the first-order axi-symmetric Navier-Stokes Equation (3.1), the continuity relation (3.2), and the equation of state for a liquid given by (3.3). The constants of integration, A and B and the parameters (eigenvalues) γ , β , and k are to be determined from the boundary conditions for a particular geometry. For a general case; that is, for a general set of boundary conditions, the transformed velocities and pressure will become

$$V_{1r} = -\sum_n \left\{ B_n \beta_n J_1(\beta_n r) + A_n \gamma_n J_1(k_n r) \right\} e^{\gamma_n z/2} \quad (3.34)$$

$$V_{1z} = \sum_n \left\{ B_n \gamma_n J_0(\beta_n r) + A_n k_n J_0(k_n r) \right\} e^{\gamma_n z/2} \quad (3.35)$$

and

$$P_1 = -\frac{\rho_0 c_0^2}{s} \sum_n B_n (\gamma_n^2 - \beta_n^2) J_0(\beta_n r) e^{\gamma_n z} \quad (3.36)$$

In the chapters which follow, boundary conditions will be applied to this solution for the case of a rigid cylindrical pipe and a cylindrical pipe with both elastic-flexible walls and elastic-stiff walls. The significance of each family of eigenvalues which result from the application of the boundary conditions will be discussed. Also, engineering models will be developed which describe average velocity and pressure conditions in a fluid conduit, thus, simplifying the mathematics. Experimental studies will be described which attempt to verify the mathematical models.

CHAPTER IV

APPLICATION OF THE EXACT SOLUTION TO THE CASE OF A RIGID FLUID CONDUIT

Introduction

The purpose of this chapter is to present a rather complete treatment of the application of the exact solution of Chapter III to the case of a rigid fluid conduit. The existence of higher order modes with respect to wave propagation in a viscous liquid will be demonstrated. A complete discussion of these modes is left for Chapter VI. The major part of this chapter will be devoted to various aspects of the zeroth mode of propagation, such as the development of approximate forms for the zeroth mode characteristic parameters (eigenvalues), a development of the zeroth mode transfer equations and discussions of frequency and transient responses. It will be seen that the approximate value obtained for the zeroth mode propagation operator corresponds to the values obtained by previous investigators through the solution of a reduced set of equations of motion. Also, the transfer equations obtained are identical in form to those previously reported.

Characteristic Equations for Eigenvalues

In Chapter III, the general solution to the first-order Navier-Stokes equation for a compressible liquid was found and expressed in the

Laplace domain form of Equations (3.34), (3.35), and (3.36) for respectively, the radial velocity, the axial velocity, and the pressure. In order that the solution can be complete for the case under consideration, the proper boundary conditions must be applied. The eigenvalues k_n , γ_n , and β_n will be specified if the relationship between velocity and pressure is specified at the wall; i.e., if the impedance at the wall is specified. The constants of integration A_n and B_n must be found from an end condition for the conduit. This means that the fluid velocity at the conduit end must be expanded as a series of the eigenfunctions and the coefficients determined.

For the case of rigid conduit walls, it is required that both the radial and axial fluid velocities go to zero at the pipe wall, $r = r_0$. Applying these conditions to Equations (3.34) and (3.35) yields

$$B_n \beta_n J_1(\beta_n r_0) + A_n \gamma_n J_1(k_n r_0) = 0 \quad (4.1)$$

and

$$B_n \gamma_n J_0(\beta_n r_0) + A_n k_n J_0(k_n r_0) = 0. \quad (4.2)$$

Elimination of A_n and B_n by combining Equations (4.1) and (4.2) gives

$$k_n \beta_n \frac{J_1(\beta_n r_0)}{J_0(\beta_n r_0)} = \gamma_n^2 \frac{J_1(k_n r_0)}{J_0(k_n r_0)} \quad (4.3)$$

which is the characteristic equation for the eigenvalues. The simultaneous solution of Equations (3.32) and (4.3) will yield the eigenvalues. The exact computation of these values can only be achieved by a numerical iteration procedure. A computer program has been set up to do this and the procedure and program are detailed in Appendix A. In general,

it must be said that the exact evaluation of the eigenvalues is not amenable to hand calculations. Fortunately, it is easy to obtain rather good approximate values for the $n = 0$ or "zeroth" mode eigenvalues. This will be discussed in the next section.

In summary, it has been found that application of the boundary conditions at the conduit wall results in a characteristic equation which may be solved for the allowed values of the parameters β_n , γ_n , and k_n . In general, there will be an infinite number of allowed values. Each set of numbers corresponds to a mode of propagation. The summation of all of these modes, weighted properly by the constants of integration A_n and B_n , give the fluid velocity and pressure at any point in the fluid conduit. The constants A_n and B_n must be evaluated in terms of end conditions; that is, it is necessary that one know the r dependence of the velocity at some axial position z_0 . The evaluation of these constants will be discussed in more detail in Chapter VI. The significance of the modes will also be discussed more fully at that time.

Approximate Form of Zeroth Mode Equations

The difficulties in exactly solving for the eigenvalues from the characteristic equation was indicated in the previous section. If it were not for two facts, the application of the exact solution to everyday engineering problems would appear difficult indeed. However:

1. For most engineering problems, the influence of the zeroth mode is predominant.
2. It is possible to get good approximate values for the zeroth mode eigenvalues.

With these two facts in mind, the approximate form of the zeroth mode

equations will be obtained. It will be seen that the approximate form of the zeroth mode propagation operator corresponds to that reported by several previous investigators.

It may be assumed that, to a first approximation, the zeroth mode value for $\beta_0 r_0$ is very small or small enough that $J_0(\beta_0 r_0)$ and $J_1(\beta_0 r_0)$ may be approximated by their small argument values

$$J_1(\beta_0 r_0) \approx \frac{\beta_0 r_0}{2} \quad (4.4)$$

and

$$J_0(\beta_0 r_0) \approx 1. \quad (4.5)$$

The validity of this assumption may be judged on the basis of the comparison between exact values for $\gamma_0 r_0$ and the approximate value which will be presented later in this section.

Substitution of Equations (4.4) and (4.5) into (4.3) gives

$$\beta_0^2 = 2\gamma_0^2 \left\{ \frac{J_1(k_0 r_0)}{k_0 r_0 J_0(k_0 r_0)} \right\} \quad (4.6)$$

or, by substituting Equation (4.6) into (3.32) yields

$$\gamma_0 = \left\{ \frac{\frac{s^2}{c_0^2 + \frac{4}{3} \gamma_0^2 s}}{1 - \frac{2 J_1(k_0 r_0)}{k_0 r_0 J_0(k_0 r_0)}} \right\}^{1/2}. \quad (4.7)$$

To complete the approximation, since $\beta_0 r_0$ is small, $k_0 \approx i\sqrt{s/v}$ for $|s| \ll c_0/v$. This yields, subject to the limitations

$$|\beta_0 r_0| \ll 1$$

and

$$|S| \ll c_0/v$$

that

$$k_0 = i \sqrt{\frac{S}{2v}} \quad (4.8)$$

and

$$\beta_0 = \left\{ \frac{2\gamma_0^2 J_1(k_0 r_0)}{k_0 r_0 J_0(k_0 r_0)} \right\}^{1/2} \quad (4.9)$$

where γ_0 is given by Equation (4.7).

To evaluate the accuracy of this approximation, Γ_r and c/c_0 have been obtained by both the exact procedure of Appendix A and with the aid of Equations (4.7) and (4.8) for the zeroth mode. The results are shown plotted in Figures 4.1 and 4.2. Note that

$$\Gamma_r \equiv \text{Real part of } \gamma r_0$$

$$\Gamma_c \equiv \text{Imaginary part of } \gamma r_0$$

$$c/c_0 \equiv \text{Normalized phase velocity} = \frac{F_{nr}}{\Gamma_c}$$

$$F_{nr} \equiv \text{Radial frequency number} = \frac{\omega r_0}{c_0}$$

$$D_{nr} \equiv \text{Radial damping number} = \frac{v}{r_0 c_0}$$

Notice that the error for Γ_r is much greater than the corresponding error for c/c_0 . With the aid of these two figures, a judgment can be made as to the validity of the approximate Γ_0 based upon the use intended. Suppose that it is desired to have an error in Γ_0 no greater than one per cent and the value of the radial damping number happens to

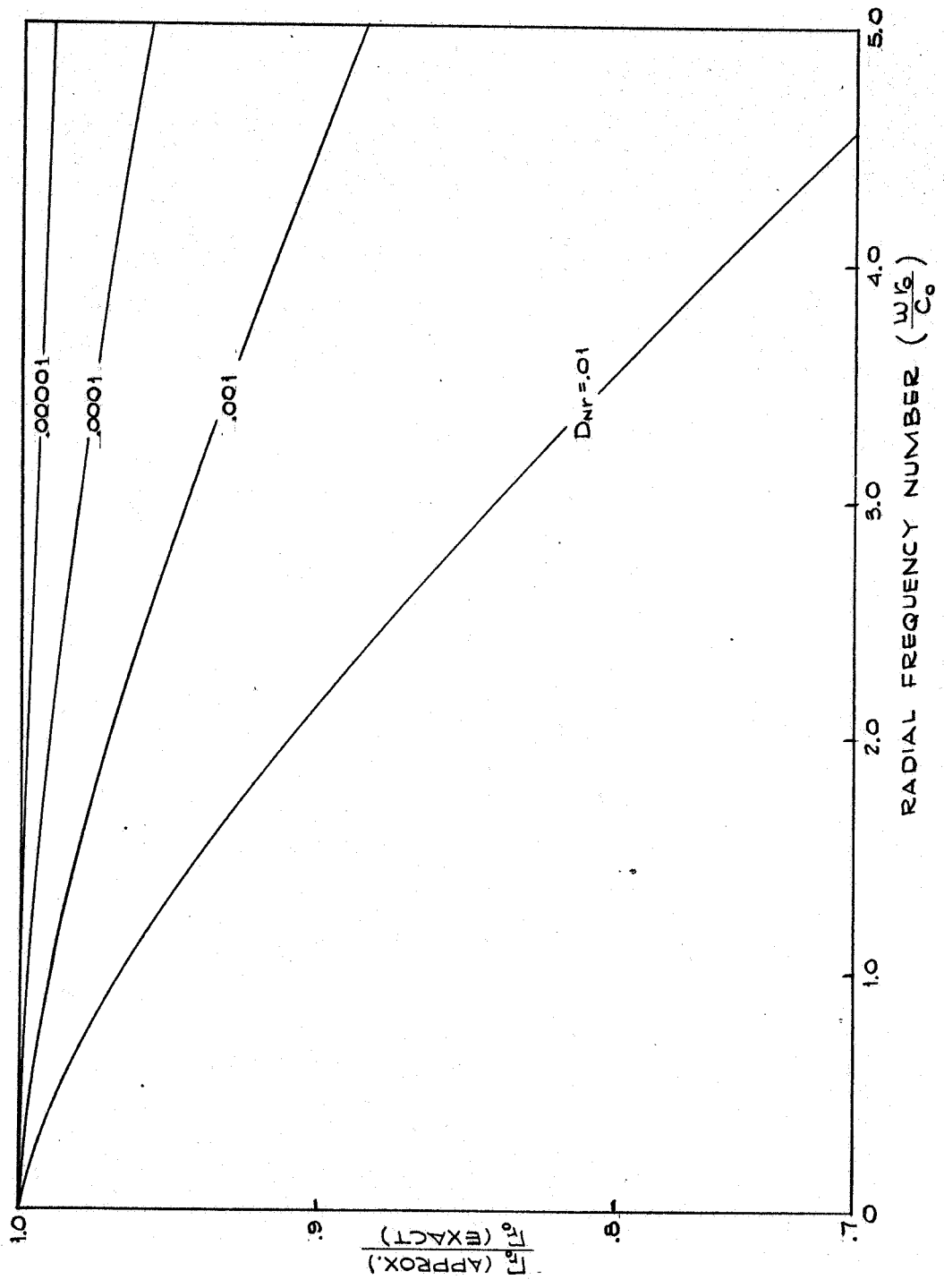


Figure 4.1. Ratio of Real Part of Propagation Operator From Equation (4.7) to Exact Value Versus Radial Frequency Number

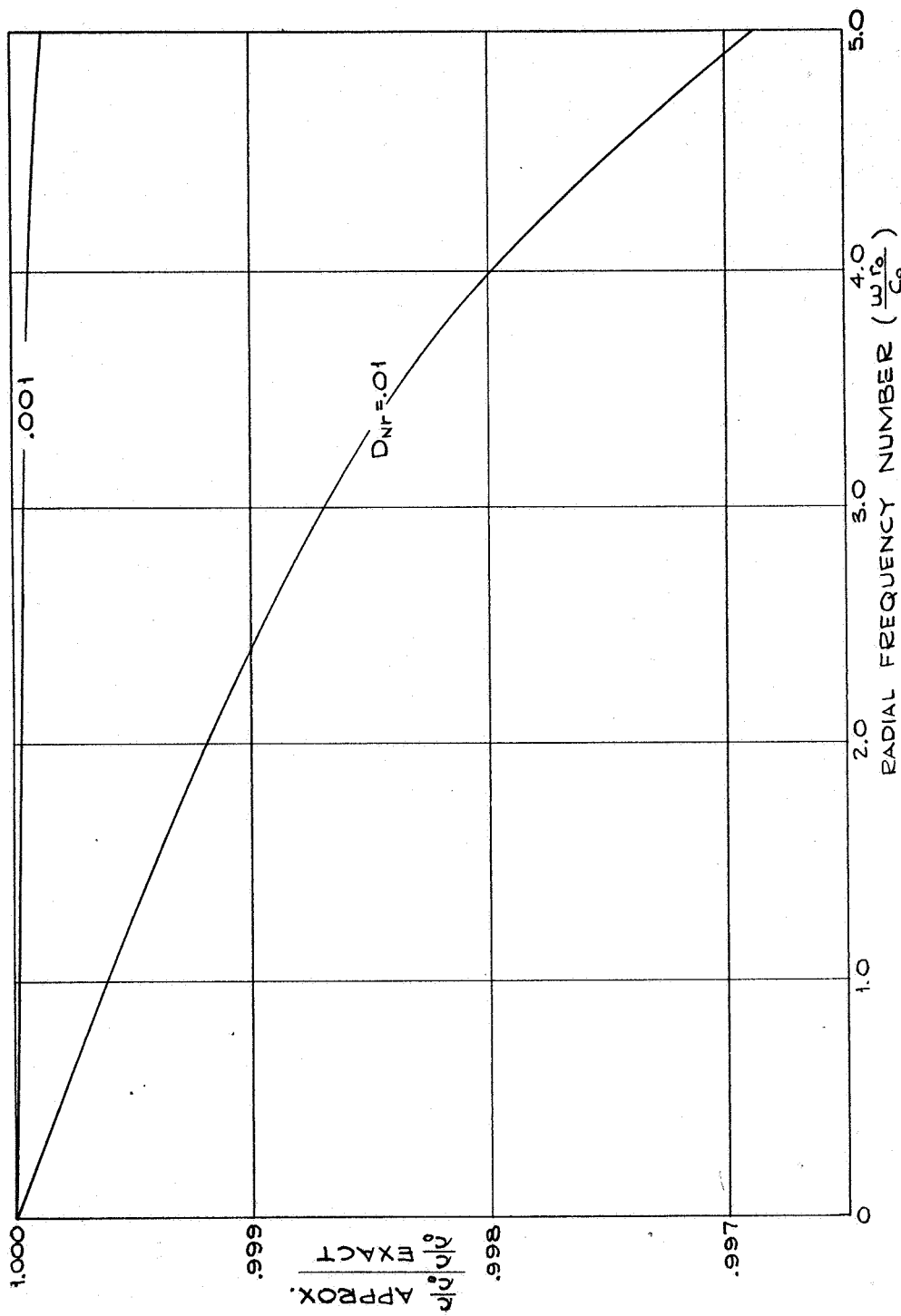


Figure 4.2. Ratio of Dimensionless Phase Velocity From Equation (4.7) to Exact Value Versus Radial Frequency Number

be .001. From Figures (4.1) and (4.2), it may be seen that the maximum radial frequency number can be about 1.0. For most engineering problems, the approximate value of Γ_0 should suffice.

It should be recognized that the approximate value of Υ_0 just derived is almost identical to that given by Equation (2.19) as reported by several previous investigators. The implication here is that the propagation operator given by these previous investigators, and which is recognized as being for the zeroth mode only, is really an approximation to the exact value of Υ_0 .

Now that the approximate forms of the eigenvalues have been demonstrated, they will be applied to the axial velocity and pressure in order to obtain the corresponding approximate forms.

The zeroth mode transformed first-order axial velocity and pressure may be written from Equations (3.35), (3.36), and (4.2) as (omitting the sub 1 for convenience)

$$V_{z0} = B_0 \gamma_0 J_0(\beta_0 r_0) \left\{ \frac{J_0(\beta_0 r)}{J_0(\beta_0 r_0)} - \frac{J_0(k_0 r)}{J_0(k_0 r_0)} \right\} e^{\gamma_0 z} \quad (4.10)$$

and

$$P_0 = - \frac{B_0 \rho_0 c_0^2}{s} (\gamma_0^2 - \beta_0^2) J_0(\beta_0 r) e^{\gamma_0 z}. \quad (4.11)$$

Applying the approximation of Equation (4.5) to (4.10) yields

$$V_{z0} = B_0 \gamma_0 \left\{ 1 - \frac{J_0(k_0 r)}{J_0(k_0 r_0)} \right\} e^{\gamma_0 z} \quad (4.12)$$

and similarly for Equation (4.11), using (3.32) and (4.5) gives

$$P_0 = -\rho_0 s B_0 e^{\gamma_0 z}. \quad (4.13)$$

Considering the response of the zeroth mode velocity to a sinusoidal pressure gradient then it is found that the time domain velocity may be expressed as

$$v_{z0} = \frac{iK}{\rho_0 \omega} \left\{ 1 - \frac{J_0(r\sqrt{-i\omega/\nu})}{J_0(r_0\sqrt{-i\omega/\nu})} \right\} e^{i\omega t}$$

where the pressure gradient is

$$\frac{dp}{dt} = K e^{i\omega t}$$

This same result has been reported by Sexl and Uchida as a result of solving a reduced form of the equations of motion. See reference (2) for a review of these results.

For values of the parameter $r_0\sqrt{\omega/\nu} < 5$. The velocity profile is essentially parabolic while for values greater than 5 the profiles begin to look like those shown in Figure 4.3. Notice that the fluid near the edges of the pipe responds more quickly than the fluid in the center of the pipe. This phenomena is called "Richardson's annular effect" and is discussed, for example, in Schlichting (2).

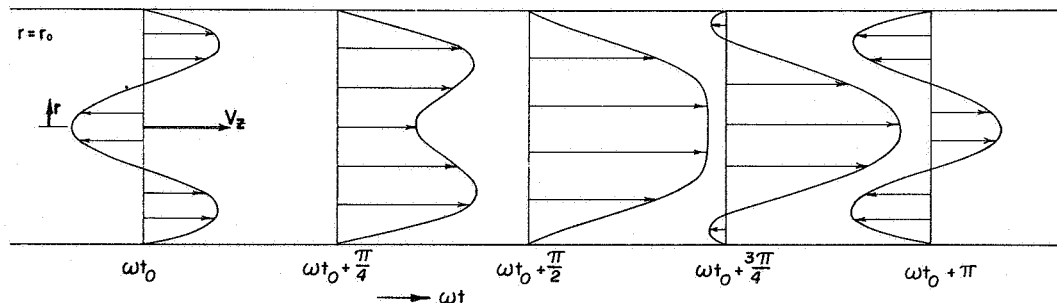


Figure 4.3. Typical Zeroth-Mode Velocity Profiles due to a Sinusoidal Axial Pressure Gradient

It has been shown that the exact solution as derived in Chapter III, when applied to the zeroth mode, can be reduced by using small argument values for $J_0(\beta_0 r_0)$ and $J_1(\beta_0 r_0)$ to give the propagation operator derived by F. T. Brown, N. B. Nichols, and others. The results of these authors was reported in Chapter II. The corresponding approximate form for the zeroth mode velocity profiles was seen to be identical to the work of Sexl and Uchida. The results of Brown, Nichols, Sexl, and Uchida was obtained from the solution of a reduced form of the equations of motion. The conclusion is that the work of the above mentioned authors is an approximation of the exact solution presented herein. The accuracy of the approximation may be partially judged on the basis of Figures 4.1 and 4.2.

In this section, concern has been given only to the discussion of the zeroth mode of propagation, or, also called the fundamental or longitudinal mode. What about the effects of the higher modes? The calculations involved in working with the higher modes is very cumbersome, as may be seen in Chapter VI. Fortunately, for most engineering applications, the effects of these higher modes appear to be negligible.

A concept useful when performing engineering calculations involving the zeroth mode will now be discussed.

Derivation of Zeroth Mode Transfer Equations

It is desirable, from an engineering point of view, to derive from Equations (4.12) and (4.13) a set of transfer equations which will describe the average conditions at some point z along the conduit in terms of the average conditions at $z = z_0$.

In the previous section, it was found that the zeroth mode axial velocity and pressure can be expressed approximately as

$$V_{z0} = B_0 \gamma_0 \left\{ 1 - \frac{J_0(k_0 r)}{J_0(k_0 r_0)} \right\} e^{\gamma_0 z} \quad (4.12)$$

and

$$P_0 = -\rho_0 s B_0 e^{\gamma_0 z} \quad (4.13)$$

Since only the zeroth mode is being discussed at this time, for the rest of this chapter "0" subscripts which refer to the zeroth mode will be omitted. Averaging Equation (4.12) across the conduit cross-section gives (the bar notation indicates the quantity has been averaged over the cross-section by integration from $r = 0$ to $r = r_0$)

$$\bar{V}_z = B \gamma \left\{ 1 - \frac{2 J_1(k r_0)}{k r_0 J_0(k r_0)} \right\} e^{\gamma z} \quad (4.14)$$

and

$$\bar{P} = -\rho_0 s B e^{\gamma z} \quad (4.15)$$

Up to this point γ has been considered, for convenience, to have only positive values; but, in general, it will have both a positive and a negative value. Positive values of γ indicate waves progressing in the negative z direction and negative γ 's indicate waves traveling in the positive z direction. Rewriting Equations (4.14) and (4.15) to include positive and negative values for γ yields

$$\bar{V}_z = \gamma \left\{ 1 - \frac{2 J_1(k r_0)}{k r_0 J_0(k r_0)} \right\} \cdot \left\{ B_1 e^{\gamma z} - B_2 e^{-\gamma z} \right\} \quad (4.16)$$

and

$$\bar{P} = -\rho_0 s \{ B_1 e^{\sqrt{z}} + B_2 e^{-\sqrt{z}} \}. \quad (4.17)$$

In Figure 4.4 is shown a diagram of a fluid conduit with appropriate end conditions. It may be seen that the boundary conditions which it is

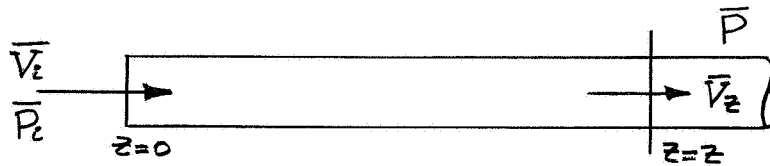


Figure 4.4. Diagram of Fluid Conduit for Zeroth Mode Transfer Equations

necessary to satisfy are

$$\bar{V}_z \Big|_{z=0} = \bar{V}_i$$

and

$$\bar{P} \Big|_{z=0} = \bar{P}_i$$

Substitution of these boundary conditions into Equations (4.16) and (4.17) gives a pair of equations from which B_1 and B_2 may be found. Substituting these values back into Equations (4.16) and (4.17) yields the familiar form of the transfer relations

$$\bar{V}_z = \bar{V}_i \cosh \sqrt{z} - \frac{\bar{P}_i}{Z_c} \sinh \sqrt{z} \quad (4.18)$$

and

$$\bar{P} = \bar{P}_i \cosh \gamma z - Z_c \bar{V}_i \sinh \gamma z \quad (4.19)$$

where

$$Z_c = \frac{\rho_0 c_0^2 \gamma}{S} \quad (4.20)$$

Equations (4.18) and (4.19) are then the zeroth mode transfer equations relating the average transformed conditions at some arbitrary z to the average transformed conditions at $z = 0$. One may rewrite these relations in another convenient and familiar form relating the conditions at some other position 2, where 2 is oriented a $+L$ distance from 1 in the z direction. See Figure 4.5.

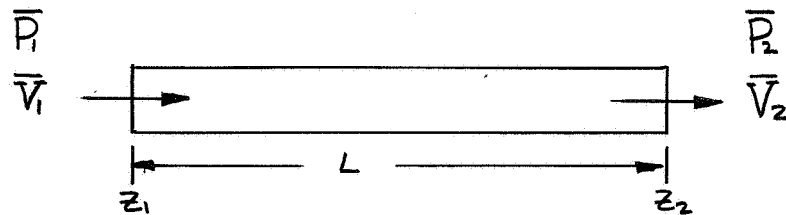


Figure 4.5. Diagram of Fluid Conduit With Averaged Quantities at Each End

This form is

$$\bar{V}_2 = \bar{V}_1 \cosh \Gamma - \frac{\bar{P}_1}{Z_c} \sinh \Gamma \quad (4.21)$$

and

$$\bar{P}_2 = \bar{P}_1 \cosh \Gamma - Z_c \bar{V}_1 \sinh \Gamma. \quad (4.22)$$

The quantity Γ appearing in Equations (4.21) and (4.22) is related to Υ by

$$\Gamma = \Upsilon L$$

and is often called the propagation operator. In Chapter II, it was noted that Υ , the propagation constant, consists of a real part and an imaginary part, or

$$\Upsilon = \Upsilon_r + i\Upsilon_c.$$

Therefore,

$$\Gamma = \Gamma_r + i\Gamma_c.$$

Figure 4.6 shows the variation of Γ_r , the spatial attenuation, with axial frequency number ($\omega L/c_0$) for various values of the axial damping number ($\nu L/c_0 r_0$). Figure 4.7 shows the variation of dimensionless phase velocity (c/c_0) with axial frequency number.

Notice that when working with a single fluid conduit, Equations (4.21) and (4.22) show that by specifying any two variables, one can find the response of a third in terms of the fourth variable. This means, for example, that if one specifies the impedance at one end (specify \bar{P} and \bar{V} for that end), then the response of \bar{P} to \bar{V} or \bar{V} to \bar{P} for the other end can be found. Further discussion of the use of transfer equations was given in Chapter II. Notice also that Equations (4.21) and (4.22) are of identical form to those reported by several previous investigators. In general, the zeroth mode transfer equations will always be of this same form, only the value of the propagation

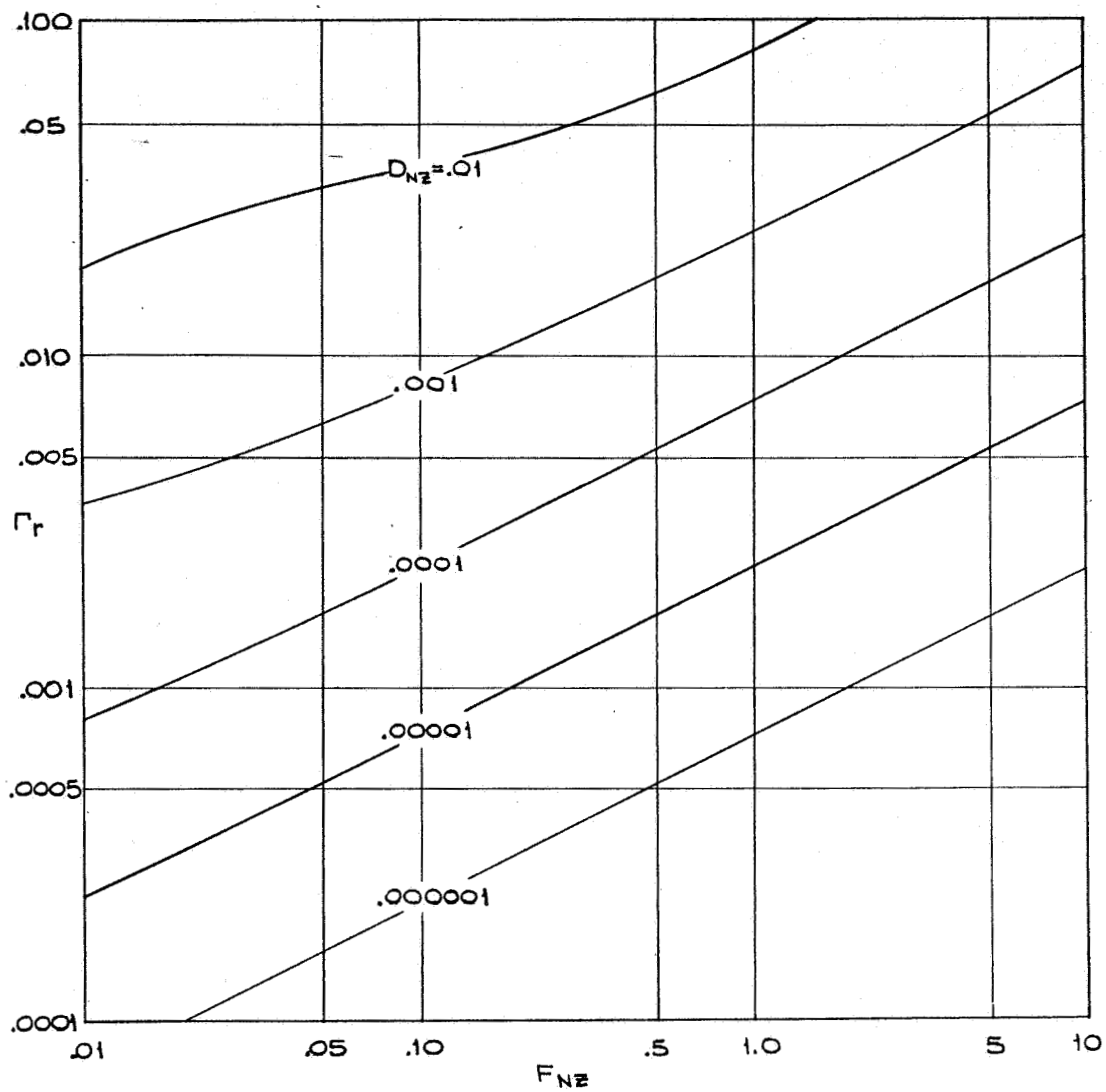


Figure 4.6. Variation of the Zeroth Mode Spatial Attenuation Factor With Axial Frequency Number

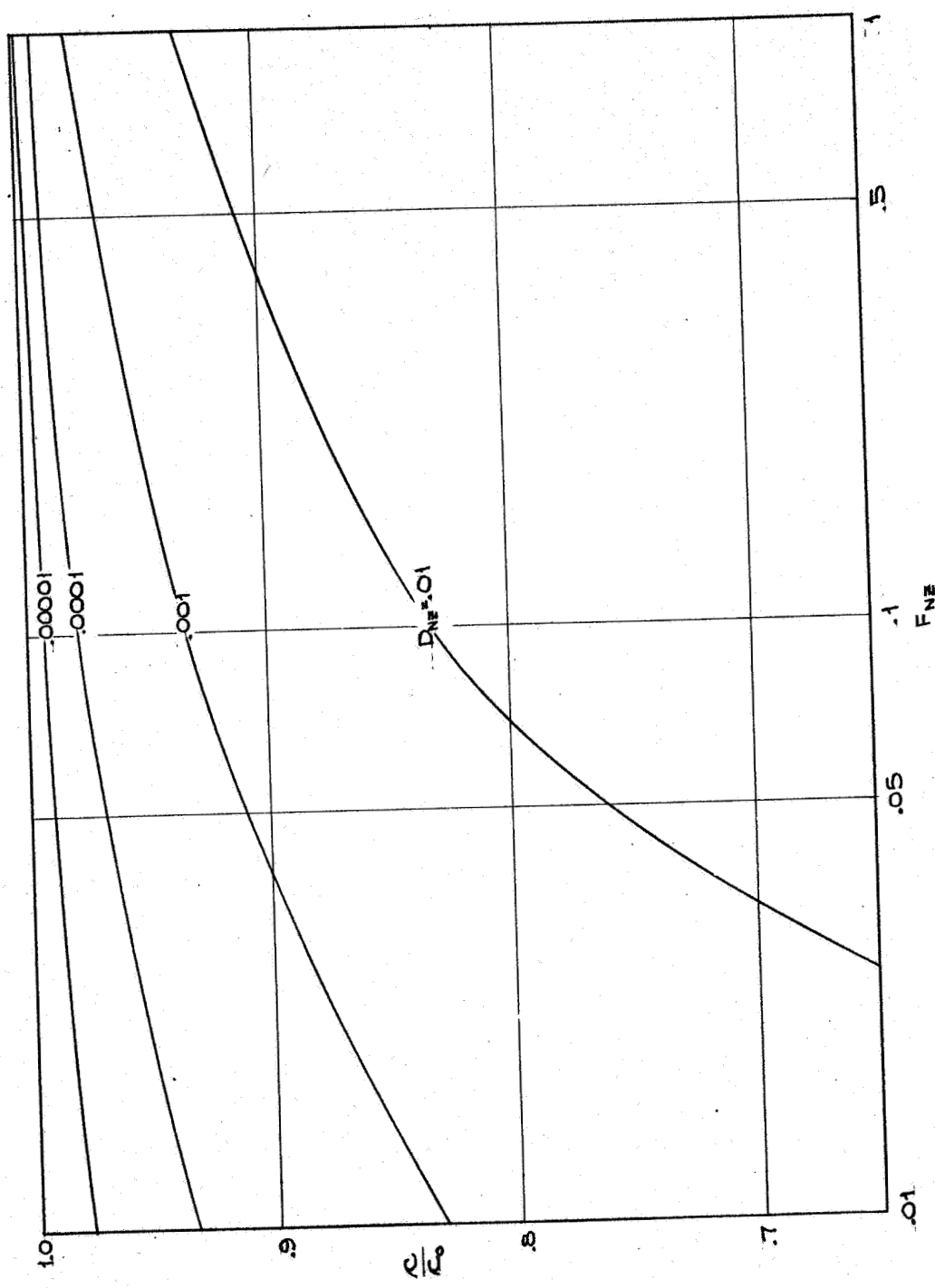


Figure 4.7. Dimensionless Phase Velocity, c/c_0 , Versus Axial Frequency Number for the Zeroth Mode

operator Γ will change, depending upon the original equations of change. These transfer equations have been presented by many previous workers and, thus, are not an original contribution of the writer. They have been derived in this section for the sake of giving a greater degree of completeness to this chapter.

Zeroth Mode Frequency Response

In this section, the frequency response of a fluid conduit with two types of terminations will be examined. The first will be for a termination impedance which is equal to the characteristic impedance of the line. The second will be for a zero termination impedance.

Consider a fluid conduit as shown in Figure 4.5. Rearranging Equations (4.21) and (4.22), they may be written in an impedance form which gives the impedance of end 1 in terms of the terminal end impedance, thus

$$\bar{Z}_1 = \frac{Z_2 \cosh \Gamma + Z_c \sinh \Gamma}{\cosh \Gamma + (Z_2/Z_c) \sinh \Gamma} \quad (4.23)$$

where $\bar{Z}_1 = \bar{P}_1/\bar{V}_1$.

Specifying the special case of a termination impedance equal to the line characteristic impedance yields

$$\bar{Z}_1 = Z_c = \frac{\rho_0 c_0^2 \gamma}{S} \quad (4.24)$$

which means that the impedance looking into end 1 will be the same as the line characteristic impedance. Figures 4.8 and 4.9 show the amplitude and phase of Z_c versus axial frequency number, $F_{nz} = \omega L/c_0$, with

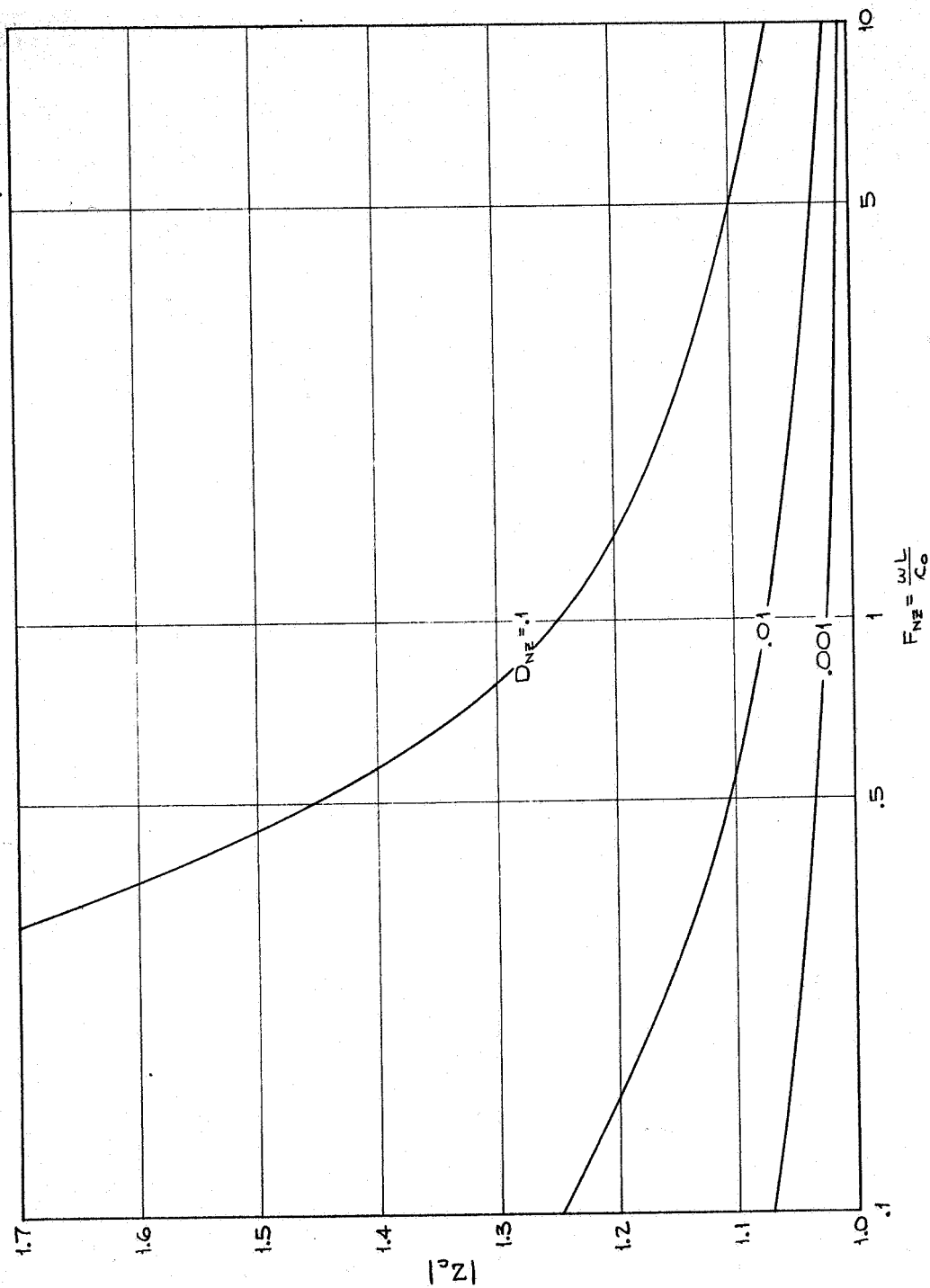


Figure 4.8. Amplitude of the Zeroth Mode Characteristic Impedance Versus Axial Frequency Number

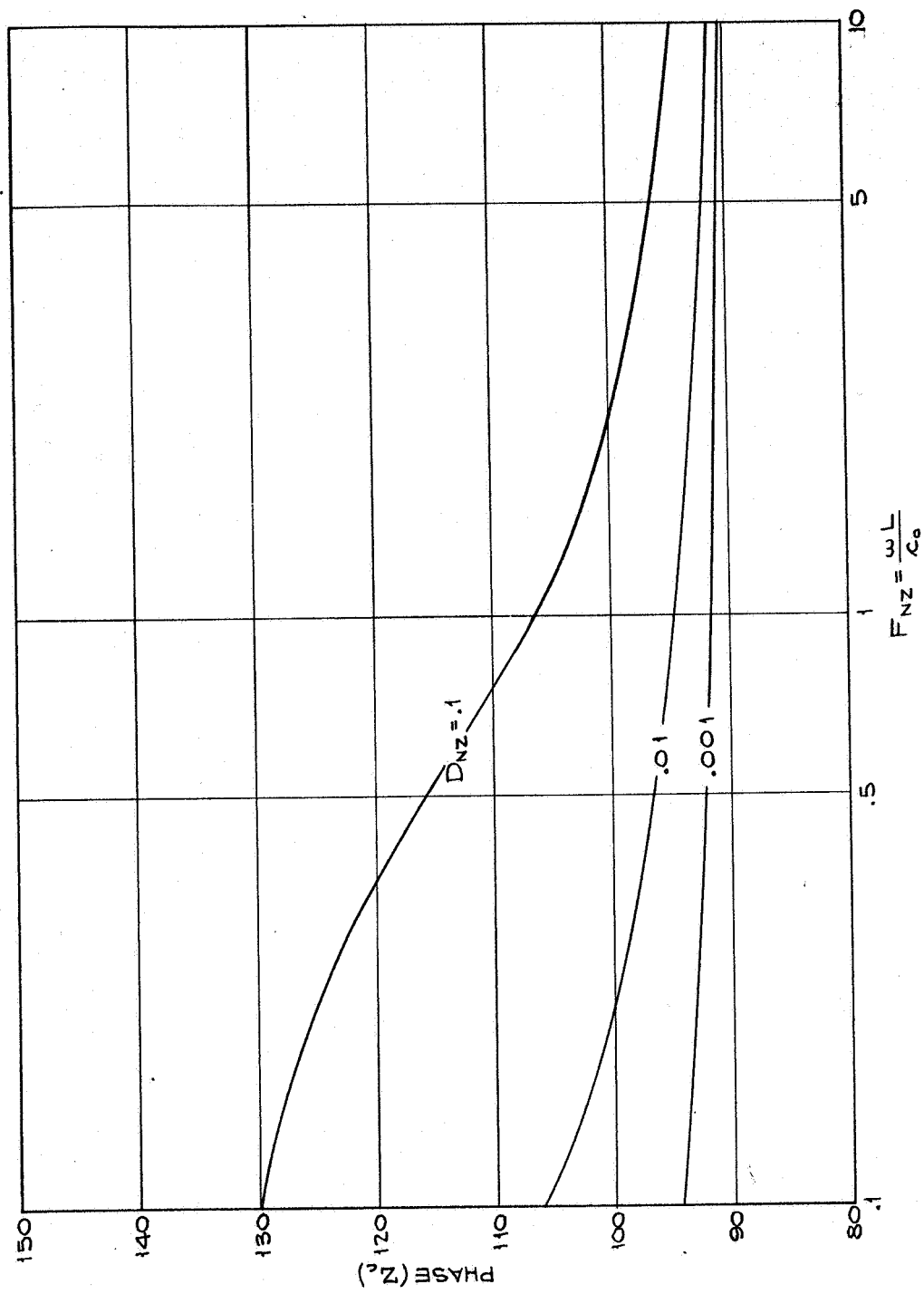


Figure 4.9. Phase of the Zeroth Mode Characteristic Impedance Versus Axial Frequency Number

the axial damping number, $D_{nz} = \nu L / c_0 r_0^2$, as a parameter. This was computed from Equations (4.24) and (4.7). Notice that the amplitude for this case is a simple monotonically decreasing function with frequency number. There are no resonant conditions. If one specifies any termination impedance other than $Z_2 = Z_c$, then there will occur resonant frequencies for the impedance looking into end 1.

As a particular example of a termination impedance other than Z_c , consider the case where $Z_2 = 0$. For this case,

$$\bar{Z}_1 = Z_c \tanh \Gamma. \quad (4.25)$$

The amplitude of $\bar{Z}_1 = [p^{(t)} / \rho_0 c_0 V_0]$ for this case is plotted in Figure 4.10 as a function of axial frequency number for various values of the axial damping number. Notice the influence of the damping number. As damping number increases, the resonant frequencies decrease. Also notice that, for a given damping number, the damping effect increases with frequency as evidenced by a decrease in resonant amplitude with each successively higher resonant frequency. This effect might also have been predicted from Figure 4.6 which shows increasing attenuation with increase in the frequency.

Zeroth Mode Transient Response

In the previous section, a study was made of the application of the zeroth-mode transfer equations to the frequency response of a fluid conduit with two types of terminal impedances and some important implications were noted. Perhaps more practical or informative type of responses to study from an engineering point of view are the time

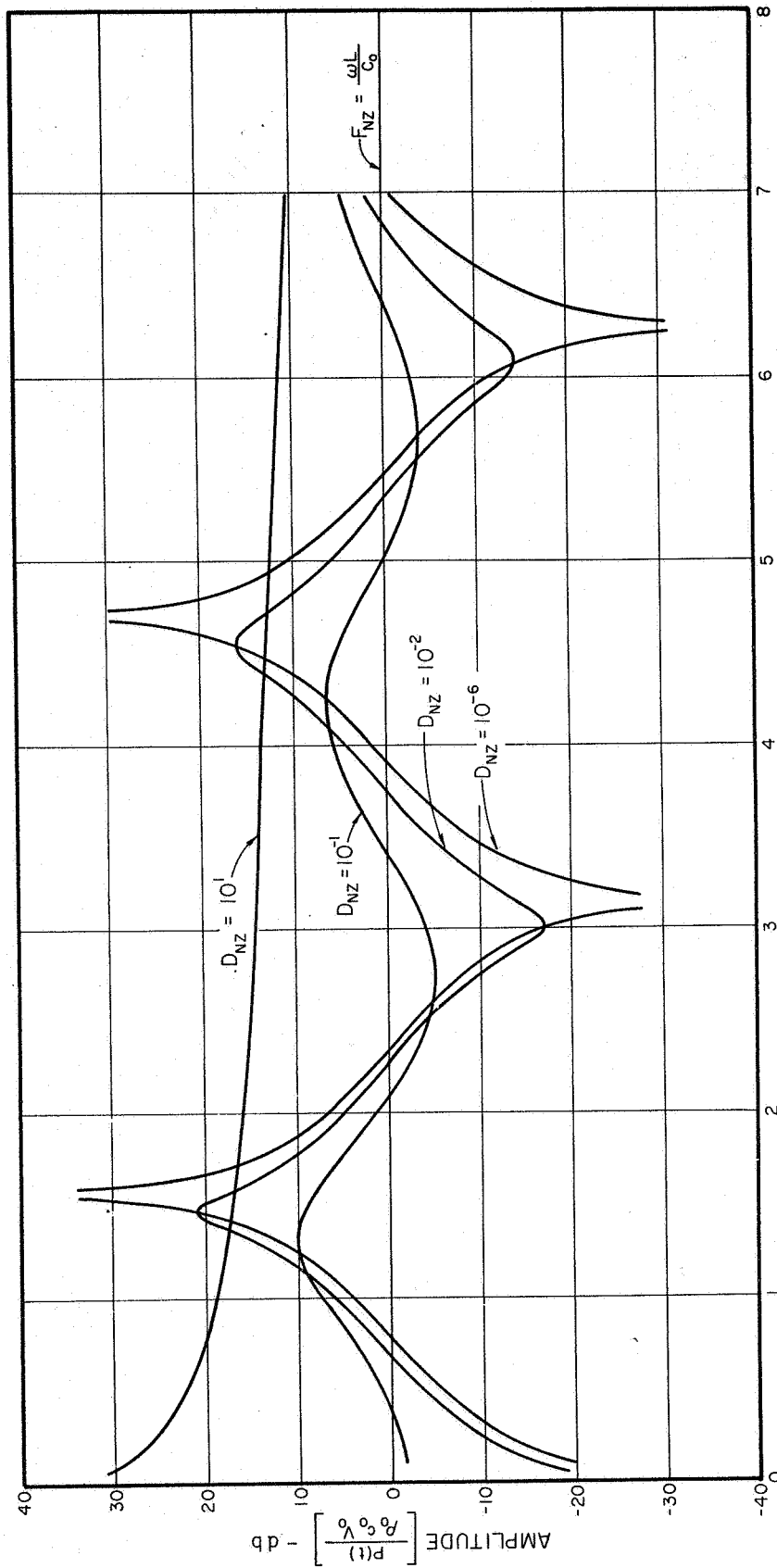


Figure 4.10. Amplitude of \bar{Z}_T from Equation (4.25) for the Case of Zero Termination Impedance

domain transients. The major problem, in this regard, is that the actual calculation of time domain transients are much more difficult than frequency type responses. In this section, the time domain responses of a fluid line with the same two types of terminal impedances as examined in the previous section will be discussed.

It should be emphasized that by specifying the impedance at one end of the line the response of any one variable to any other variable for the line can be determined. This is not obvious from the impedance form obtained in Equation (4.23). Take first the case of a terminal impedance $\bar{Z}_2 = Z_c$. The line equations now become

$$\begin{aligned}\bar{P}_2 &= \bar{P}_1 \cosh \Gamma - Z_c \bar{V}_1 \sinh \Gamma \\ &= \bar{V}_2 Z_c = Z_c \left\{ \bar{V}_1 \cosh \Gamma - \frac{\bar{P}_1}{Z_c} \sinh \Gamma \right\}.\end{aligned}\quad (4.26)$$

Examination of Equation (4.26) will reveal that it is now possible, because of having specified the impedance at one end of the line, to obtain the response of \bar{P}_1 to \bar{V}_j , \bar{P}_1 to \bar{P}_j , \bar{V}_1 to \bar{V}_j or \bar{V}_1 to \bar{P}_j . The time responses of \bar{V}_1 to \bar{P}_1 and \bar{P}_2 to \bar{P}_1 for impulses of P_1 will now be discussed. From Equation (4.26)

$$\bar{V}_1 = \frac{\bar{P}_1}{Z_c}$$

and

$$\bar{P}_2 = \bar{P}_1 e^{-\Gamma}$$

are the response equations. Letting \bar{P}_1 be an impulse

$$\bar{V}_1(s) = \frac{1}{Z_c(s)} \quad (4.27)$$

and

$$\bar{P}_2(s) = e^{-\Gamma(s)} \quad (4.28)$$

To obtain the time domain responses, use is made of the inverse Laplace transformation, or

$$f(t) = \frac{1}{2\pi i} \int_{c-i\infty}^{c+i\infty} F(s) e^{st} ds. \quad (4.29)$$

From Equations (4.27), (4.28), and (4.29)

$$\bar{V}_1(t) = \frac{1}{2\pi i} \int_{c-i\infty}^{c+i\infty} \frac{e^{st}}{Z_c(s)} ds \quad (4.30)$$

and

$$\bar{P}_2(t) = \frac{1}{2\pi i} \int_{c-i\infty}^{c+i\infty} e^{st - F(s)} ds. \quad (4.31)$$

The actual inversion of these equations is rather involved because of mathematical difficulties. F. T. Brown has done an extensive amount of work in the calculation of fluid line impulsive responses along lines similar to those indicated by Equations (4.30) and (4.31) making the numerical evaluation of these equations by the writer superfluous.

Proceeding now to the case for which the terminal impedance is zero, the equations become

$$\bar{P}_1 \cosh \Gamma - Z_c \bar{V}_1 \sinh \Gamma = 0$$

and

$$\bar{V}_2 = \bar{V}_1 \cosh \Gamma - \frac{\bar{P}_1}{Z_c} \sinh \Gamma.$$

It may be readily seen that one can now find the response of any one variable to any other. This is again due to having specified the impedance at one end of the line. For the purposes of this example, the response of \bar{P}_1 to a unit step in \bar{V}_1 will be calculated. Thus, putting $\bar{V}_1 = 1/s$,

$$\bar{P} = Z_c \tanh \Gamma \cdot \bar{V}_1 = \frac{Z_c \tanh \Gamma}{s} \quad (4.32)$$

or, in the time domain

$$P(t) = \frac{1}{2\pi i} \int_{c-i\infty}^{c+i\infty} \frac{Z_c(s)}{s} \tanh \Gamma(s) e^{st} ds. \quad (4.33)$$

Evaluation of Equation (4.33) has been performed by a summation of the residues as described in Appendix B. The results are plotted in Figures 4.11, 4.12, 4.13 and depict the pressure history typical of water hammer for three values of the damping number. These figures clearly show the dispersive and dissipative effects which viscosity has upon the temporal response of a fluid line. The dissipation results in the attenuation of all frequency components with greater attenuation of the higher frequency being evidenced by the fact that principally the fundamental frequency remains after some finite number of oscillations. Dispersion results in the "tailing off" effect for each oscillation due to the faster traveling high frequency terms.

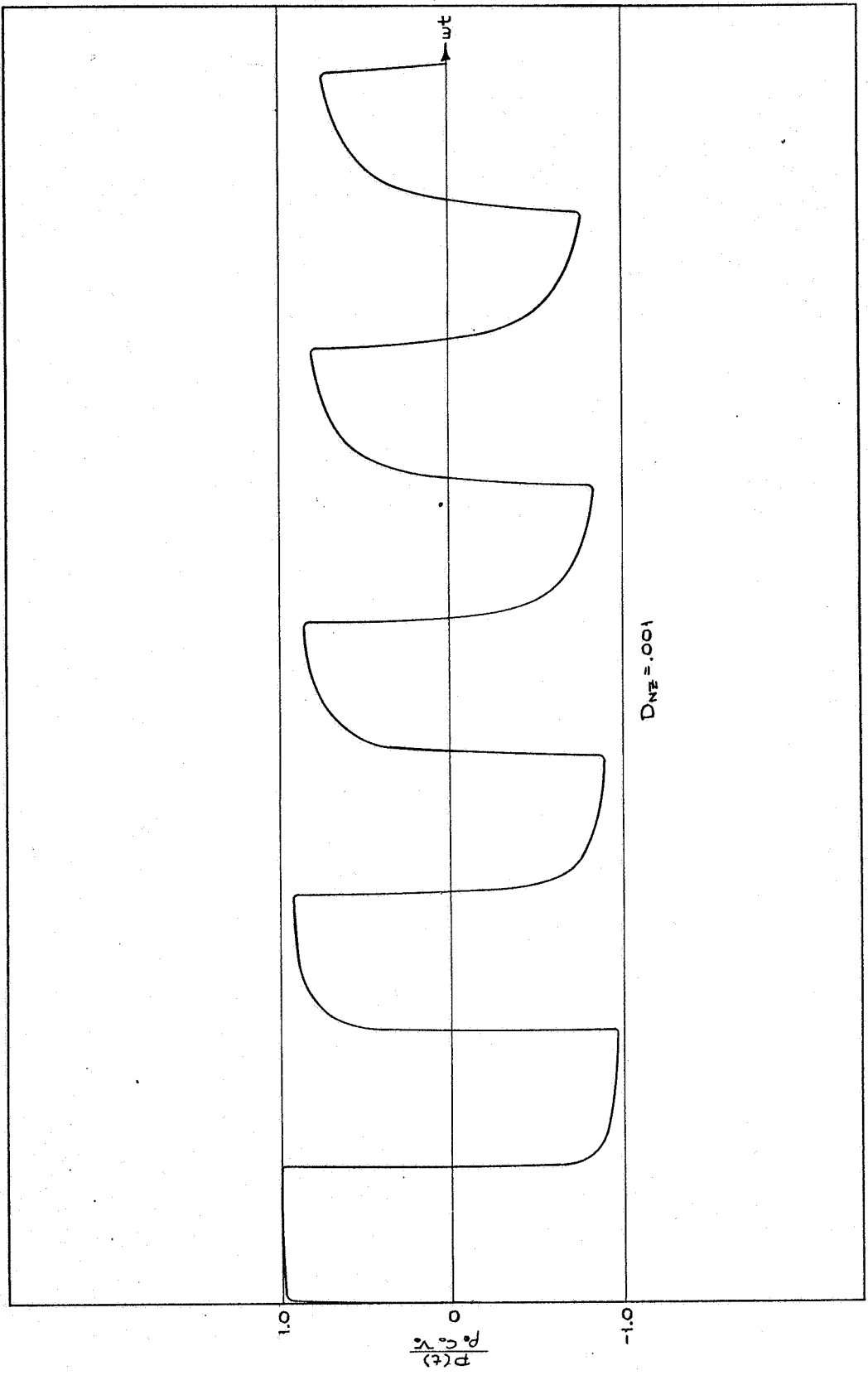


Figure 4.11. Water Hammer Pressure History From Equation (4.33), Axial Damping Number 0.001

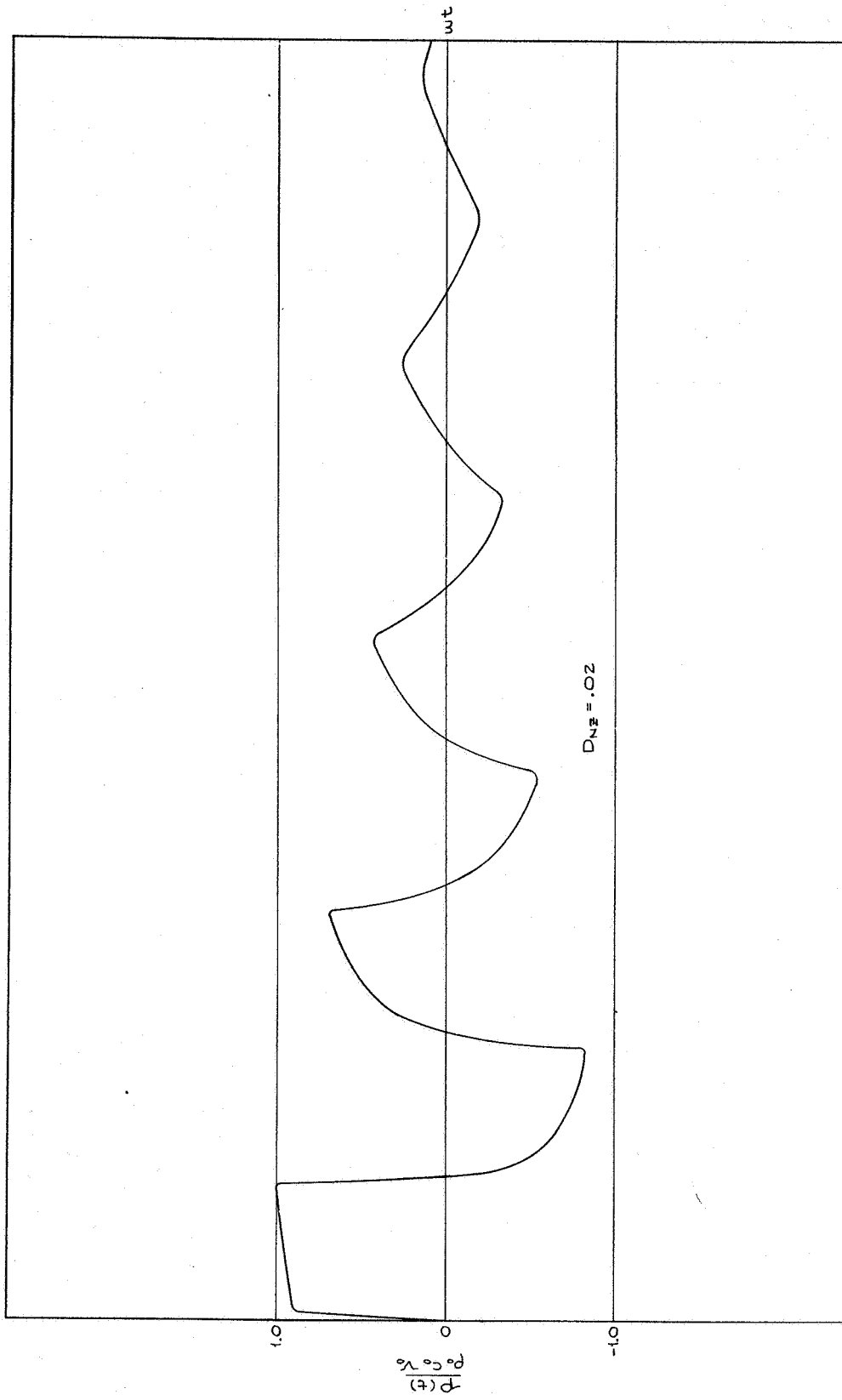


Figure 4.12. Water Hammer Pressure History From Equation (4.33),
Axial Damping Number 0.02

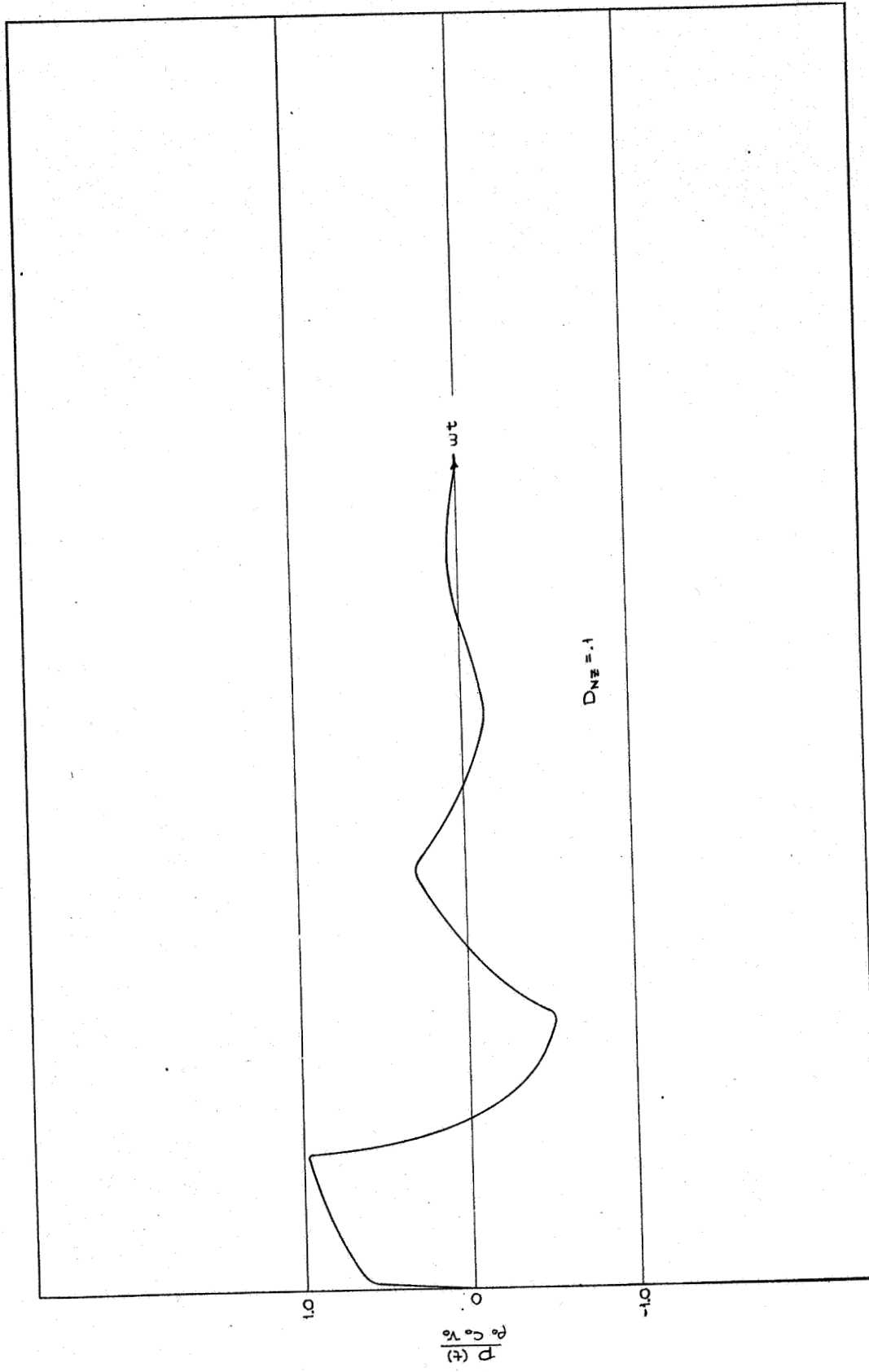


Figure 4.13. Water Hammer Pressure History From Equation (4.33),
Axial Damping Number 0.1

CHAPTER V

EXPERIMENTAL VERIFICATION OF ZEROETH MODE TRANSFER EQUATIONS

Introduction

To determine the validity of the transfer equations developed in the previous chapter for the zeroth mode, an experimental study was designed and conducted. The experimental models were chosen on the basis of having the greatest possible control of the accuracy of the variables concerned. Both frequency response and transient responses were studied.

Experimental Frequency Response

To experimentally verify the zeroth mode transfer equations from a frequency response standpoint, the apparatus schematically shown in Figure 5.1 was constructed. With this apparatus, the impedance at the reservoir end was maintained at zero. Because of the piston driver at the other end, the velocity there could be varied in a sinusoidal manner at frequencies from 0 to about 100 cps. Since the piston amplitude and driver oscillation frequency were accurately controllable, the velocity of the fluid at the driver end was therefore precisely known. By positioning a pressure transducer near the piston, the impedance amplitude at the driver end could then be obtained from recorded values of

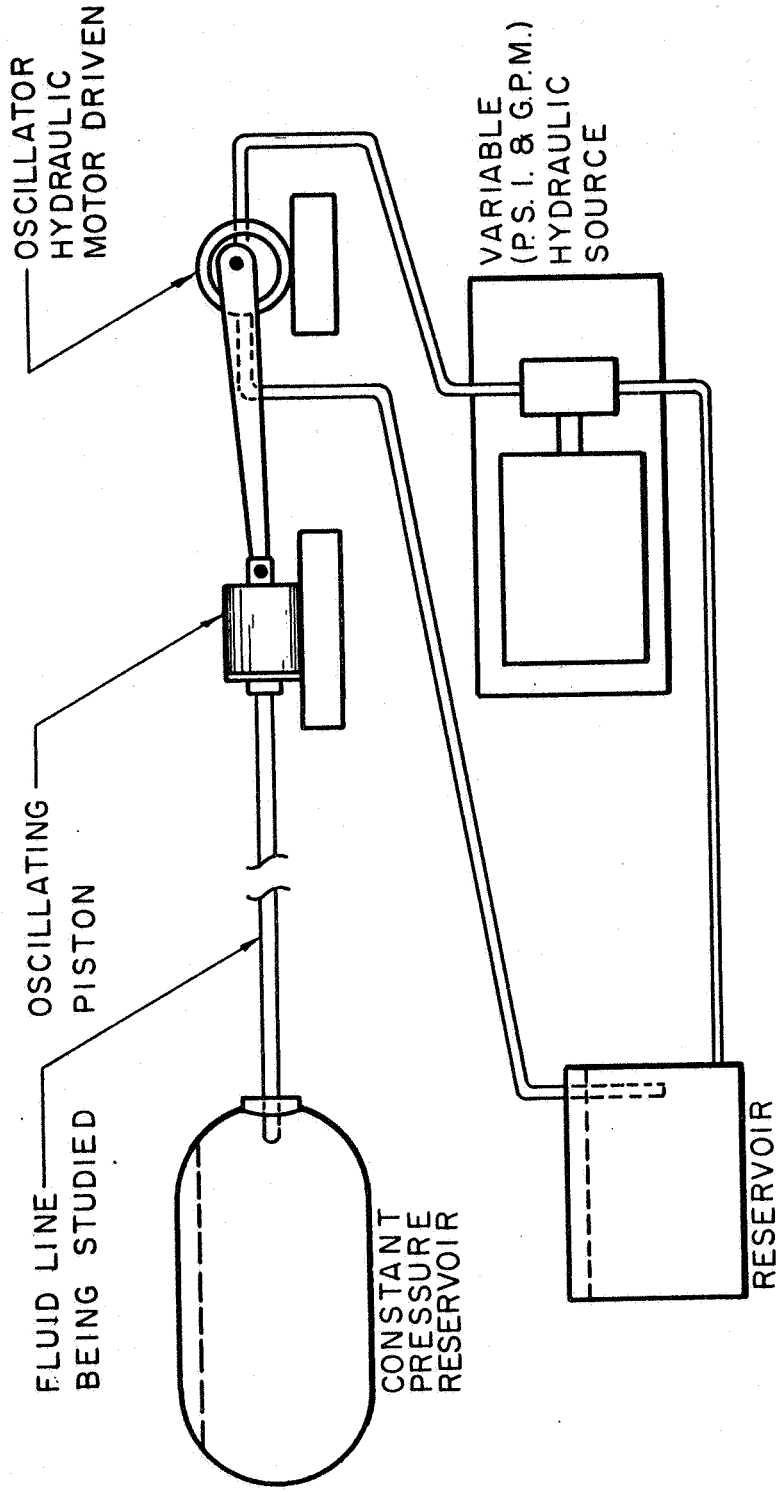


Figure 5.1. Experimental Model for Studying the Frequency Response of a Fluid Line

pressure and velocity amplitudes by simply taking their ratio.

Figures 5.2 and 5.3 display results of experiments performed with the above described apparatus. These figures also show the corresponding theoretical predictions of the zeroth mode transfer equations which, for this case, reduce to Equation (4.25). Note the excellent agreement between the experimental results and the theoretical predictions of the zeroth mode equations. This fine agreement substantiates the validity of the zeroth mode transfer equations for the range of parameters given.

Experimental Transient Response

To examine the validity of the zeroth mode equations from a time domain point of view, an experimental model has been chosen which represents the conditions of the classical water-hammer problem. Figure 5.4 shows the physical layout of this model. It consists of a line with a constant pressure source at one end and a fast acting valve at the other end. With the valve initially open, fluid flows from the reservoir through the line, valve and flow meter into a second reservoir. When the valve is suddenly closed, the transducer located at the valve can be used to monitor the pressure response to the step change in flow resulting from the valve closure.

Figure 5.5 displays typical experimental pressure traces resulting from sudden valve closure with the above described apparatus. Comparison of these results with the theoretical predictions of Figure 4.11 demonstrates, as for the frequency response case, an excellent agreement between theory and experiment. This further substantiates the validity of the zeroth mode transfer equations developed in Chapter IV.

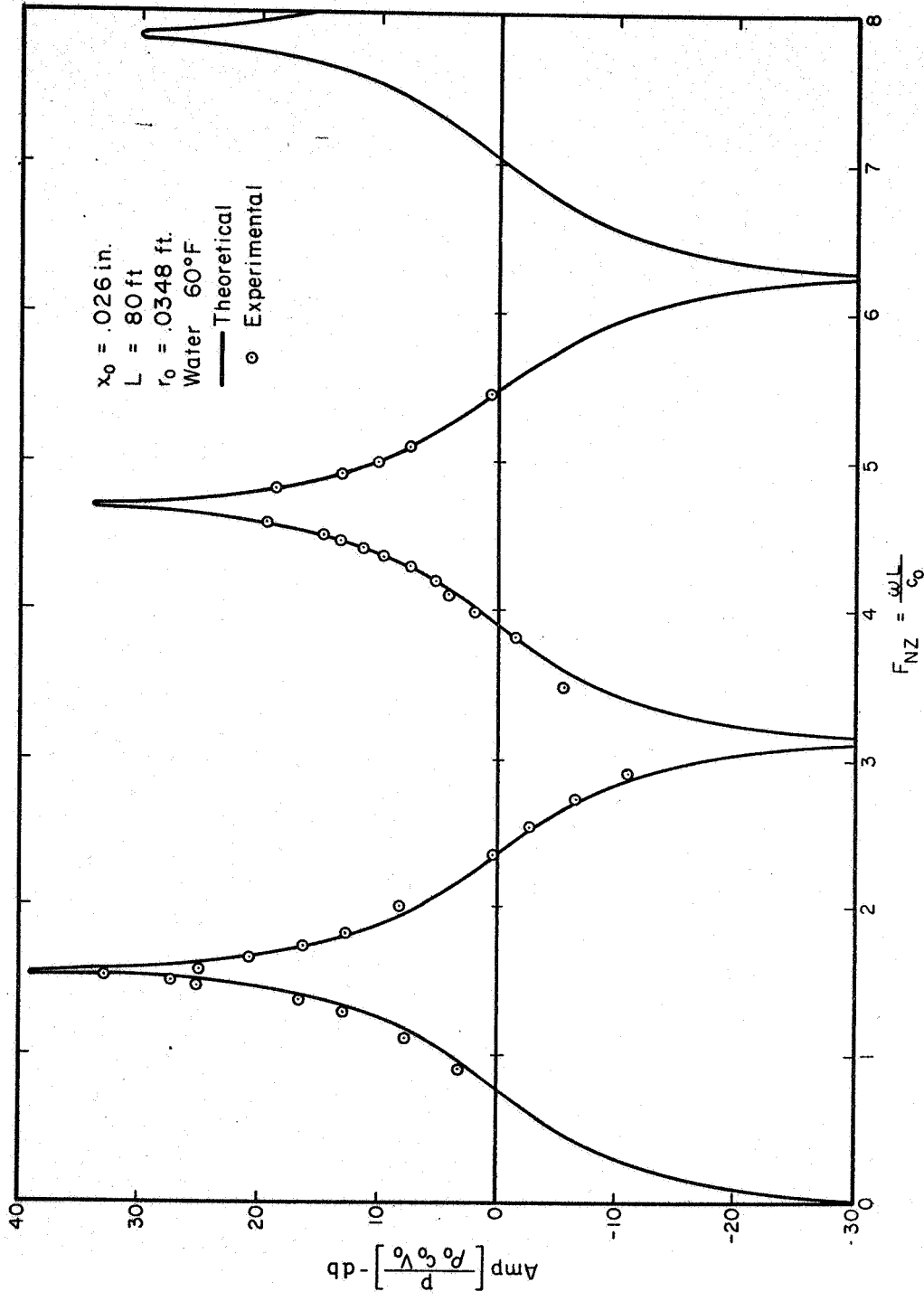


Figure 5.2. Experimental Amplitude, $\left[\frac{p}{\rho_0 c_0 V_0} \right]$, Obtained From the Frequency Analysis of an 80 Foot Line With Water as the Working Fluid

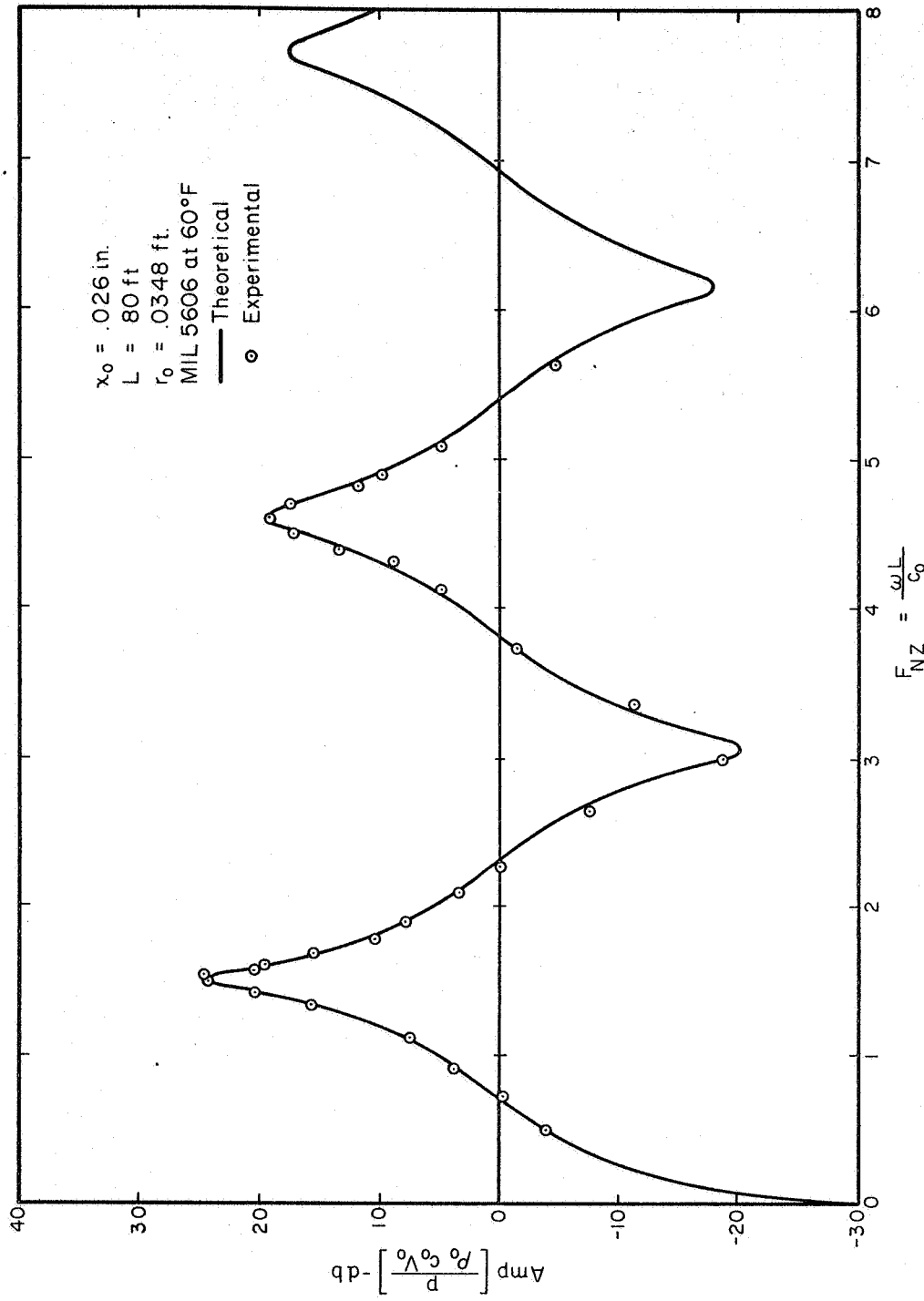


Figure 5.3. Experimental Amplitude, $[\frac{p}{\rho c_0 V_0}]$, Obtained From the Frequency Analysis of an 80 Foot Line With MIL 5606 as the Working Fluid

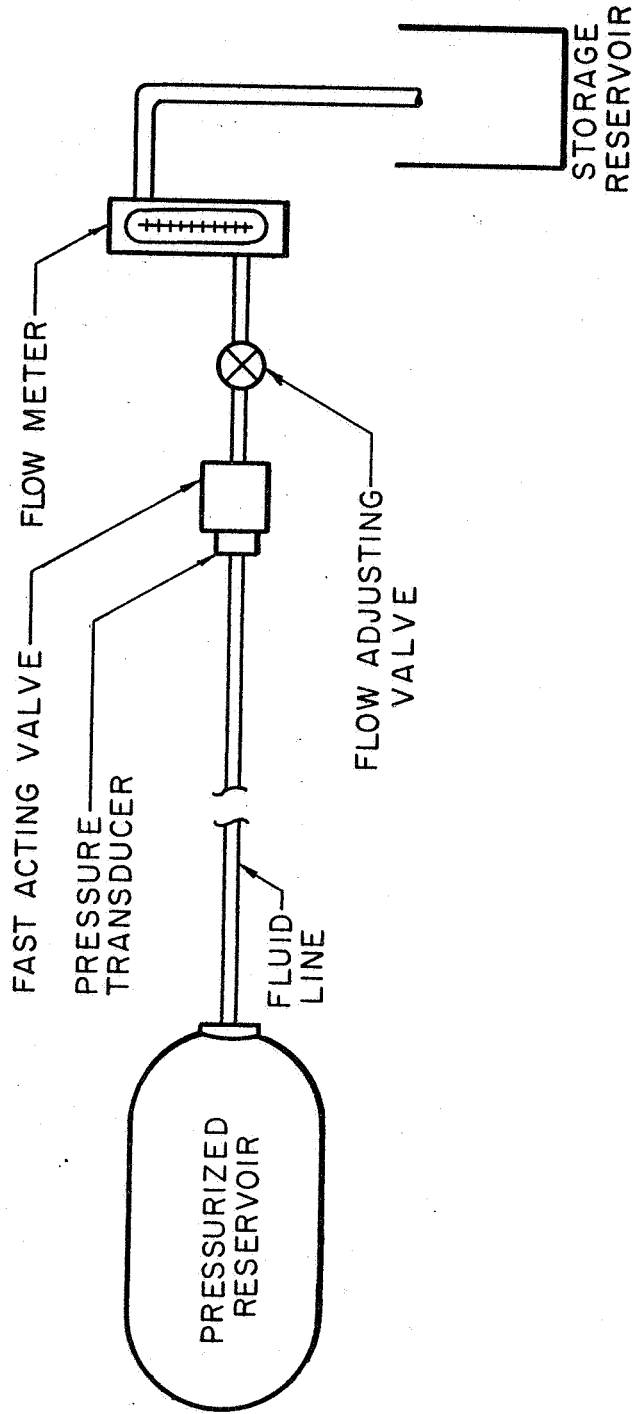


Figure 5.4. Experimental Model for Studying the Transient Response

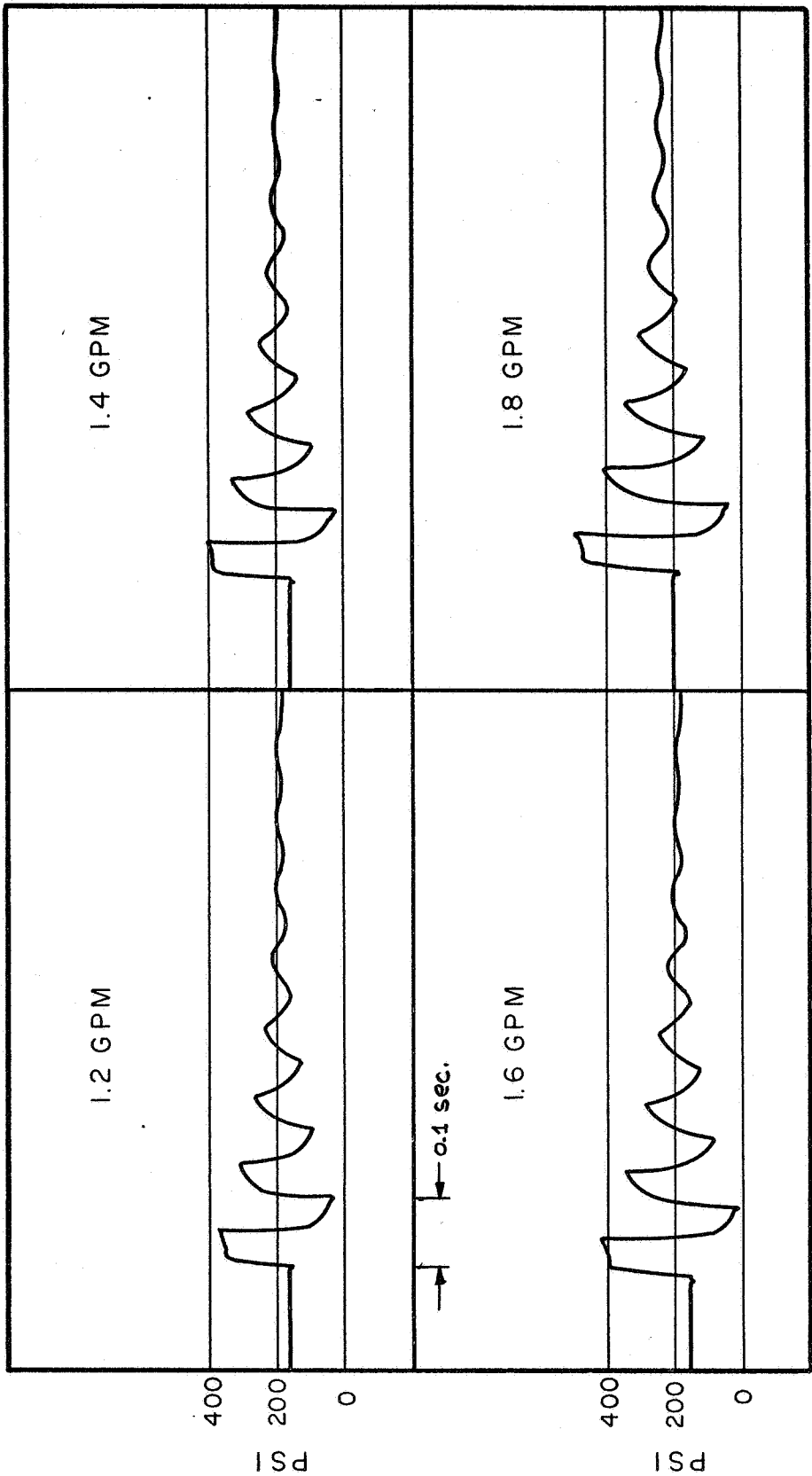


Figure 5.5. Typical Pressure History Traces Obtained From the Model of Figure 5.4

As a result of the excellent agreement between theoretical and experimental results, it may be concluded that the zeroth mode transfer equations are a good model in the range of parameters of the tests conducted. In terms of damping numbers and frequency numbers, the range for these tests was

$$0.0001 < D_{nz} < 0.02$$

$$0.5 < F_{nz} < 10.0.$$

CHAPTER VI

THE HIGHER MODES OF VISCOUS PROPAGATION

Introduction

In Chapter IV, it was found that the application of the condition of zero fluid velocity at the wall of a rigid conduit led to a set of equations relating the parameters β , k , and γ . Solution of these equations yielded an infinite set of the eigenvalues with each set corresponding to a mode of propagation. The general expressions for the transformed velocities and pressure were given by Equations (3.34), (3.35), and (3.36) and consisted of an infinite summation of all the modes. The purpose of this chapter is to delve more completely into the mathematics and physical meaning of these modes.

Discussions of higher modes of propagation of acoustic type waves are extensive in the literature (e.g., 26, 27, 31); however, these all deal with waves where viscosity has been neglected. In this chapter, viscous propagation will be discussed.

Higher Mode Eigenvalues for Rigid Conduit

The characteristic equations for the eigenvalues of a rigid fluid-filled conduit were demonstrated in Chapter IV to be

$$k_n \beta_n \frac{J_1(\beta_n r_0)}{J_0(\beta_n r_0)} = \gamma_n^2 \frac{J_1(k_n r_0)}{J_0(k_n r_0)} \quad (6.1)$$

and

$$\gamma_n^2 = k_n^2 + \frac{s}{2\nu} = \beta_n^2 + \frac{s^2}{c_0^2 + \frac{4}{3}\nu s} \quad (6.2)$$

For each set of values of s , ν , c_0 and r_0 , there exists an infinite number of discrete values of the parameters γ_n , k_n , and β_n , hence, eigenvalues. Each family of numbers, represented by a value for n , corresponds to a mode of fluid motion. The $n = 0$ or zeroth mode was discussed extensively in Chapter IV and found to be of considerable importance in the modeling of a fluid conduit. It was found that the most important of the parameters was γ , the propagation constant, and that

$$\gamma = \gamma_r + i\gamma_c$$

where γ_r represented the spatial attenuation factor and $c = \frac{\omega}{\gamma_c}$ represented the phase velocity of the disturbance. For the higher modes, γ is also important and has the same physical significance.

By use of the procedure described in Appendix A, Equations (6.1) and (6.2) have been solved for the γ 's of three modes. Figure 6.1 shows a plot of $\gamma_r \cdot r_0$ versus the radial frequency number, $\frac{\omega r_0}{c_0}$, for a typical value of the radial damping number, $\frac{\nu}{r_0 c_0}$. Figure 6.2 shows the corresponding dimensionless phase velocity, c/c_0 , for these three modes. Figures 6.3 and 6.4 demonstrate the variation of the real part of γ and c/c_0 with radial damping number for the first mode. It is important to note that a discontinuity occurs in each of the higher mode values of γ . This discontinuity might be termed a cutoff frequency since it separates frequency regions of very high spatial attenuation and very low spatial

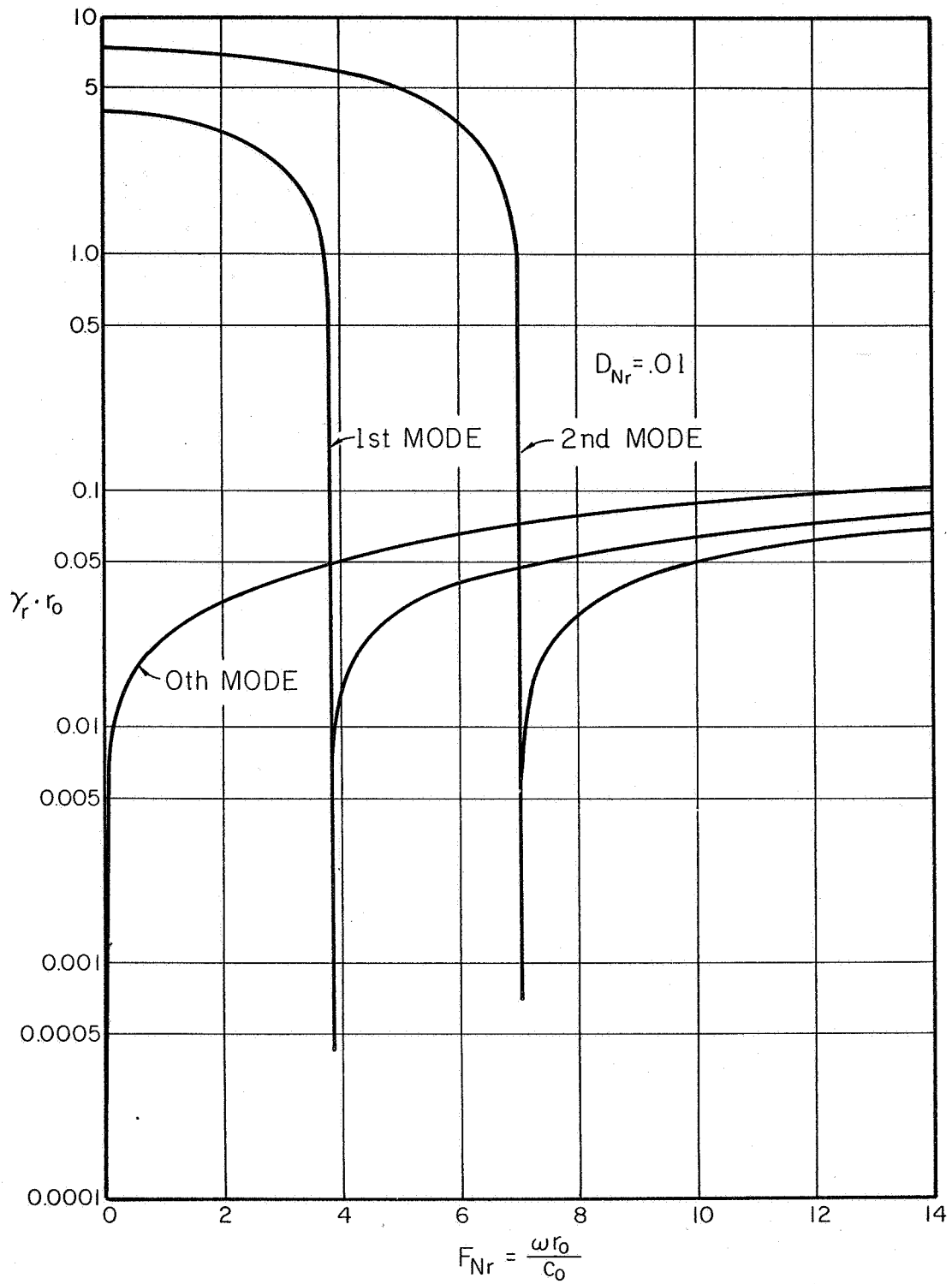


Figure 6.1. Plot of the Spatial Attenuation Factor Versus Radial Frequency Number for Three Modes

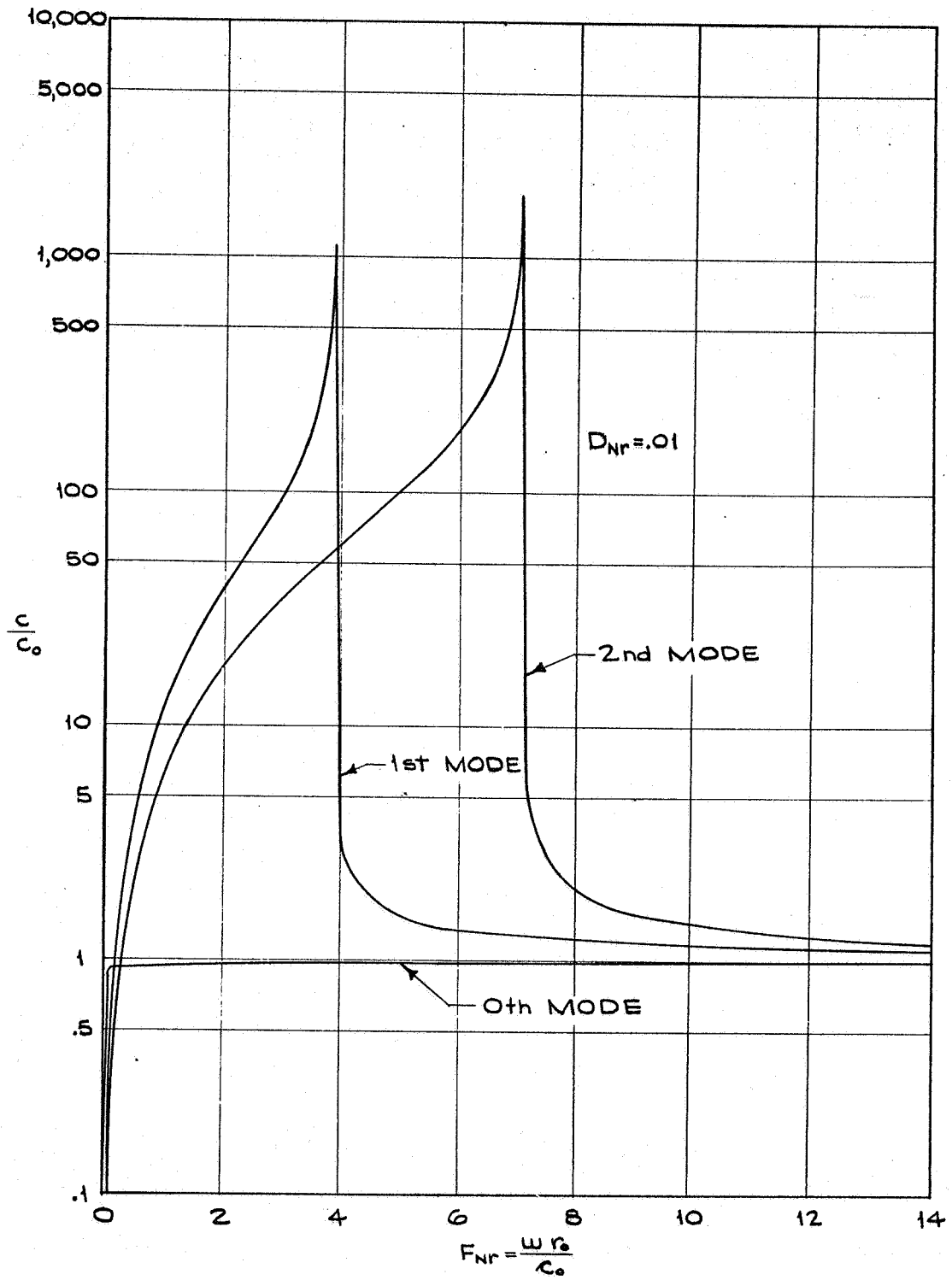


Figure 6.2. Plot of the Dimensionless Phase Velocity Versus Radial Frequency Number for Three Modes

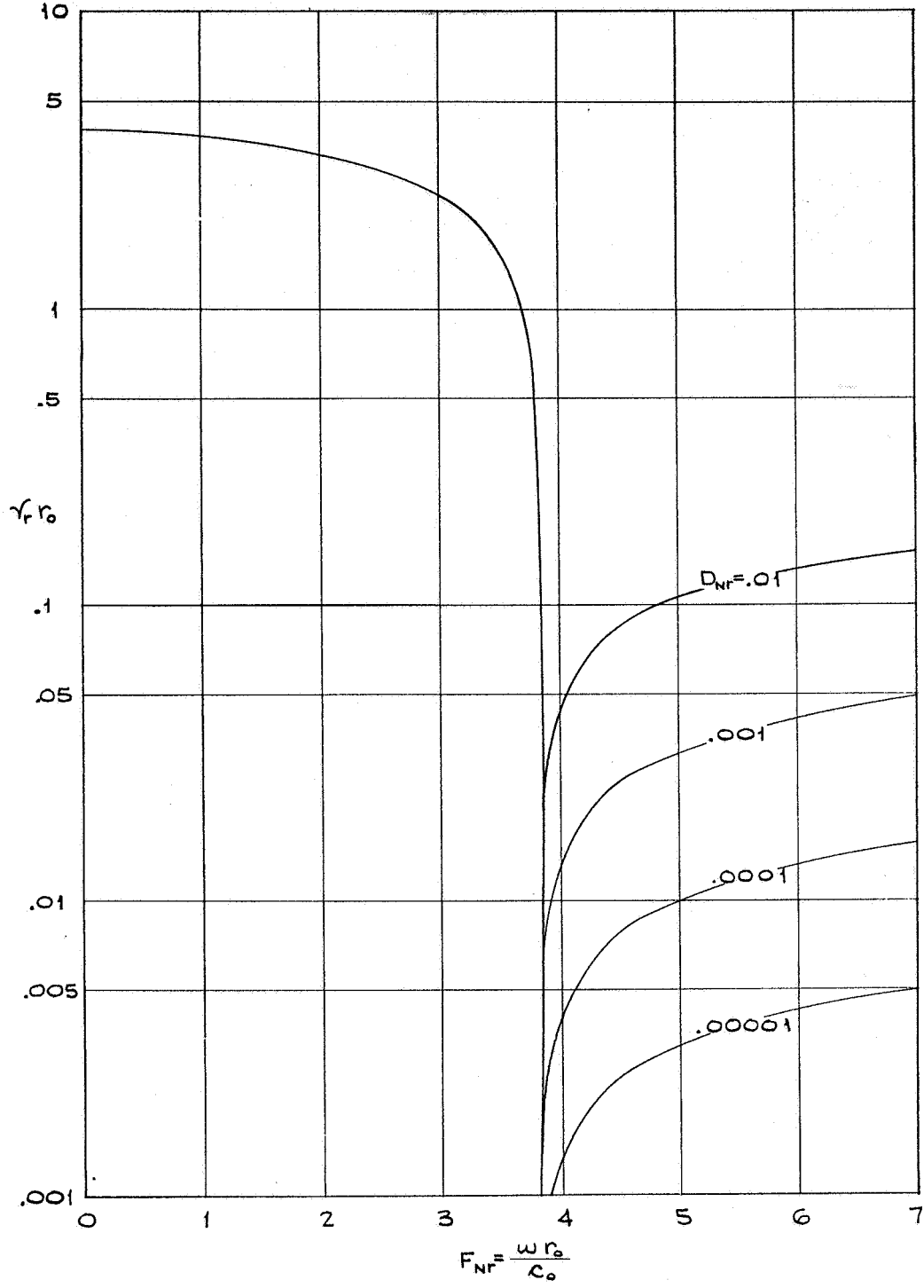


Figure 6.3. Spatial Attenuation Factor γ_{r_0} Versus Radial Frequency Number for the First Mode

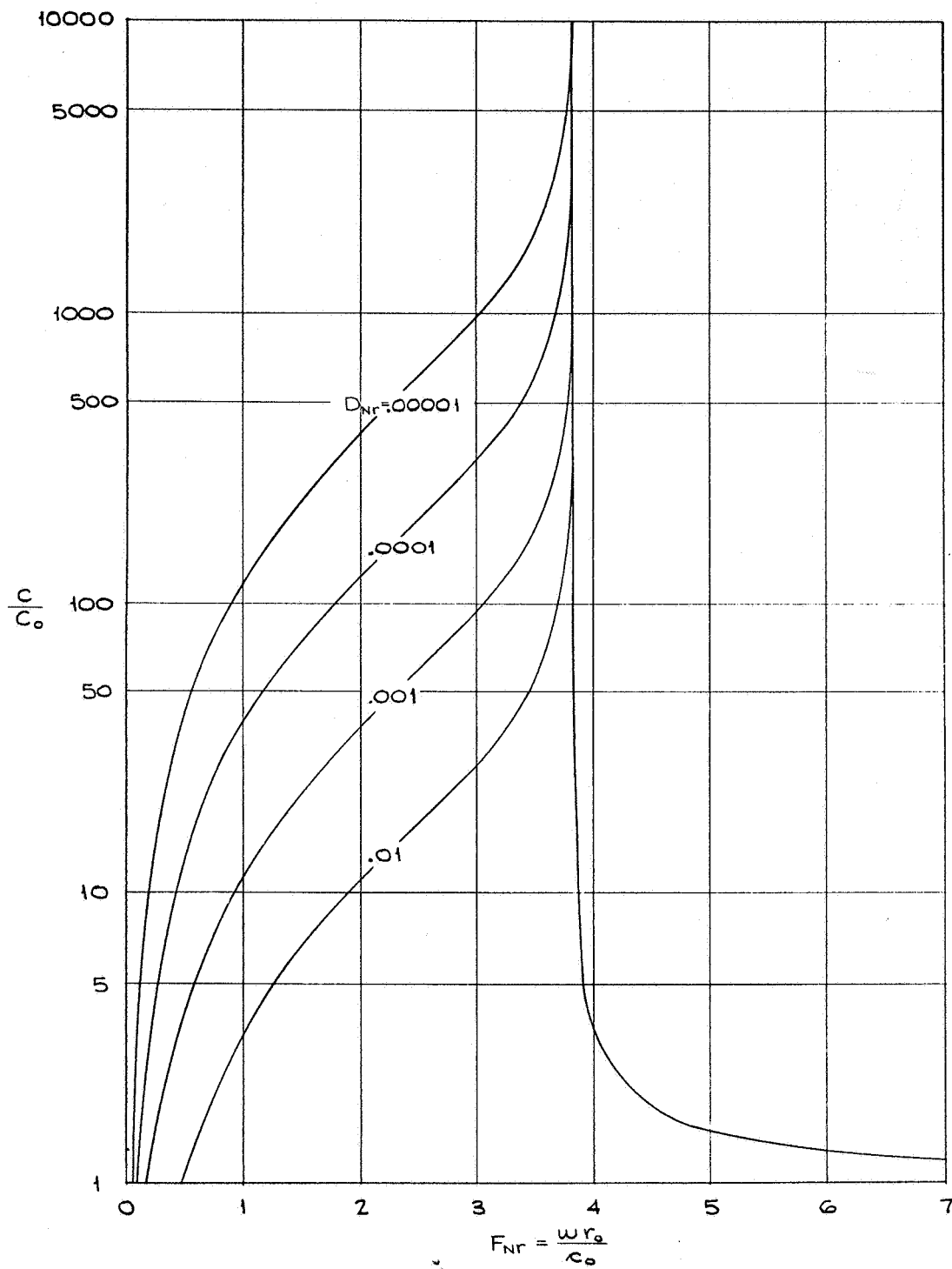


Figure 6.4. Dimensionless Phase Velocity c/c_0 Versus Radial Frequency Number for the First Mode

attenuation. Below this cutoff frequency, the contribution of a particular mode to the over-all disturbance will be damped in a relatively short distance from its point of origin, leaving only the zeroth mode to be propagated any significant distance. This becomes very evident if an example is considered. Take the case of a disturbance in the first mode in a pipe at a radial frequency number of 1.0. From Figure 6.3, it may be seen that the spatial attenuation factor is $\gamma_r r_0 = 3.9$. This means that in a distance of one pipe radius from the source, the disturbance will have decayed by a factor of $e^{-\gamma_r r_0}$ or 0.02. Thus, the disturbance (first mode), in magnitude, had decayed to two per cent of its original value.

It is interesting to contrast the higher mode spatial attenuation and phase velocity for viscous propagation as shown in Figures 6.1 through 6.4 with the corresponding no viscosity case as presented in the literature. For the case of no viscosity, the spatial attenuation for each mode would be zero above the cutoff frequency. The zeroth mode would have zero spatial attenuation for all frequencies. The phase velocity for the case of no viscosity is zero below the cutoff frequency in contrast to a finite value of phase velocity below the cutoff when viscosity is included.

Velocity Profiles

To get a better physical feeling for the higher modes, the axial velocity profiles for the first few modes for a rigid fluid conduit will now be obtained. From Equation (3.35), the general expression for the axial velocity in the Laplace domain was found to be

$$V_{1z} = \sum_n \left\{ B_n \gamma_n J_0(\beta_n r) + A_n k_n J_0(k_n r) \right\} e^{\gamma_n z} \quad (3.35)$$

The condition of zero axial velocity at the wall yields the equation

$$B_n \gamma_n J_0(\beta_n r_0) + A_n k_n J_0(k_n r_0) = 0$$

which along with Equation (3.35), gives

$$\begin{aligned} V_{1z} &= \sum_n B_n \gamma_n J_0(\beta_n r_0) \left\{ \frac{J_0(\beta_n r)}{J_0(\beta_n r_0)} - \frac{J_0(k_n r)}{J_0(k_n r_0)} \right\} e^{\gamma_n z} \\ &= \sum_n B_n \gamma_n J_0(\beta_n r_0) F_{zn}(r) e^{\gamma_n z} \end{aligned} \quad (6.3)$$

The function $F_{zn}(r)$ will be called the axial velocity profile function for the n^{th} mode. For a given damping number and frequency number, this profile function may be calculated for each mode as a function of r . In general, $F_{zn}(r)$ is complex, having both real and imaginary parts. This function has been calculated for four modes (0, 1, 2, and 3) for various combinations of frequency number and damping number. Figures 6.5, 6.6, and 6.7 display the results of these calculations. Note that the higher modes (1, 2, and 3) retain the same general shape for the various combinations of frequency number and damping number. The zeroth mode profile, on the other hand, has a shape which is highly dependent upon these two parameters.

Series Expansion

Thus far all efforts have been concentrated on satisfying the

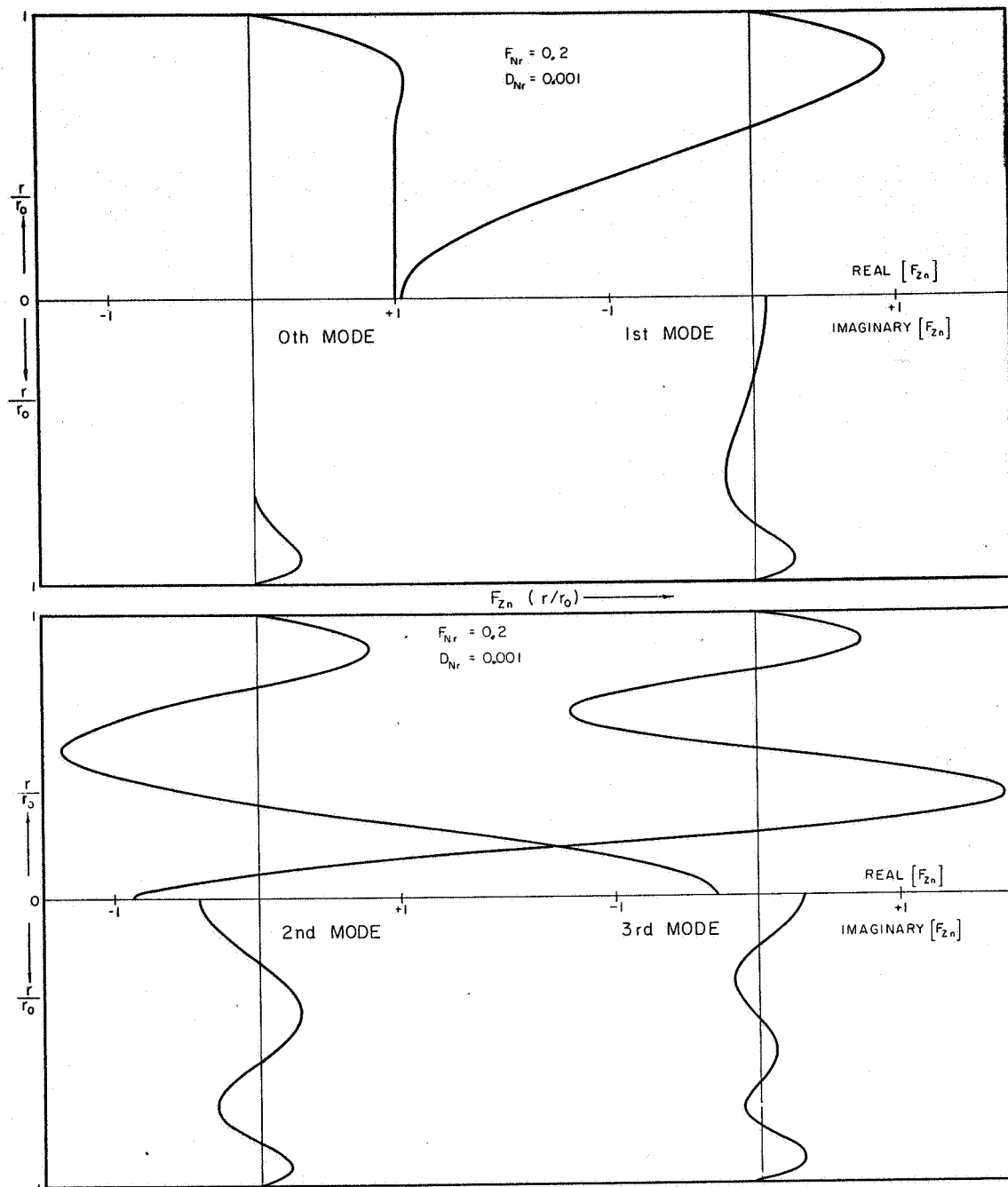


Figure 6.5. Axial Velocity Profile Function, $F_{zn}(r)$, for Four Modes ($F_{Nr} = 0.2$, $D_{Nr} = 0.001$).

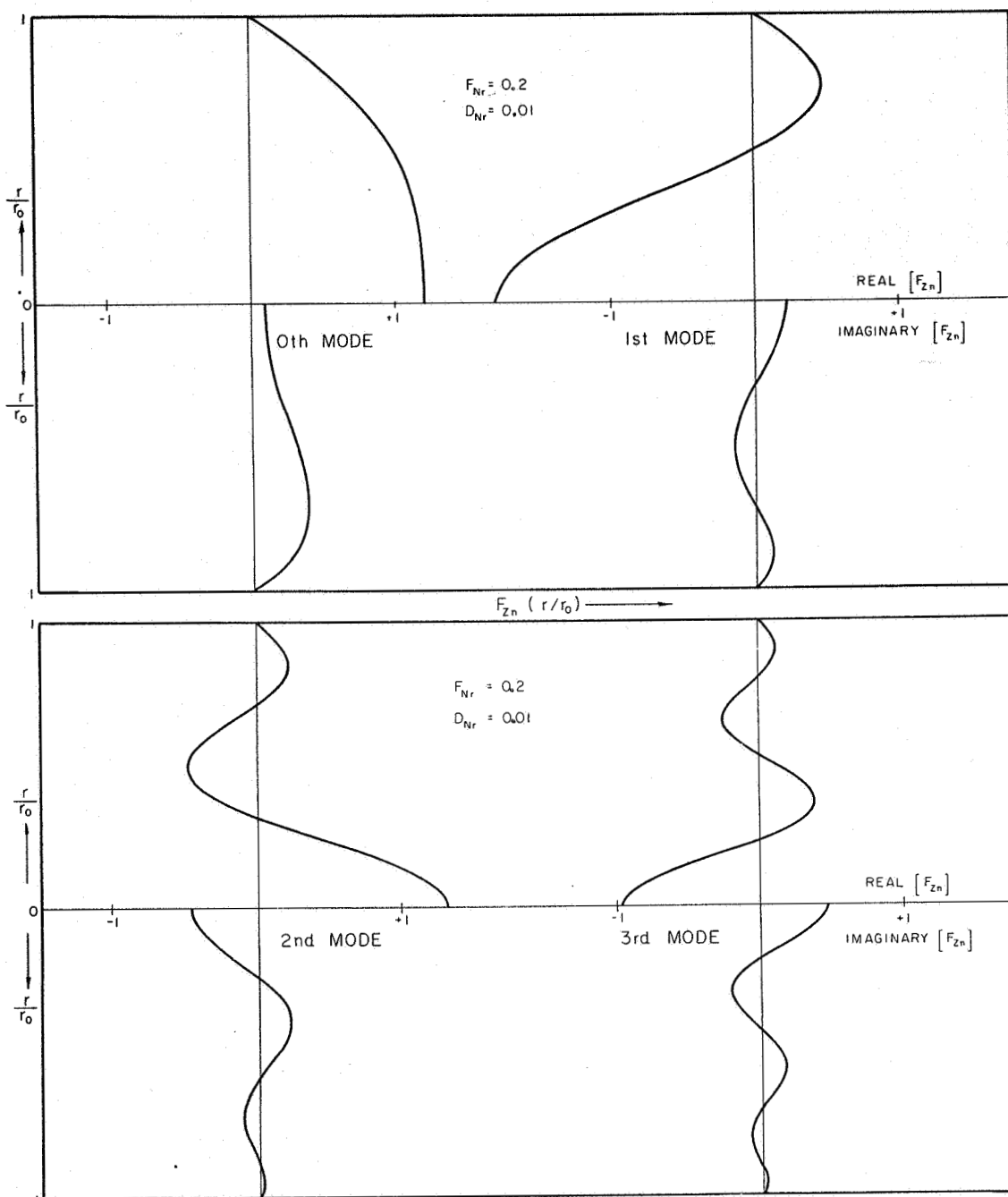


Figure 6.6. Axial Velocity Profile Function, $F_{zn}(r)$, for Four Modes ($F_{Nr} = 0.2$, $D_{Nr} = 0.01$)

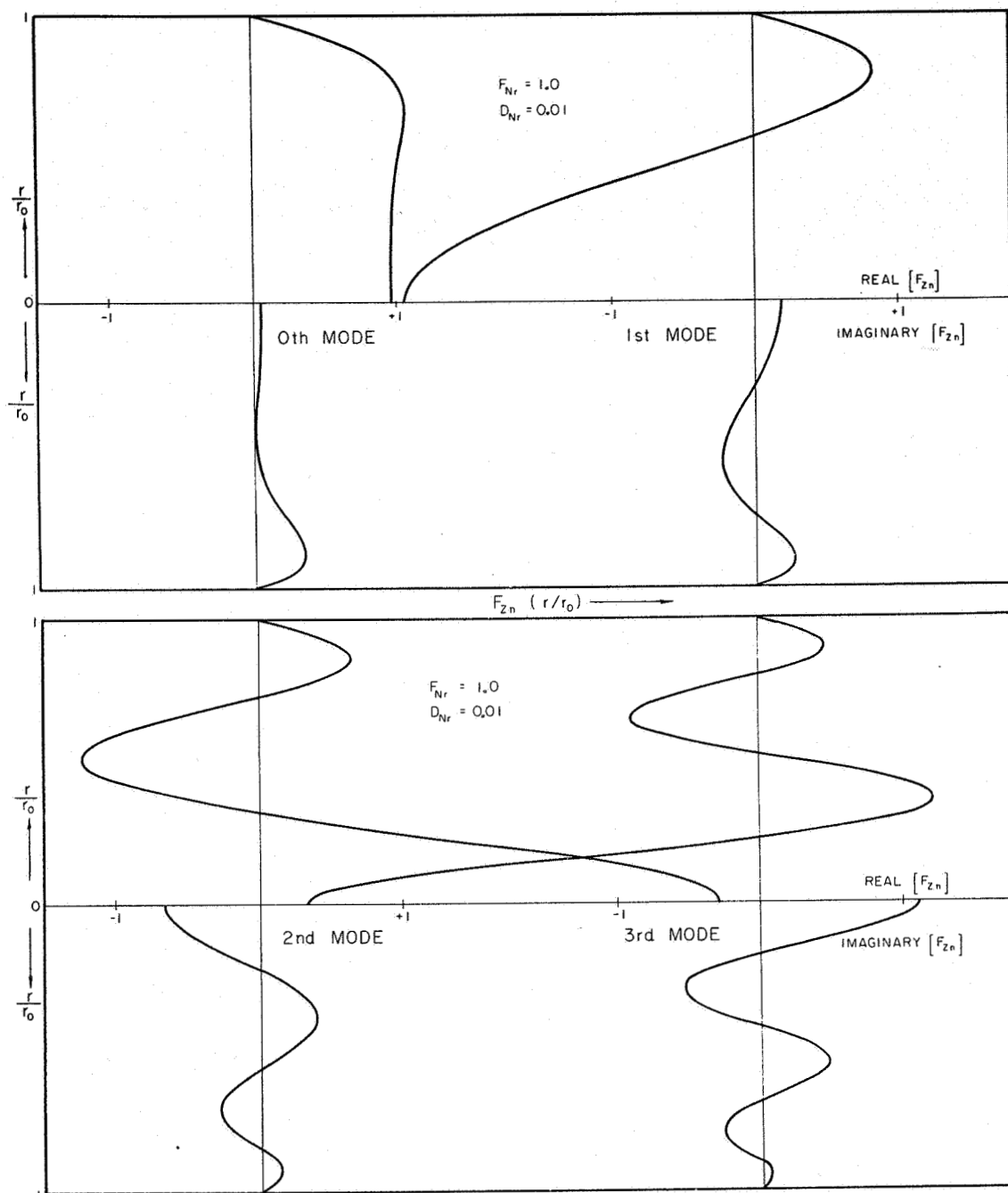


Figure 6.7. Axial Velocity Profile Function, $F_{zn}(r)$, for Four Modes ($F_{Nr} = 1.0$, $D_{Nr} = 0.01$)

fluid conditions at the conduit wall and obtaining the results eigenfunctions. What about satisfying end conditions for a fluid conduit? Suppose that the transformed condition at the end $z = 0$ for a fluid conduit is $G(r)$; that is,

$$V|_{z=0} = G(r)$$

The problem is to calculate the coefficients in the expansion given by Equation (6.3); that is, to find B_n such that

$$G(r) = \sum_n B_n \gamma_n J_0(\beta_n r_0) F_{zn}(r). \quad (6.4)$$

One might think that since $F_{zn}(r)$ is a linear sum of the eigenfunctions $J_0(\beta_n r)$ and $J_0(k_n r)$ that this problem would be a simple extension of ordinary Fourier-Bessel expansion methods. Such is not the case. This is because a set of normalizing functions is not obvious. Suppose that one could obtain a set of functions $F'_{zm}(r)$ such that

$$\int_0^{r_0} F_{zn}(r) \cdot F'_{zm}(r) \cdot dr = \begin{cases} 0, & m \neq n \\ 1, & m = n \end{cases}.$$

One could then multiply both sides of Equation (6.4) by the orthogonal functions $F'_{zm}(r)$ and integrate to yield¹

$$B_n = \frac{1}{\gamma_n J_0(\beta_n r_0)} \int_0^{r_0} G(r) \cdot F'_{zn}(r) \cdot dr. \quad (6.5)$$

¹It should be noted that this discussion makes no mention of the usual mathematical problems of convergence, uniqueness, etc. The writer's purpose is not to examine the mathematical delicacies, but rather to attempt to "get an answer".

Thus far the writer has not found a set of normalizing functions; however, a scheme is presented below which will be seen to show all indications of satisfying the desires proposed of Equation (6.4).

Kaplan (32), in his discussion of Fourier series has given the following theorem:

Theorem Let $f(x)$ be piecewise continuous for

The coefficients of the partial sum

$$\frac{1}{2} a_0 + a_1 \cos x + b_1 \sin x + \dots + a_n \cos nx + b_n \sin nx$$

of the Fourier series of $f(x)$ are precisely those among all coefficients of the functions

$$g_n(x) = p_0 + p_1 \cos x + q_1 \sin x + \dots + p_n \cos nx + q_n \sin nx$$

which render the square error

$$\int_{-\pi}^{\pi} [f(x) - g_n(x)]^2 dx$$

a minimum. Furthermore, the minimum square error E_n

satisfies the equation

$$E_n = \int_{-\pi}^{\pi} [f(x)]^2 dx - \pi \left[\frac{1}{2} a_0^2 + \sum_{k=1}^n (a_k^2 + b_k^2) \right].$$

In a manner analogous to the preceding theorem, the coefficients of Equation (6.4) will be evaluated. Assume that the coefficients of a partial sum, $S_k(r)$, are known; that is

$$S_k(r) = \sum_{n=0}^k B_n \gamma_n J_0(\beta_n r_0) F_{2n}(r). \quad (6.6)$$

Define a square error as

$$E_k = \int_0^{r_0} [G(r) - S_k(r)]^2 \cdot r \cdot dr. \quad (6.7)$$

Hypothesize that the coefficients B_n are those that minimize E_k . This means that the coefficients can be evaluated one at a time, starting with B_0 , by simply minimizing E_k with respect to B_k . Suppose it is desired to find the coefficient B_{k+1} where the first k are known. Then

$$E_{k+1} = \int_0^{r_0} [G(r) - S_k(r) - B_{k+1} \gamma_{k+1} J_0(\beta_{k+1} r_0) F_{z(k+1)}(r)]^2 \cdot r \cdot dr. \quad (6.8)$$

If E_{k+1} is to be a minimum with respect to B_{k+1} , it is necessary to have

$$\frac{\partial E_{k+1}}{\partial B_{k+1}} = 0. \quad (6.9)$$

Applying the condition of Equation (6.9) to Equation (6.8) gives

$$B_{k+1} = \frac{\int_0^{r_0} [G(r) - S_k(r)] \gamma_{k+1} J_0(\beta_{k+1} r_0) F_{z(k+1)}(r) \cdot r \cdot dr}{\int_0^{r_0} [\gamma_{k+1} J_0(\beta_{k+1} r_0) F_{z(k+1)}(r)]^2 \cdot r \cdot dr}. \quad (6.10)$$

This method has been used to evaluate the first six coefficients for the case of a piston oscillating in a rigid conduit. Since this implies a constant velocity at the piston face, $G(r) = 1$ was used for the boundary condition. The results of the calculation are tabulated in Table III. Utilizing these coefficients, the six term approximation of the transformed axial velocity has been calculated for various axial distances from the piston face. The relationship describing this approximation is given by the first six terms of Equation (6.3). The results are graphically demonstrated in Figure 6.8. Note the transition of the profile from flat at the piston to essentially the zeroth mode profile beyond $\frac{z}{D} = 0.5$. The frequency number for these calculations was

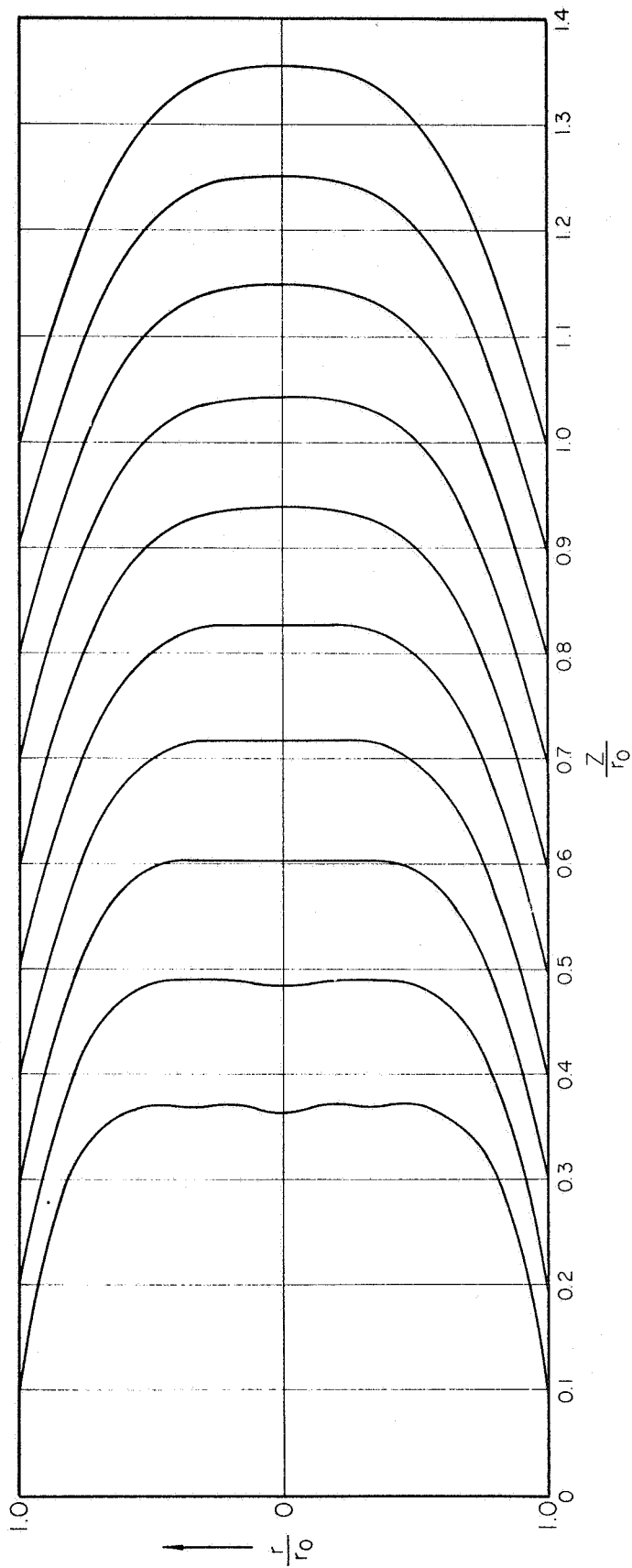


Figure 6.8. Near Piston Velocity Profile (r Dependent Part Only) Calculated From Six Terms of Equation (6.3) With $F_{nr} = 0.2$; $D_{nr} = 0.01$

0.2 which is well below the cutoff frequency for all of the higher modes. This explains why only the zeroth mode is propagated any great distance from the piston.

TABLE III

TABULATION OF THE FIRST SIX COEFFICIENTS OF THE SERIES EXPANSION
FOR A PISTON OSCILLATING IN A RIGID CONDUIT

$$(F_{nr} = .2, D_{nr} = .01)$$

$$B_0 \gamma_0 J_0(\beta_0 r_0) = 1.100 - 0.2957i$$

$$B_1 \gamma_1 J_0(\beta_1 r_0) = 0.4187 - 0.1686i$$

$$B_2 \gamma_2 J_0(\beta_2 r_0) = 0.4951 + 0.0653i$$

$$B_3 \gamma_3 J_0(\beta_3 r_0) = 0.5076 + 0.1756i$$

$$B_4 \gamma_4 J_0(\beta_4 r_0) = 0.5000 + 0.2331i$$

$$B_5 \gamma_5 J_0(\beta_5 r_0) = 0.4572 + 0.2174i$$

Experimental Investigation of Viscous Modes

As a result of mathematically demonstrating the existence of the infinite set of viscous modes of propagation, the writer became eager to obtain an experimental demonstration of their existence. By viewing the action of a birefringent fluid in the neighborhood of an oscillating piston in a plexiglass tube, the effects of the higher modes have been observed.

Figure 6.9 schematically describes the experimental apparatus used.

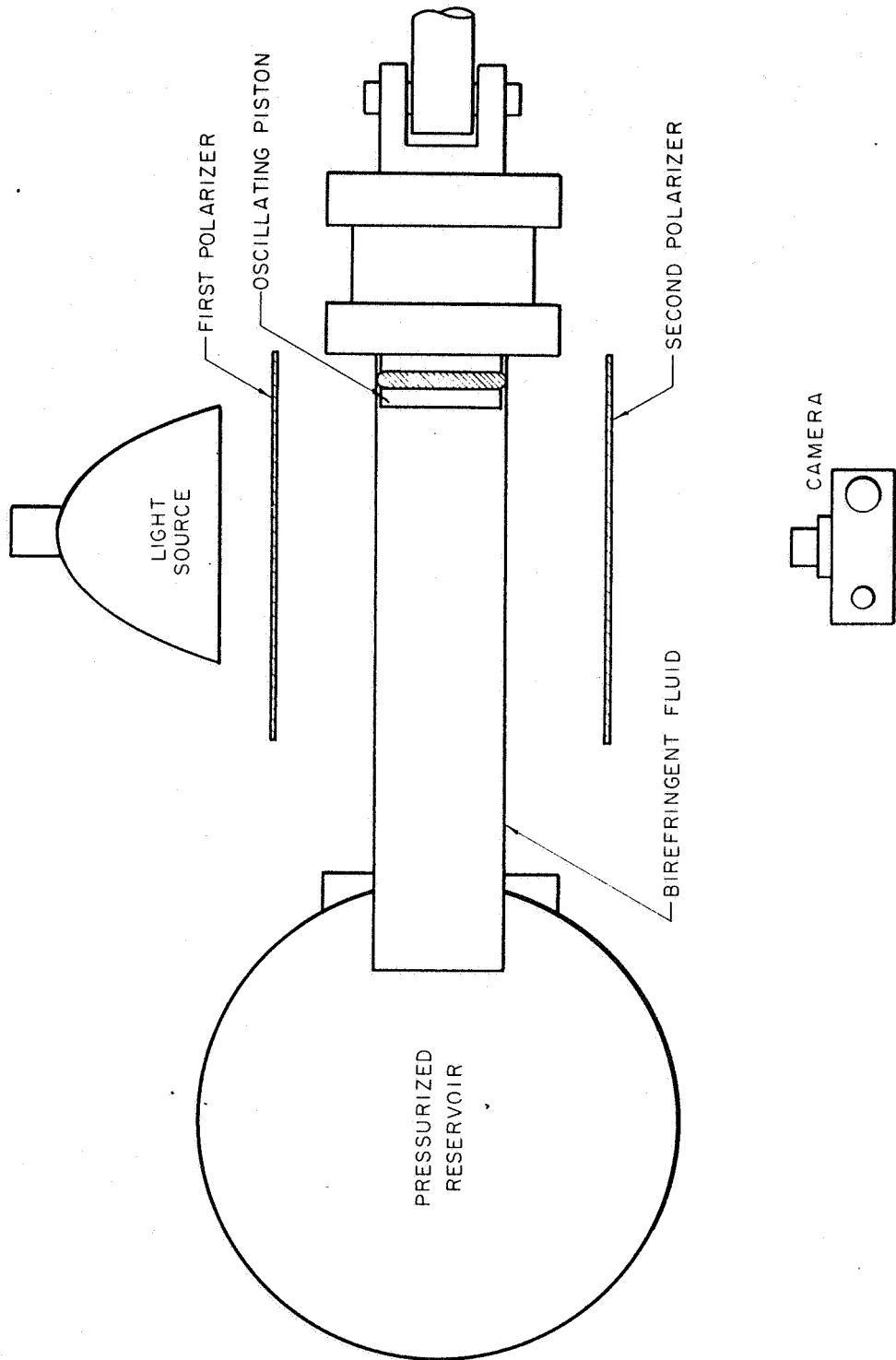


Figure 6.9. Schematic of Experimental Apparatus Used to Visually Observe the State of Shear Stress Near an Oscillating Piston

The working fluid consisted of the following components by weight:

water - 85%

milling yellow dye - 1.4%

glycerine - 13.6%

This fluid exhibited the property of optical birefringence² when in a state of shear stress.

The test section was viewed between crossed polarizer planes with a light source behind the first polarizer. The piston was oscillated at a constant frequency of about 2 cps and several photographs were taken to record the visual effect. These photographs are displayed in Figure 6.10. The patterns observed represent the state of shear stress within the fluid. Since the phenomena was viewed across a cylindrical tube, the observed effect was actually an integration of all the effects across the tube. The patterns were observed to change with time depending upon the position of the piston. This accounts for the difference between the photographs. No record was made of piston position when the pictures were taken. The important phenomena which is demonstrated by these pictures is that there appears to be a boundary effect near the piston which is damped out at a Z/D of about .5 measured axially from the piston face. The patterns for $Z/D > .5$ represent the state of shear stress of the zeroth mode only, since all higher modes are damped out. The patterns for $Z/D < .5$ represent the state of shear stress for the sum of all the modes.

Referring back to Figure 6.8, which represented the near piston

²A considerable amount of work with birefringent liquids has been done by Thurston (33). Frenkel (34) also gives a discussion of the theory of liquid birefringence.

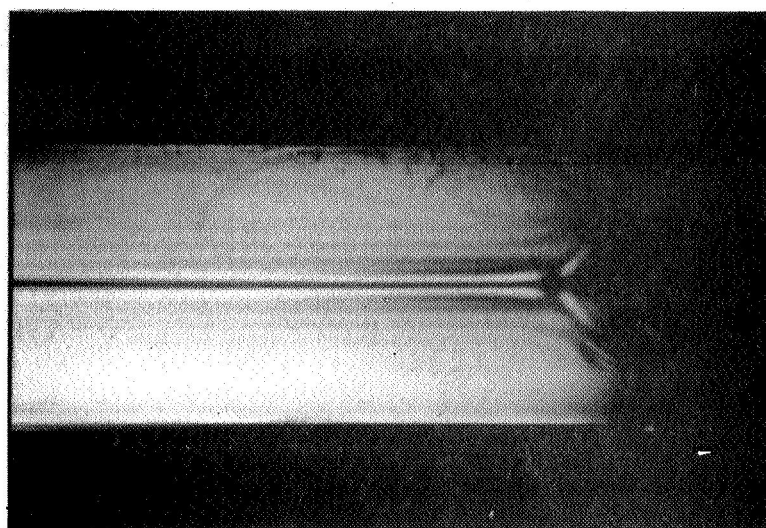
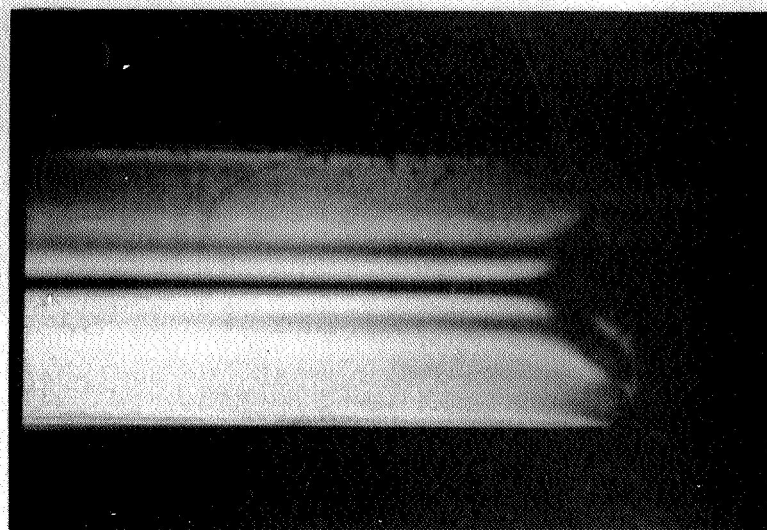


Figure 6.10. Photographs of Experimentally
Observed State of Shear
Stress

velocity profiles obtained from a summation of a few modes, an interpretation of the stress patterns obtained experimentally will now be given. For the axi-symmetric case here being discussed, the transformed shear stress may be expressed as

$$\hat{\tau}_{rz} = \mu \left\{ \frac{\partial v_r}{\partial z} + \frac{\partial v_z}{\partial r} \right\}. \quad (6.11)$$

The lines observed in Figure 6.10 represent the conditions for which $\hat{\tau}_{rz} = \text{constant}$. If one approximates $\hat{\tau}_{rz}$ by

$$\hat{\tau}_{rz} \approx \mu \frac{\partial v_z}{\partial r}$$

lines of constant shear stress can be obtained from the predicted near piston axial velocity profiles of Figure 6.8. Typical results of such a procedure are shown in Figure 6.11. Note the obvious similarity between the theoretical state of shear stress displayed in this figure and the experimental results shown in Figure 6.10. This excellent agreement between theory and experiment appears to substantiate the existence of these higher modes of viscous propagation as predicted by the theory.

Discussion

This chapter has been devoted to a theoretical and experimental investigation of the higher modes of viscous propagation. The results may be summarized as follows:

1. The higher modes were shown to have a relative cutoff frequency, below which their spatial attenuation is very great. These modes demonstrate a finite phase velocity below this cutoff frequency which is opposed to the results which have been published concerning higher modes

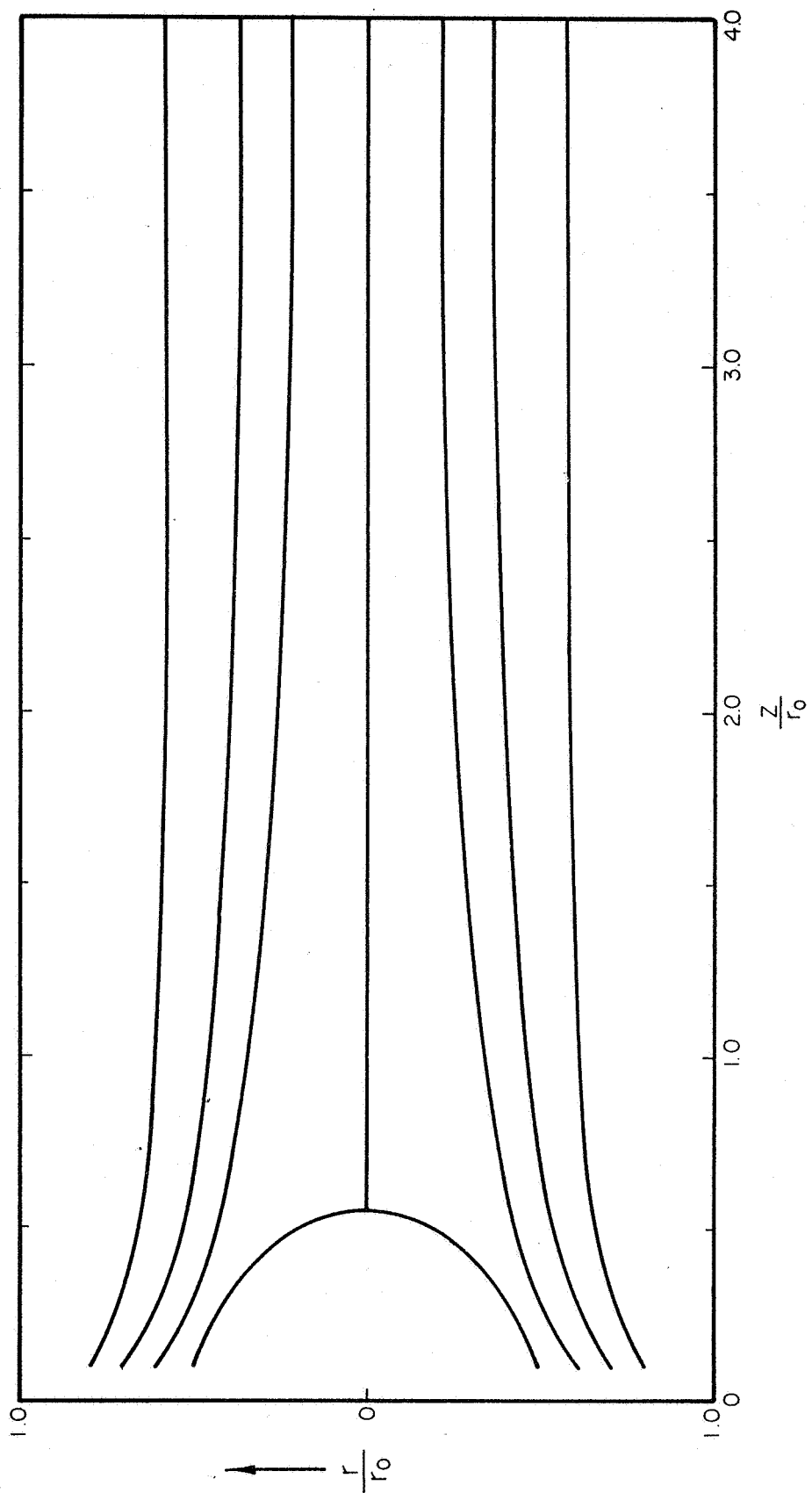


Figure 6.11. Lines of Constant Axial Velocity Gradient Obtained From Figure 6.8

of propagation neglecting viscosity (27). Above their cutoff frequency, the higher modes have spatial attenuation, but of a much smaller magnitude than below the cutoff.

2. The r dependent part of the axial velocity was found to be representable, for each mode, in terms of a profile function, $F_{zn}(r)$, having, in general, a real and imaginary part. The profile shape for the zeroth mode was found to be sensitive to values of the frequency and damping numbers. For the higher modes, the general shape stayed much the same, regardless of the values of these two numbers.
3. In order to satisfy end conditions for a fluid transmission line, it was found necessary to obtain a series expansion in terms of the velocity profile functions (eigenfunctions). The coefficients of this expansion were not obtainable by ordinary methods since a set of orthogonal functions (orthogonal to the eigenfunctions) was not known. It was found to be possible, however, to evaluate the coefficients one at a time by a method of minimizing the square error. The absolute validity of this method is undetermined at this time, but the results seem to demonstrate its practicality.
4. A flow visualization technique was used to obtain photographic records of the state of shear stress near an oscillating piston in a tube. Interpretation of the results in terms of the theoretical predictions seem to

validate the existence of the higher modes.

To the best of the writer's knowledge, the discussion of the higher modes of viscous propagation as given in this treatise is the first ever presented. It is hoped that it may represent an advance in the state of the art.

CHAPTER VII

NON-RIGID WALL EFFECTS

Introduction

The purpose of this chapter is to outline an analytical approach to the problem of determining the effects which non-rigid walls have on the transmission properties a viscous fluid carrying conduit. Basically, there are four types of conduit walls:

1. Rigid walls - Those walls which are assumed perfectly rigid and do not give under the influence of a pressure force. This type of wall has an infinite radial impedance, i.e., $\frac{p}{v_r} = \infty$.
2. Pressure release walls - Those walls which just contain the fluid but exert no force on the fluid. This type has a zero radial impedance.
3. Elastic flexible walls - Those walls which give under pressure and have some finite radial impedance but do not propagate a disturbance in the axial direction.
4. Elastic stiff walls - Those walls which have a finite radial impedance and do propagate a disturbance in the axial direction.

The model for a rigid conduit was developed in Chapter IV. The remainder of this chapter will be devoted to discussions of conduits

with elastic flexible and elastic stiff walls.

Elastic Flexible Walls

If one is studying the dynamic characteristics of fluid-filled elastic tubes, such as rubber, where the major effects are those due to tube inertia and tensile stress in the wall, then the equation of motion for the tube is (35)

$$\rho_t h \frac{d^2 \delta_r}{dt^2} + \delta_r (h E_t / r_o^2) = p_t \quad (7.1)$$

where

h = tube wall thickness

r_o = tube radius

E_t = Young's modulus for tube material

δ_r = wall radial deflection

p_t = fluid pressure at tube wall

ρ_t = density of tube wall.

Applying the Laplace transformation to Equation (7.1) gives

$$\rho_t h s^2 \hat{\delta}_r + \hat{\delta}_r (h E_t / r_o^2) = P_t$$

or

$$\hat{\delta}_r = \frac{P_t}{(\rho_t h s^2 + h E_t / r_o^2)}$$

Noting that the transformed radial velocity and deflection for the tube wall are related by $V_{rt} = s \hat{\delta}_r$, the radial impedance for the tube wall becomes

$$\frac{P_t}{V_{rt}} = \frac{P_t h s^2 + h E_t / r_0^2}{s}. \quad (7.2)$$

For these calculations, it will be assumed that the wall deflections are small compared with the tube radius so the conditions at the wall require that the axial fluid velocity be zero and the fluid radial impedance at the wall equals the tube radial impedance. From Equations (3.30) and (3.33), the fluid radial impedance at the wall is

$$\frac{P}{V_r} = \left(\frac{\rho_0 c_0^2}{s} \right) \left\{ \frac{B(\gamma^2 - \beta^2) J_0(\beta r_0)}{B\beta J_1(\beta r_0) + A\gamma J_1(kr_0)} \right\}. \quad (7.3)$$

The condition of zero axial fluid velocity at the wall yields from Equation (3.31)

$$B\gamma J_0(\beta r_0) + Ak J_0(kr_0) = 0. \quad (7.4)$$

Combining (7.3) and (7.4) to eliminate the arbitrary constants, A and B yield

$$\frac{P}{V_r} = \frac{(\gamma^2 - \beta^2)(\rho_0 c_0^2 / s)}{\left\{ \frac{\beta J_1(\beta r_0)}{J_0(\beta r_0)} - \frac{\gamma^2 J_1(kr_0)}{k J_0(kr_0)} \right\}} \quad (7.5)$$

which is the radial impedance of the fluid at the wall. Equating this to Equation (7.3) gives the characteristic equation

$$\frac{(\gamma^2 - \beta^2)(\rho_0 c_0^2)}{\left\{ \frac{\beta J_1(\beta r_0)}{J_0(\beta r_0)} - \frac{\gamma^2 J_1(kr_0)}{k J_0(kr_0)} \right\}} = P_t h s^2 + h E_t / r_0^2. \quad (7.6)$$

which, along with the equations

$$\gamma^2 = k^2 + \frac{s}{\mathcal{D}} = \beta^2 + \frac{s^2}{c_0^2} \quad (7.7)$$

completely relate the eigenvalues. For the case of a rigid wall, which was discussed previously, the eigenvalues were found to depend only upon two dimensionless parameters; the radial damping number and the radial frequency number. For the case now being considered, the eigenvalues are found to also depend upon the tube wall parameters, as might have been expected.

Equations (7.6) and (7.7) have been solved to obtain γ for the zeroth and first modes. This was done for one set of the tube wall parameters and the results are displayed in Figures 7.1, 7.2, 7.3, and 7.4 in comparison with the rigid wall results. The calculations were performed with the aid of an IBM 7040 by a procedure similar to that outlined in Appendix A. Examination of the graphical results reveals the following:

1. For the zeroth mode, the spatial attenuation is increased due to the flexible wall as opposed to a rigid wall. The increase is so great in the higher frequency regions that one can consider the flexible conduit to act as a low-pass filter. The cutoff frequency corresponds approximately to the natural frequency of the tube wall.
2. Also for the zeroth mode, the elastic flexible wall is seen to decrease the phase velocity with the minimum value occurring near the natural frequency of the tube wall.

Statements (1) and (2) above appear to be generally valid regardless of the fluid and tube wall parameters. Examination of Figures 7.3 and 7.4 show that, while there is a considerable effect of the elastic wall upon the first mode spatial attenuation and phase velocity, no

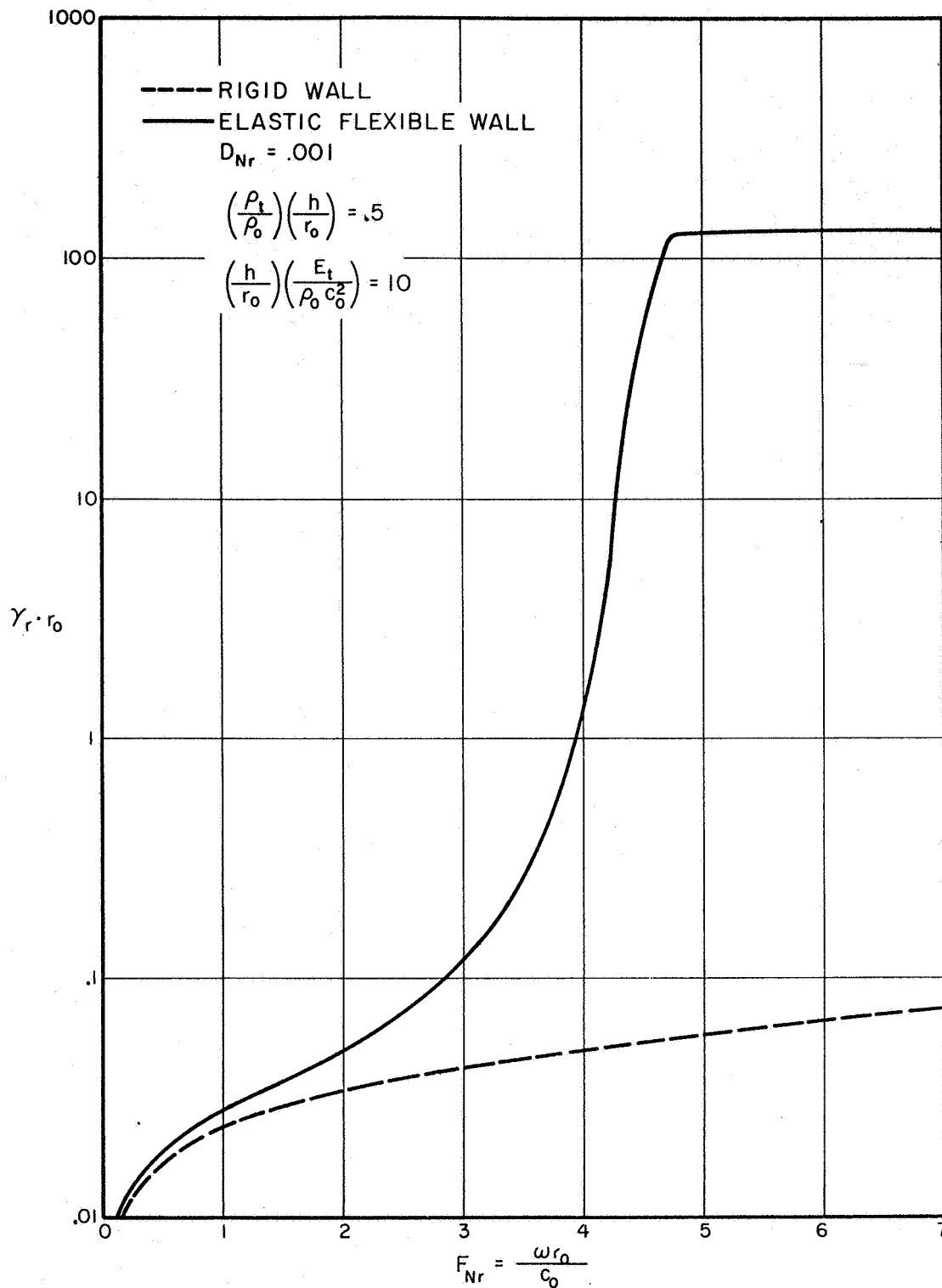


Figure 7.1. Zeroth Mode Spatial Attenuation Versus F_{Nr} for a Rigid and an Elastic Flexible Wall

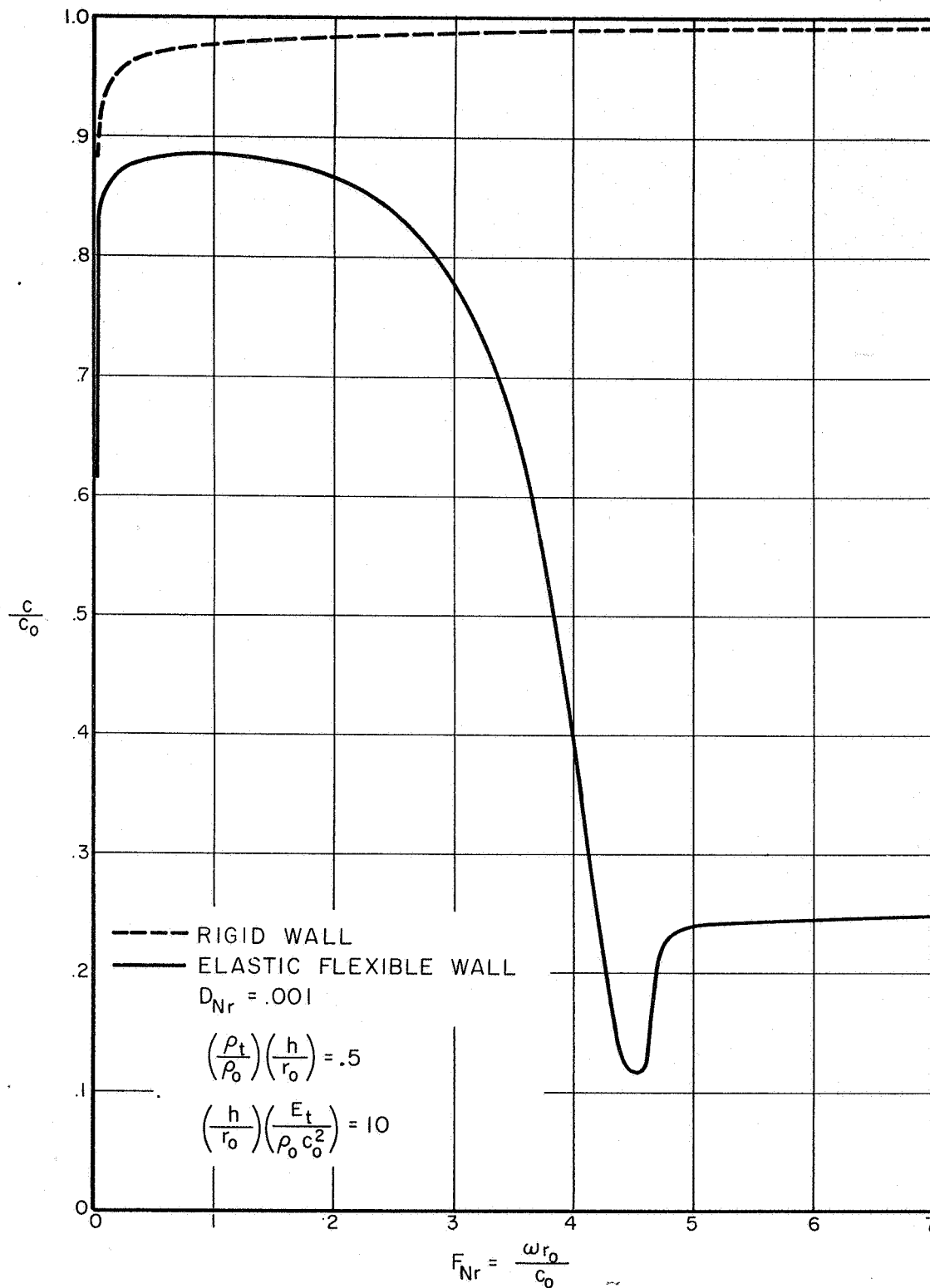


Figure 7.2. Dimensionless Phase Velocity, c/c_0 , Versus F_{Nr} for a Rigid and an Elastic Flexible Wall

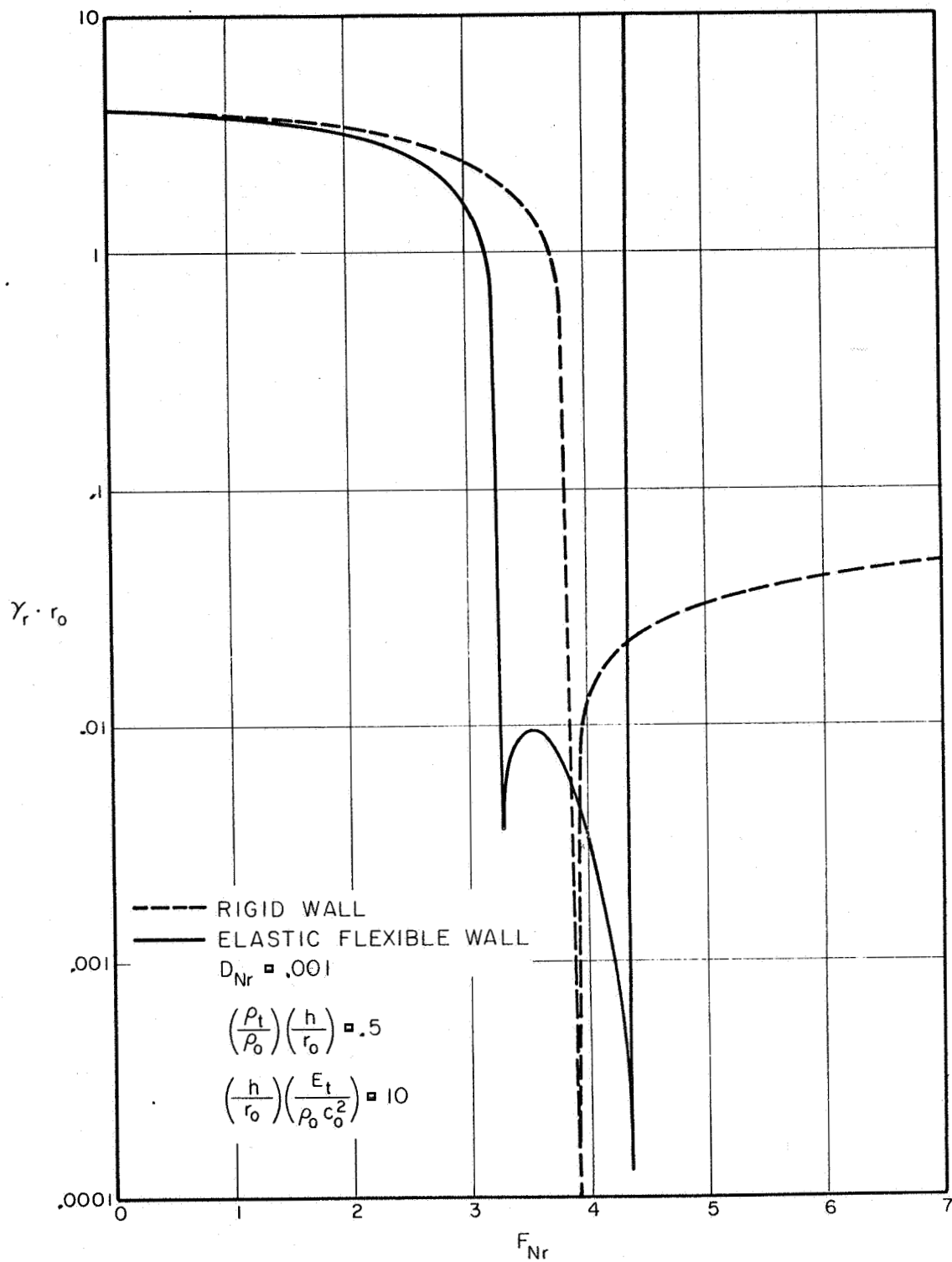


Figure 7.3. First Mode Spatial Attenuation Versus F_{Nr} for a Rigid and an Elastic Flexible Wall

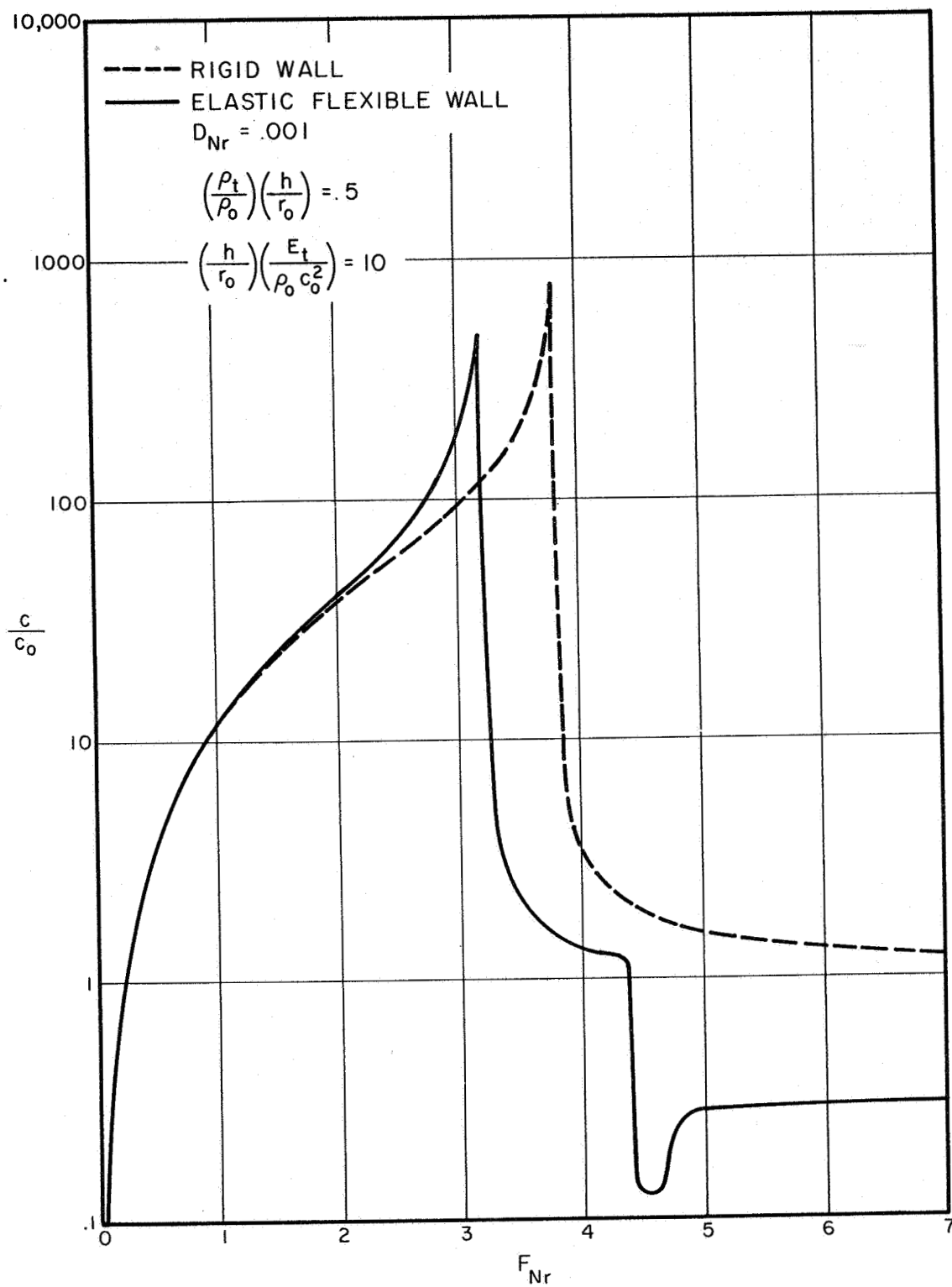


Figure 7.4. Dimensionless Phase Velocity, c/c_0 , Versus F_{Nr} for a Rigid and an Elastic Flexible Wall

general statements can be made regarding the effects as was true for the zeroth mode.

Elastic Stiff Walls

The approximate equations of motion for a thin-walled elastic stiff pipe as given by Lin and Morgan (29, 36) are, neglecting rotary inertia effects

$$\rho_t h \frac{\partial^2 \bar{\delta}_z}{\partial t^2} = \frac{h E_t}{(1-\lambda^2)} \left\{ \frac{\partial^2 \bar{\delta}_z}{\partial z^2} + \frac{\lambda}{r_0} \frac{\partial \bar{\delta}_r}{\partial z} \right\}$$

$$\rho_t h \frac{\partial^2 \bar{\delta}_r}{\partial t^2} = K G h \frac{\partial}{\partial z} \left\{ \frac{\partial \bar{\delta}_r}{\partial z} - \xi \right\} - \frac{h E_t}{(1-\lambda^2)} \left\{ \frac{\bar{\delta}_r}{r_0^2} + \frac{\lambda}{r_0} \frac{\partial \bar{\delta}_z}{\partial z} \right\} + \rho_t \left(1 - \frac{h}{2r_0} \right)$$

and

$$\frac{E_t h^3}{12(1-\lambda^2)} \frac{\partial^2 \xi}{\partial z^2} + K G h \left\{ \frac{\partial \bar{\delta}_r}{\partial z} - \xi \right\} = 0$$

where the tube wall axial and radial particle displacements are given by the perturbation equations

$$\delta_z(r, z, t) = \bar{\delta}_z(z, t) + (r_0 - r) \xi(z, t)$$

and

$$\delta_r(r, z, t) = \bar{\delta}_r(z, t).$$

For these equations, the following definitions hold:

$\lambda \equiv$ Poisson's ratio

$h \equiv$ tube wall thickness

$K \equiv$ shear constant (29, 36)

$G \equiv$ modulus of rigidity.

These equations of motion were used by Lin and Morgan to study the propagation of disturbances in non-viscous liquids. Using these equations to find the wall impedance, the characteristic equation for propagation in a viscous liquid will now be derived. To the best knowledge of the writer, this represents the first such discussion of the propagation in a compressible, viscous liquid contained within an elastic-stiff conduit.

Transforming the equations of tube motion and assuming solutions of the form

$$\hat{\delta}_z = \delta_{z0} e^{\lambda t z}$$

$$\hat{\delta}_r = \delta_{r0} e^{\lambda t z}$$

$$\hat{\xi} = \xi_0 e^{\lambda t z}$$

where \wedge indicates transformed quantities, yields, after eliminating δz_0 and ξ_0 ,

$$\delta_{r0} a_3(s, \lambda t) = a_2 P_t / e^{\lambda t z}$$

$$a_3(s, \lambda t) = \left\{ \frac{s^2}{c_p^2} + \left(\frac{h^2}{12} \right) \frac{\lambda^4 t^4}{(1 - a_1 \lambda^2 t^2)} + \frac{1}{r_0^2} + \frac{\left(\frac{\lambda \lambda t}{r_0} \right)^2}{(s^2 / c_p^2 + \lambda^2 t^2)} \right\}$$

$$a_1 = \frac{P_t h^2 c_p^2}{12 KG}$$

$$a_2 = \frac{1 - h/2r_0}{P_t h c_p^2}$$

and

$$c_p^2 = \frac{E t}{P_t (1 - \lambda^2)}$$

Solving for the radial tube impedance gives

$$\frac{P_t}{s \bar{\delta}_r} = \frac{P_t}{V_{rt}} = \frac{a_3(s, \nu)}{s a_2} \quad (7.8)$$

It should be recognized that Equation (7.8) is the counterpart of (7.3) which was the tube wall impedance equation for the case of elastic flexible walls. Proceeding in the same manner as previously done, that is, setting the tube wall impedance equal to the fluid impedance of the wall yields the equation

$$\frac{(\nu^2 - \beta^2)(\rho_0 c_0^2 / s)}{\left\{ \frac{\beta J_1(\beta r_0)}{J_0(\beta r_0)} - \frac{\nu^2 J_1(k r_0)}{k J_0(k r_0)} \right\}} = \frac{a_3(s, \nu)}{s a_2} \quad (7.9)$$

Equations (7.7) and (7.9) now completely describe the eigenvalues for an elastic-stiff viscous fluid carrying conduit.

From this point, the calculations of the eigenvalues for various types of walls must be done with the computer in a manner similar to that employed earlier in this chapter. The eigenvalues have not been calculated for this case.

CHAPTER VIII

DEVELOPMENT OF TAPERED-LUMPED MODEL

Introduction

In Chapter IV, a detailed discussion of a fluid conduit model based upon the zeroth mode transfer equations was given. In Chapter V, the validity of this model was experimentally established. It must be said, however, that despite its validity and accuracy, the model is mathematically unwieldy when used to solve everyday engineering problems in the time domain. As an example, see Appendix B which describes the inverse transformation for the water hammer problem discussed in Chapter IV. A considerable amount of time and work was needed to solve this very simple case involving a single line. Practical everyday engineering problems may involve many lines interconnected with valves, accumulators, etc. The frequency analysis of such a system can be handled with the aid of a digital computer, but a time domain analysis would be almost impossible. The need should be evident, therefore, for a simplified or approximate engineering model which would be useful in the time domain analysis of complex fluid systems. The approach taken here is to expand the hyperbolic functions, $\cosh \Gamma(s)$ and $\sinh \Gamma(s)$ which appear in the zeroth mode transfer equations, as infinite products of second order polynomial terms. This method is not new, having been reported most recently by Oldenberger and Goodson (12), but the approach taken here

results in a set of tables or curves from which the engineer can obtain the proper coefficients to be used in the polynomial terms.

Development of Model

Recall that the conduit transfer equations may be written in the form

$$\bar{P}_2(s) = \bar{P}_1(s) \cosh \Gamma(s) - Z_c(s) \bar{V}_1(s) \sinh \Gamma(s)$$

and

$$\bar{V}_2(s) = \bar{V}_1(s) \cosh \Gamma(s) - \frac{\bar{P}_1(s)}{\bar{V}_1(s)} \sinh \Gamma(s).$$

For the solution of problems requiring a time domain analysis, inverse transformations involving the above equations are extremely time consuming. It becomes, therefore, desirable to develop valid engineering approximations to these equations if possible.

Consider the possibility of expressing the hyperbolic operator functions in the infinite product forms.

$$\cosh \Gamma(s) = \prod_{n=0}^{\infty} \left\{ 1 + 2 \zeta_{cn} s / \omega_{cn} + s^2 / \omega_{cn}^2 \right\} \quad (8.1)$$

and

$$\sinh \Gamma(s) = \Gamma(s) \prod_{n=1}^{\infty} \left\{ 1 + 2 \zeta_{sn} s / \omega_{sn} + s^2 / \omega_{sn}^2 \right\}. \quad (8.2)$$

The values of the constants ζ_{cn} , ζ_{sn} , ω_{cn} and ω_{sn} are to be obtained by solving for the values of S_n at the zeroes of $\cosh \Gamma(s)$ and $\sinh \Gamma(s)$.

ζ and ω_n may then be found by noting that

$$S_n = -\zeta_n \omega_n \pm i \sqrt{1 - \zeta_n^2} \omega_n. \quad (8.3)$$

Figures 8.1, 8.2, 8.3, and 8.4 display plots of ζ_{cn} , ζ_{sn} , F_{cn} , and F_{sn} versus axial damping number. To use these plots, it is necessary only to calculate the dimensionless damping number for a line

$$D_{Nz} = \frac{\nu L}{c_o r_o^2} \quad (8.4)$$

and then read off the corresponding values for ζ_n and F_n . ω_n is then given by

$$\omega_n = \frac{F_n c_o}{L} \quad (8.5)$$

In the above equations

ν \equiv fluid viscosity

L \equiv conduit length

c_o \equiv Isentropic speed of sound in fluid

r_o \equiv inside conduit radius.

Having now developed this approximate engineering model, its validity and limitations remain to be determined.

Comparison of Exact and Approximate Models

Since the engineering model which has just been developed is an approximation of the "exact" model or zeroth mode transfer equations, the measure of its accuracy can be easily determined by directly comparing the two models. This may be done by studying the frequency and transient responses for the two cases. Consider then the approximations of Equations (8.1) and (8.2) or

$$\cosh(\Gamma(s)) = \prod_{n=0}^{\infty} \left\{ 1 + 2 \zeta_{cn} s / \omega_{cn} + s^2 / \omega_{cn}^2 \right\}$$

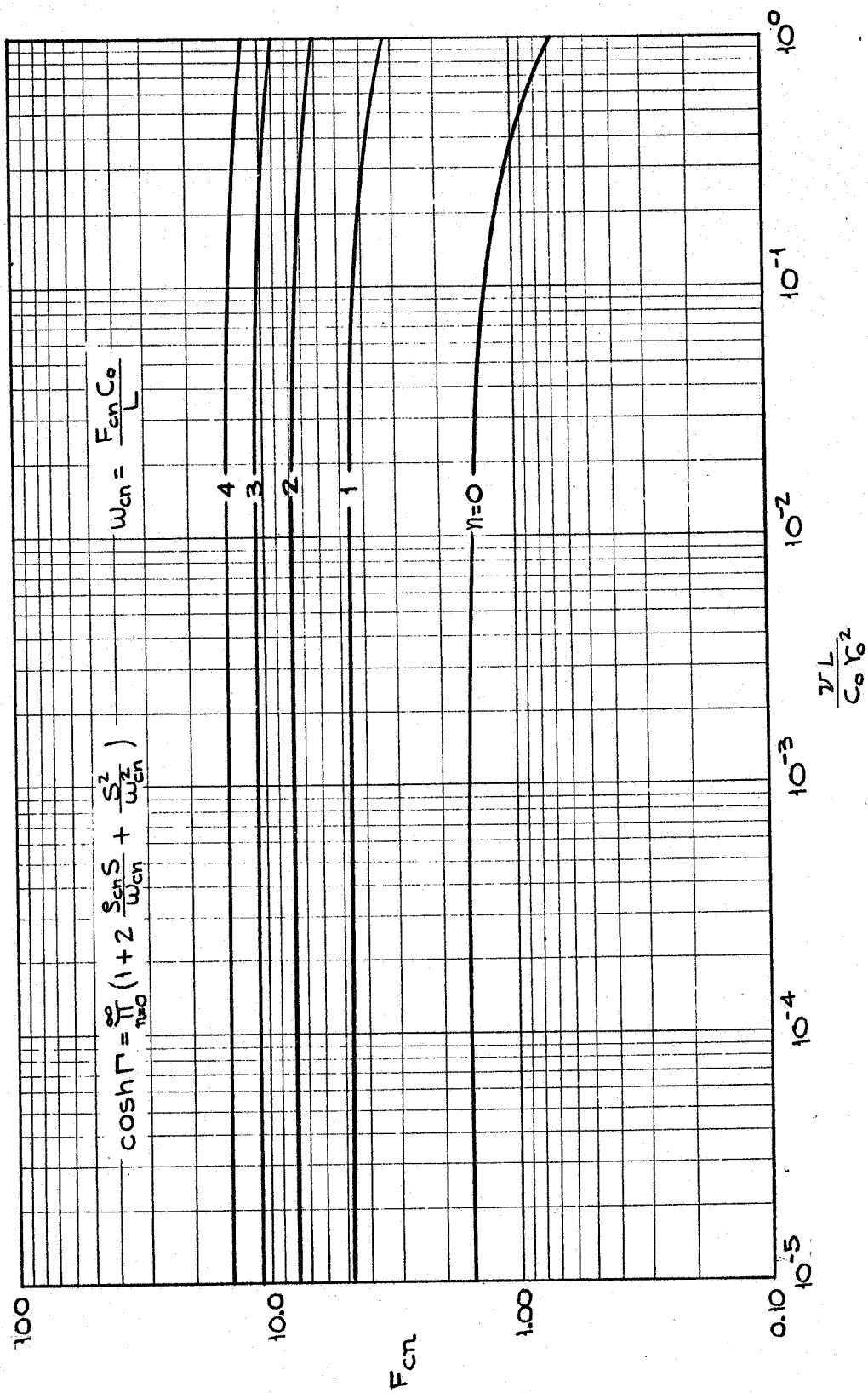


Figure 8.1. Variation of the Approximate Model Parameter Fcn With Axial Damping Number

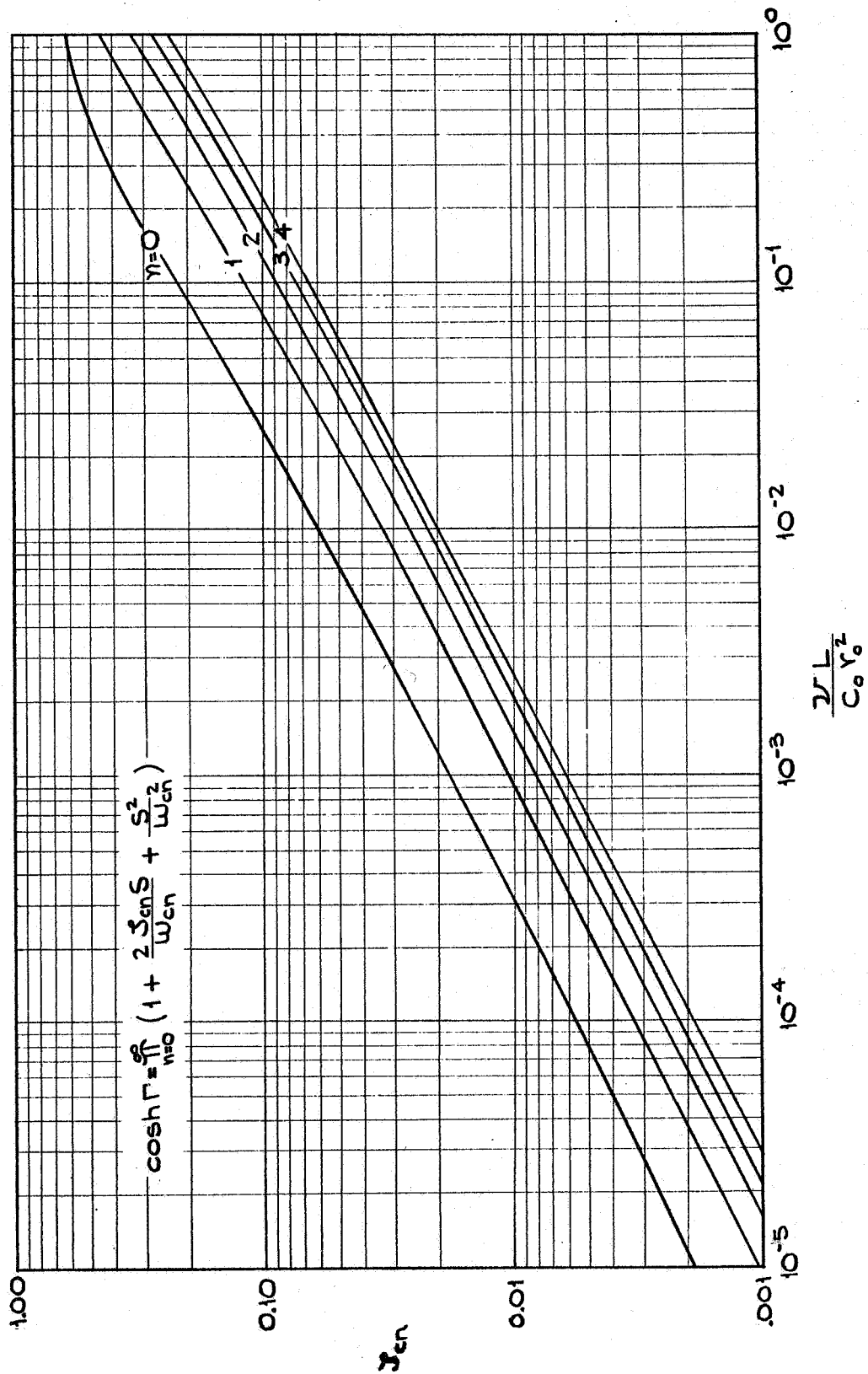


Figure 8.2. Variation of the Approximate Model Parameter ζ_{cn} With Axial Damping Number

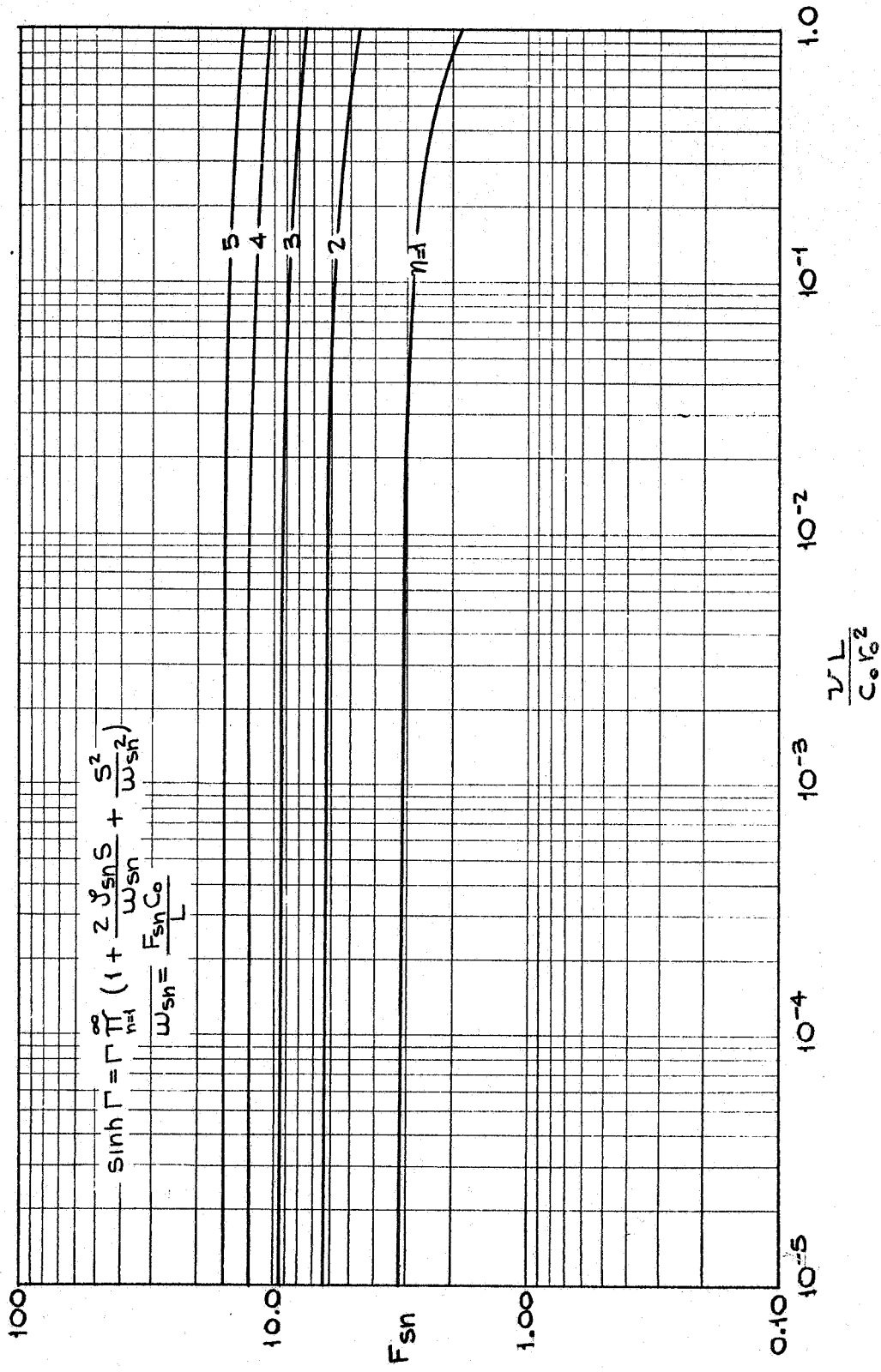


Figure 8.3. Variation of the Approximate Model Parameter F_{sn} With Axial Damping Number

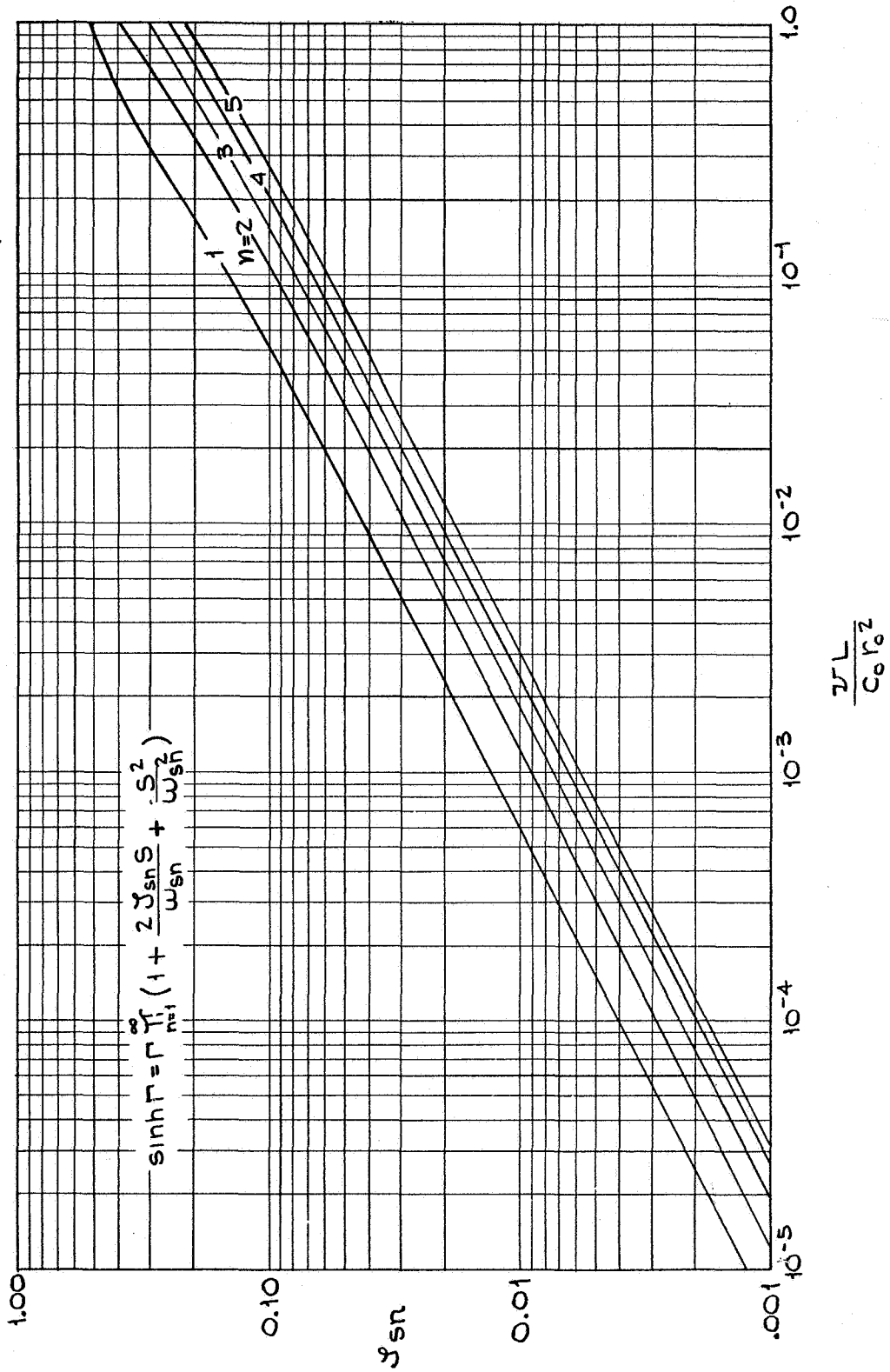


Figure 8.4. Variation of the Approximate Model Parameter S_n With Axial Damping Number

and

$$\sinh \Gamma(s) = \left(\frac{sL}{L_0} \right) \prod_{n=1}^{\infty} \left\{ 1 + 2 \zeta_{sn} s / \omega_{sn} + s^2 / \omega_{sn}^2 \right\}.$$

Here $\Gamma(s)$ is being approximated by sL/c_0 in the $\sinh \Gamma(s)$ equation. Figures 8.5 and 8.6 display plots of the amplitude and phase of $\cosh \Gamma(s)$ versus frequency number for two typical values of damping number. Also shown are the corresponding one-term approximations. Figure 8.7 and 8.8 show similar comparisons for two terms of the approximate model. The corresponding comparisons for $\sinh \Gamma(s)$ were not plotted since the results are much the same.

From the results of the frequency response comparison of the exact and approximate models, it may be concluded that the use of a one-term approximation gives excellent results up to somewhat beyond the first critical frequency. The use of two terms of the approximation improves the result up to just beyond the first critical frequency, but does not predict well the values around the second critical frequency. The use of more terms would improve the result around the second critical frequency. It now remains to compare the exact and approximate models from a transient response standpoint.

As an example, consider the water hammer problem which was analytically studied by use of the zeroth mode transfer equations in Chapter IV and which was experimentally studied as described in Chapter V. Figure 5.4 shows the physical layout of the model. The Laplace domain response for the pressure at the valve due to a V_0 amplitude step change in the velocity is found from Equation (4.32), or

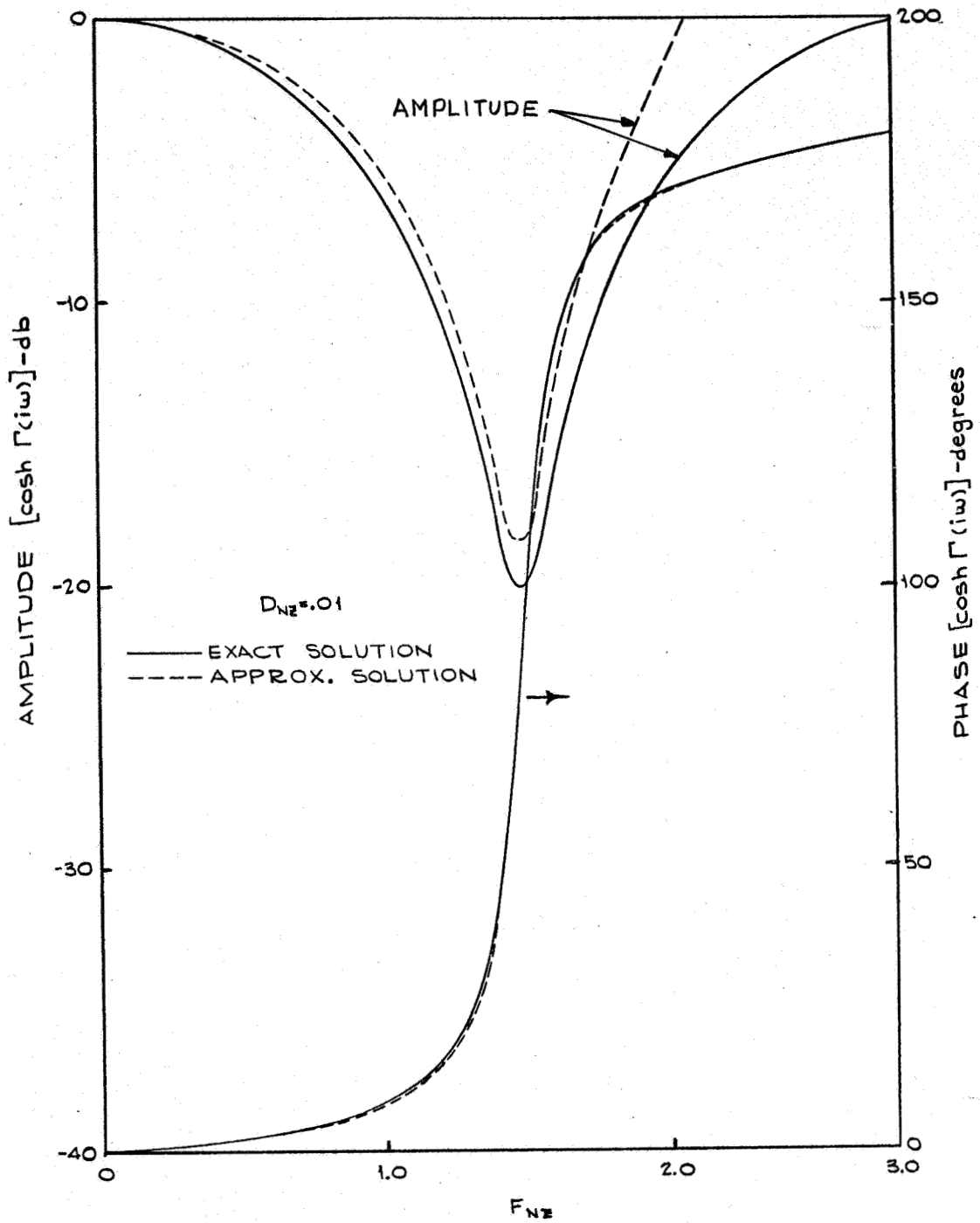


Figure 8.5. Comparison of One-Term Approximation of $\cosh \Gamma(i\omega)$ With Exact Value (Amplitude and Phase), $D_{NZ} = 0.01$

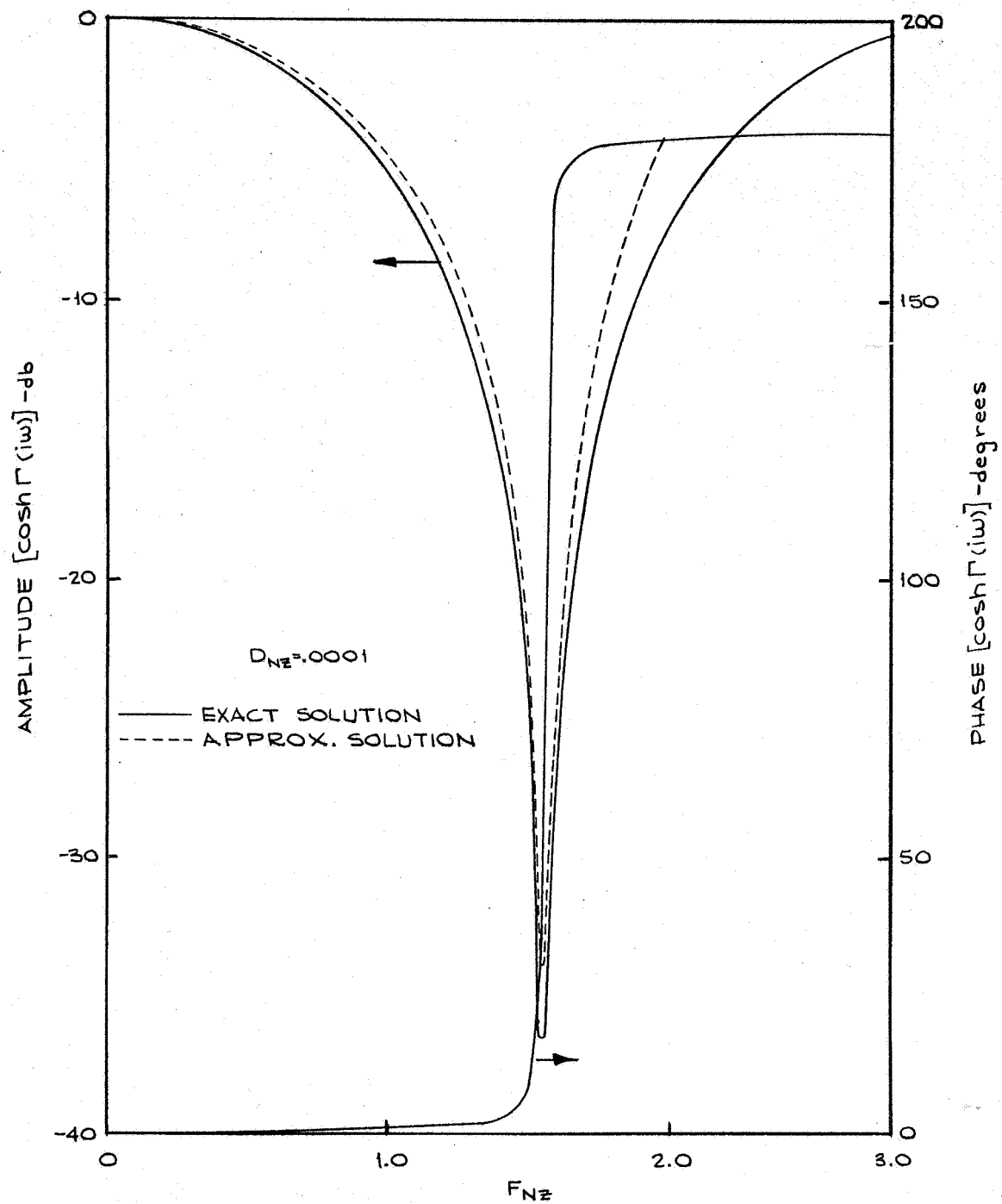


Figure 8.6. Comparison of One-Term Approximation of $\cosh \Gamma(i\omega)$ With Exact Value (Amplitude and Phase) $D_{NZ} = 0.0001$

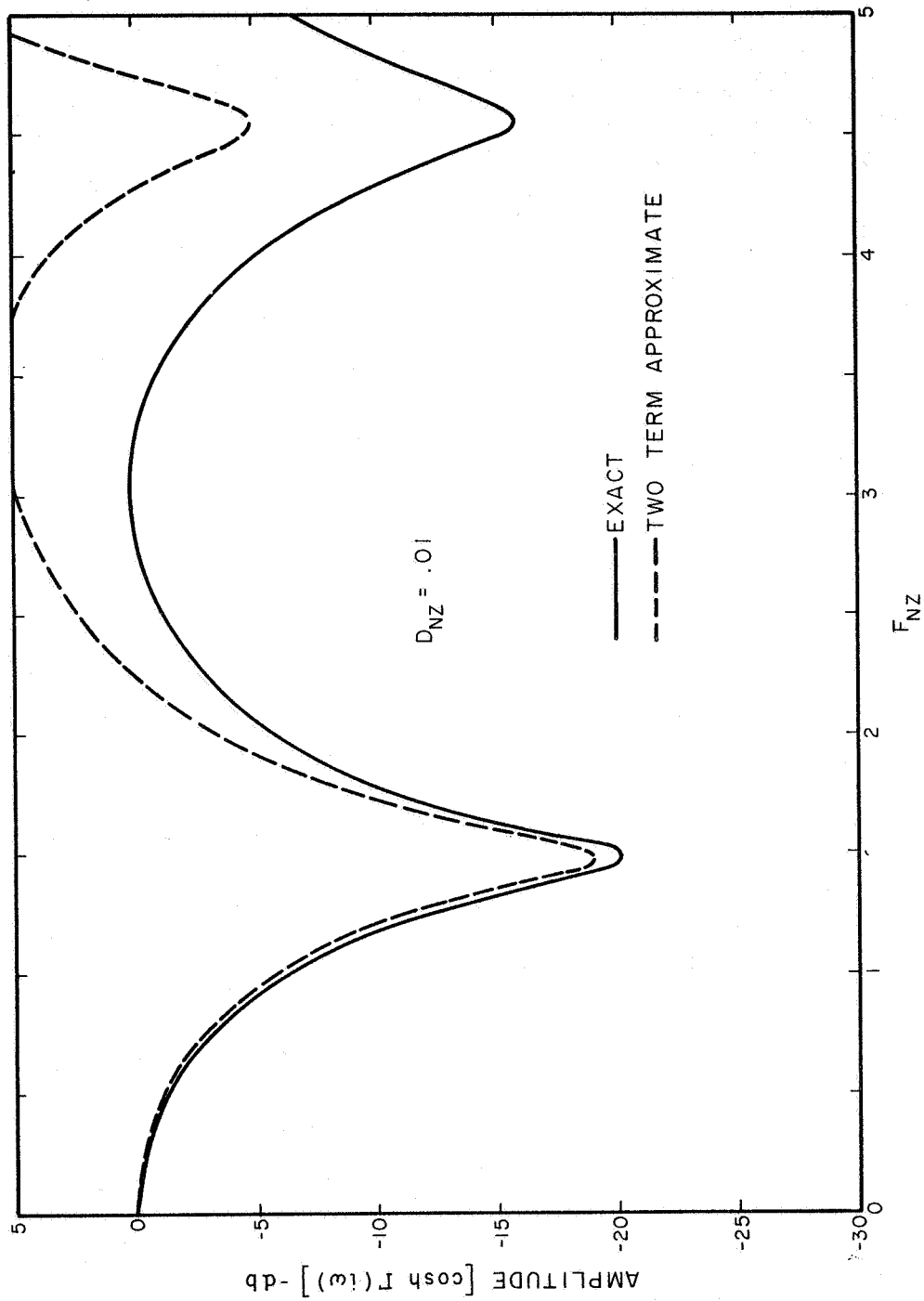


Figure 8.7. Comparison of Two-Term Approximation of Cosh $\Gamma(i\omega)$ With Exact Value (Amplitude and Phase), $D_{nz} = 0.01$

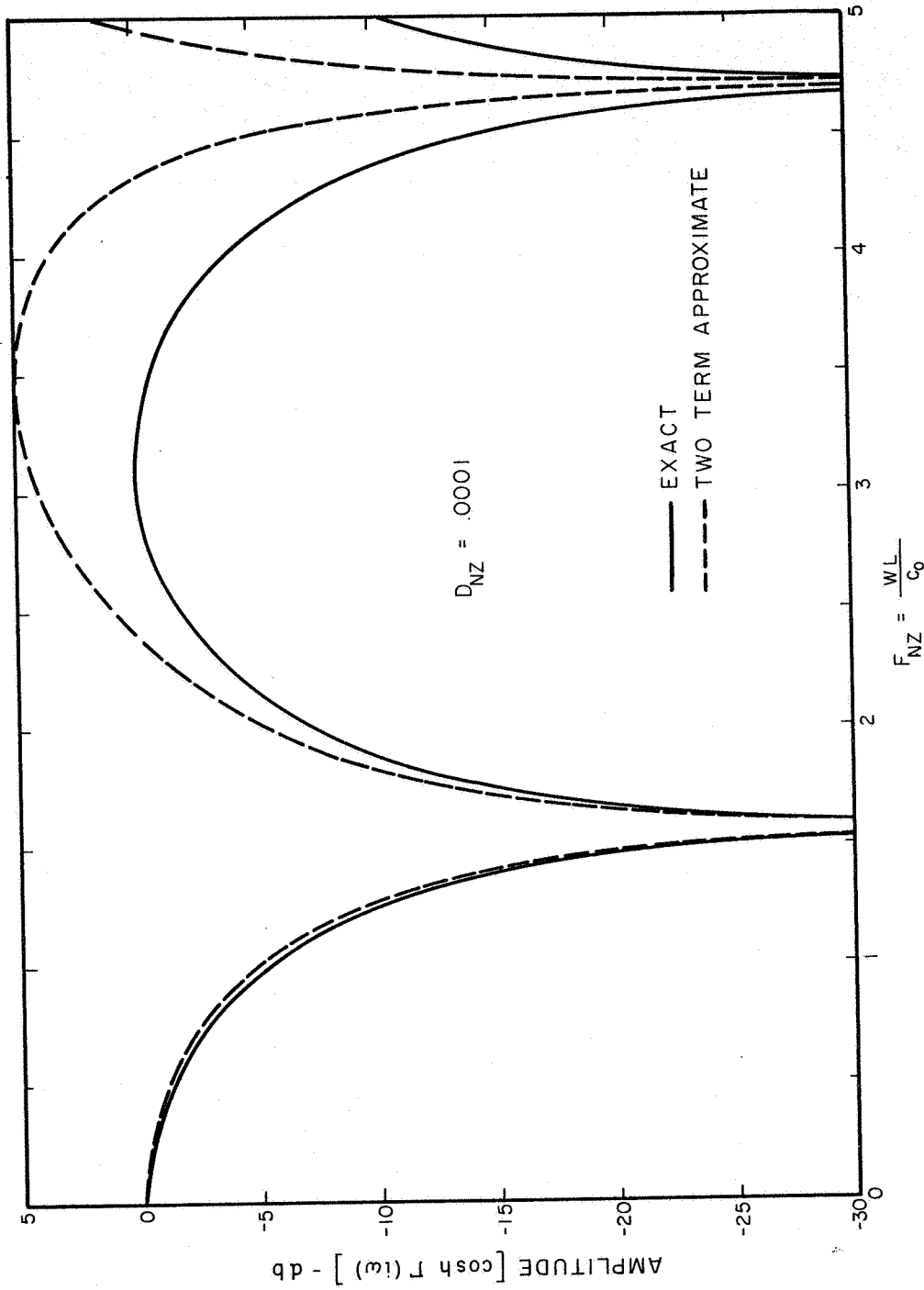


Figure 8.7. Comparison of Two-Term Approximation of Cosh $\Gamma(i\omega)$ With Exact Valve (Amplitude and Phase), $D_{nz} = 0.0001$

The evaluation of the exact inverse of this equation, as discussed in Appendix B, was cumbersome and impractical for most cases. Therefore, the $n = 0$ terms of the approximate model will now be used to predict the same pressure transients due to the sudden valve closure. Using the value of the damping number for the line which was studied experimentally, i.e., $Dn = .02$, it may be seen from Figures 8.1 and 8.2 that

$$\xi_{c_0} = 0.088$$

$$F_{c_0} = 1.5.$$

Since $c_0 = 4400$ ft/sec and $L = 100$ ft for this case

$$\omega_{c_0} = (1.5)(44) = 66 \text{ rad/sec.}$$

The response equation now becomes

$$\frac{P(s)}{P_0 c_0 V_0} = \left(\frac{1}{44} \right) \frac{1}{\left[1 + 0.176s/66 + s^2/(66)^2 \right]}.$$

The inversion of the above equation may be easily accomplished and yields

$$\frac{P(t)}{P_0 c_0 V_0} = 1.5 e^{-5.8t} \sin(66t).$$

This approximate solution is shown plotted in Figure 8.9 in comparison with the exact results given previously in Chapter IV. The approximate model appears to match well the exact result from a frequency standpoint and also in regard to the attenuation of the fundamental frequency component. For many typical engineering calculations, results such as this would be welcome considering the difficulties encountered in obtaining exact answers.

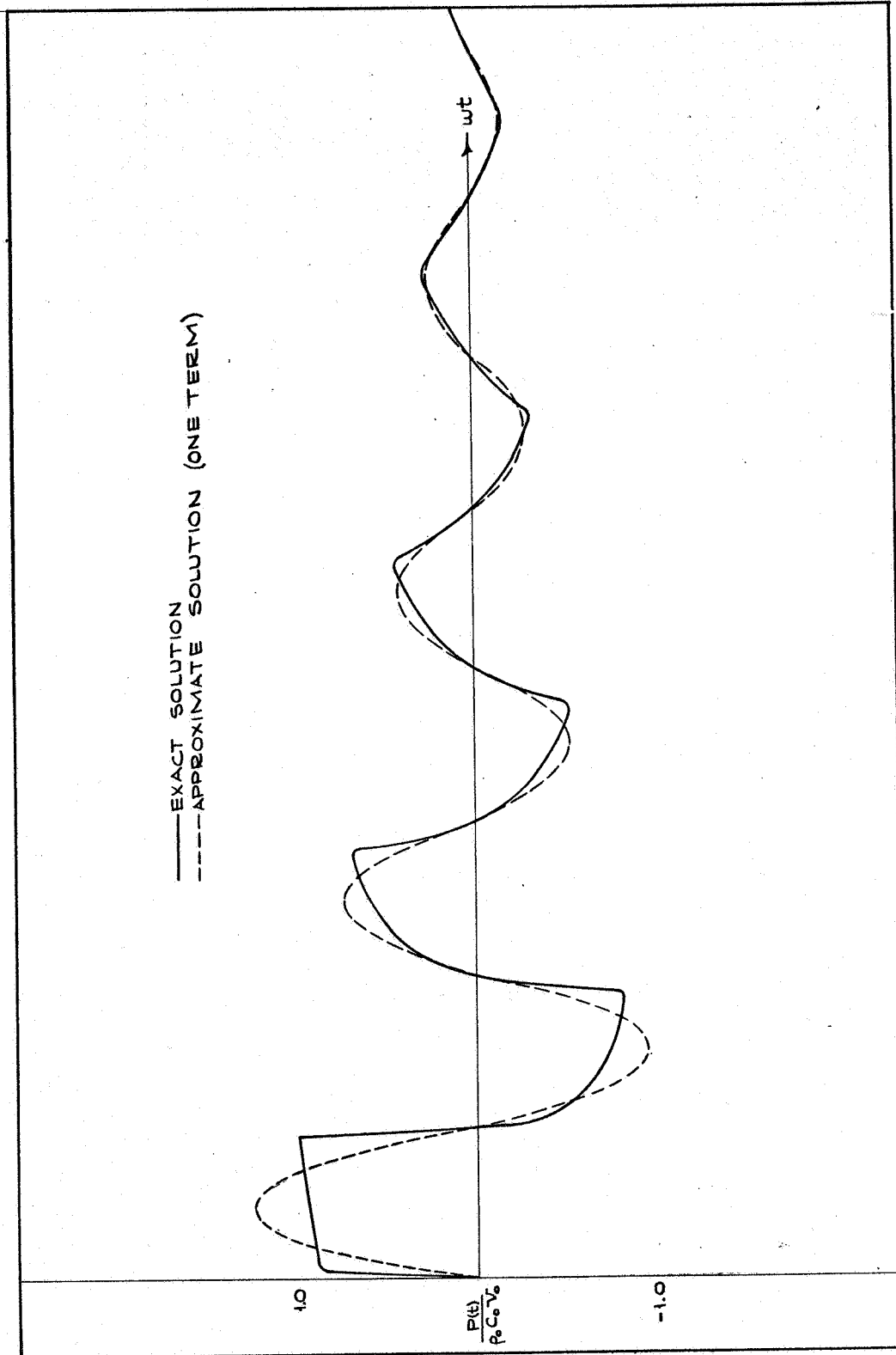


Figure 8.9. Comparison of Exact Solution (Zeroth Mode) and One Term of the Tapered-Lumped Model for the Water Hammer Problem

Application of Model in Problem Solution

In this section, use will be made of the approximate model in the solution of two typical problems. In this way, its utility can be demonstrated.

Example Problem 1

Consider the fluid system illustrated in Figure 8.10. Water is initially flowing from one reservoir through the line and valve into another reservoir. The valve is then closed in such a manner that the valve area versus time history is as shown in Table IV. The problem is to determine the corresponding pressure history upstream of the valve.

The Laplace domain response equation for the pressure upstream of the valve in terms of the corresponding fluid velocity is the same as for the water hammer problem of Chapter IV. This response equation is

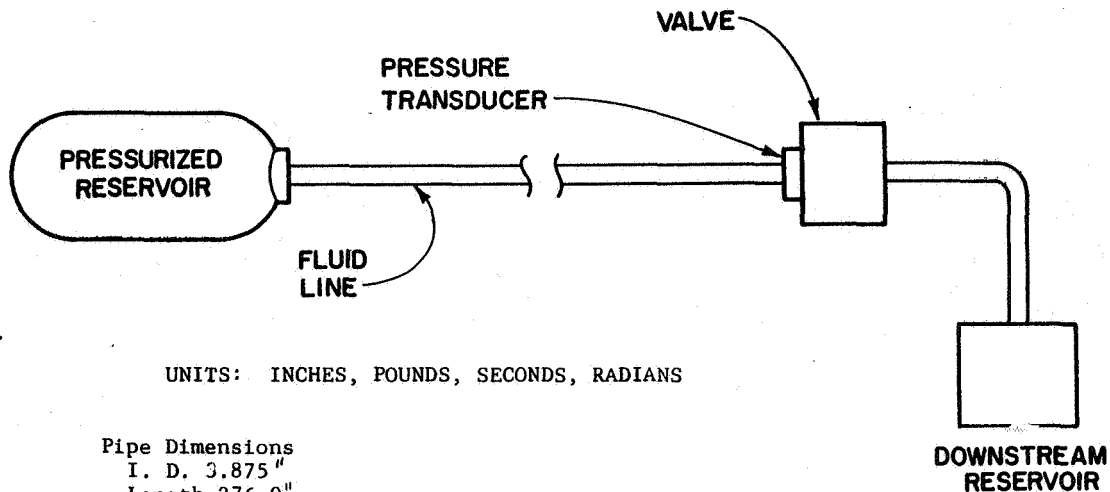
$$P(s) = -Z_c(s) \tanh \Gamma(s) V(s).$$

Utilizing one term of the approximate model yields

$$(1 + 2S_{co}s/\omega_{co} + s^2/\omega_{co}^2) P(s) = -\rho_0 L_0 \left(\frac{SL}{L_0} \right) V(s). \quad (8.6)$$

For the problem here being considered, this response equation can best be solved in the time domain since the valve area history is a complicated polynomial in time. Expressing Equation (8.6) in the time domain yields (including a linear flow resistance term, $R_1 q(t)$)

$$(1 + 2S_{co}D/\omega_{co} + D^2/\omega_{co}^2) P(t) = \frac{\rho_0 L}{A_L} Dq(t) - R_1 q(t). \quad (8.7)$$



UNITS: INCHES, POUNDS, SECONDS, RADIANS

Pipe Dimensions
 I. D. 3.875"
 Length 276.0"
 Wall Thickness 0.0625"
 Youngs Modulus of Elasticity 12×10^6

Adiabatic Modulus of Elasticity of Fluid 32×10^4
 Atmospheric Pressure 8.7 (Static pressure maintained below
 valve during closure, psia).
 Fanning Friction Factor 0.012
 Initial Static Pressure at Valve 21.42 psia
 Fluid Density at Valve 0.036995

Figure 8.10. Schematic of Physical Layout for Example Problem 1

TABLE IV

VALVE AREA DATA FOR EXAMPLE PROBLEM 1

Effective Flow Area of Valve vs Time

Time	Area
0.000	8.34
0.010	8.30
0.030	7.49
0.050	6.36
0.078	4.74
0.110	3.47
0.142	2.39
0.175	1.57
0.205	.84
0.236	.35
0.261	.00

$$Q(t) = A_v \sqrt{\frac{2g \Delta P}{\rho (1 - A_v^2/A_c^2)}}$$

9th degree equation of above points

$$\text{Area} = 36,098,169T^9 - 27,651,150T^8 + 5,290,046T^7 + 662,432T^6 - 210,542T^5 - 41,747T^4 + 16,928T^3 - 1,707T^2 + 9.226T + 8.347$$

Here, $q(t)$ is the flow rate at the valve.

Solution of Equation (8.7) has been carried out on the digital computer and the results are plotted in Figure 8.11. Also shown in this figure are results of an experiment carried out at the Marshall Space Flight Center, Huntsville, Alabama. The analytical predictions agree well with the experimental results in the early stages of valve closure but deviate considerably in the later stages. This deviation is believed to be principally due to error in the analytical expression for the valve area compared with the actual valve area which occurred during the experiment.

Example Problem 2

For this example consider the simple hydraulic system shown in Figure 8.12. It is assumed that the dynamics of the valve and load are described by the three equations

$$m \frac{d^2x}{dt^2} + b \frac{dx}{dt} + kx = K_y(t) - P_1 A \quad (8.8)$$

$$q_1 = C \Delta p x \quad (8.9)$$

and

$$P_2 = Z_L q_2. \quad (8.10)$$

The constants of the system are given below.

$$m = 0.0002 \text{ lb-sec}^2/\text{in}$$

$$b = 0.01 \text{ lb-sec/in}$$

$$k = 50 \text{ lb/in}$$

$$A = 0.2 \text{ in}^2$$

$$C = 0.00126 \text{ in}^4/\text{lb-sec}$$

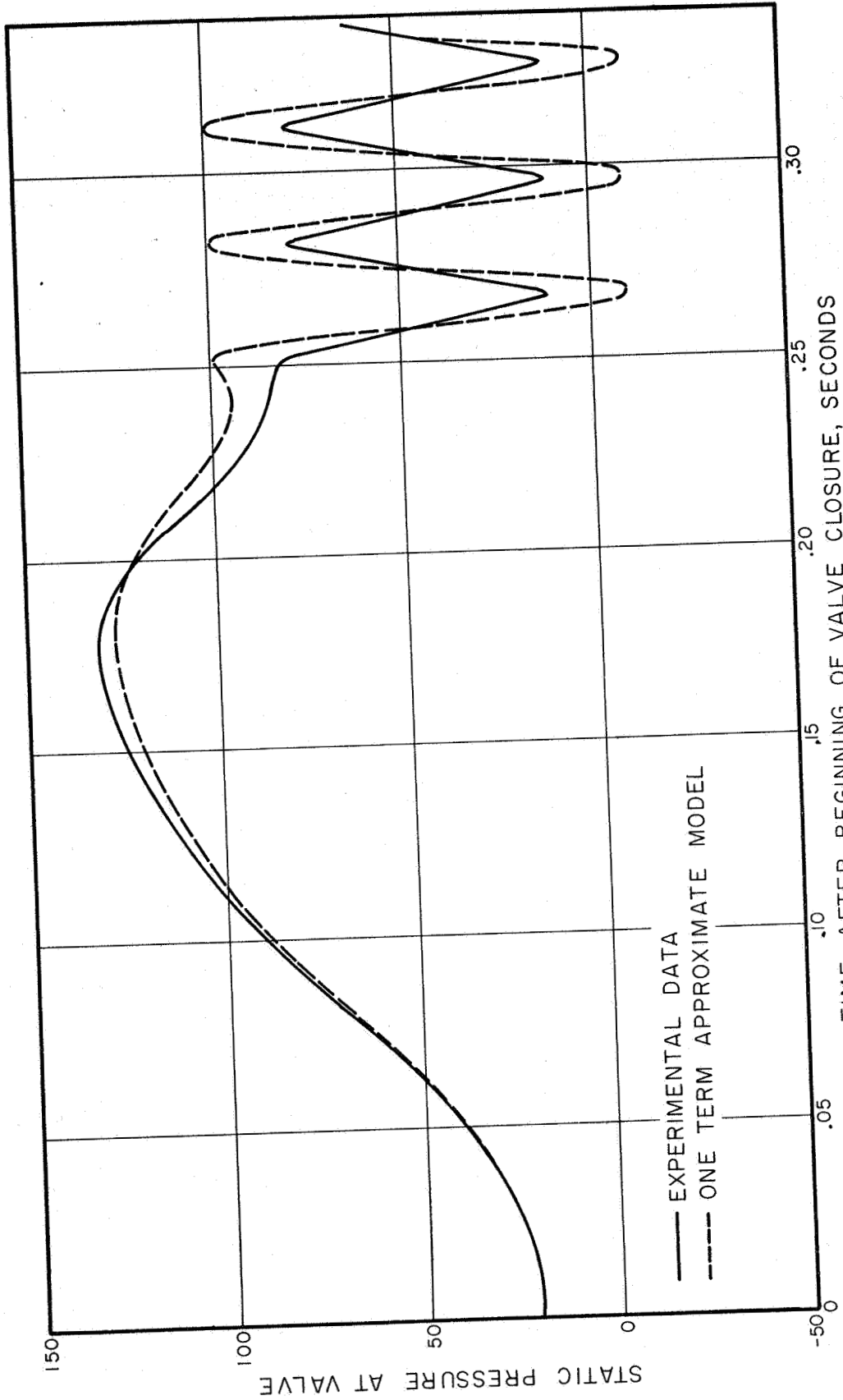


Figure 8.11. Comparison of Analytical Prediction Using One Term of Model With Experimental Results Obtained by NASA

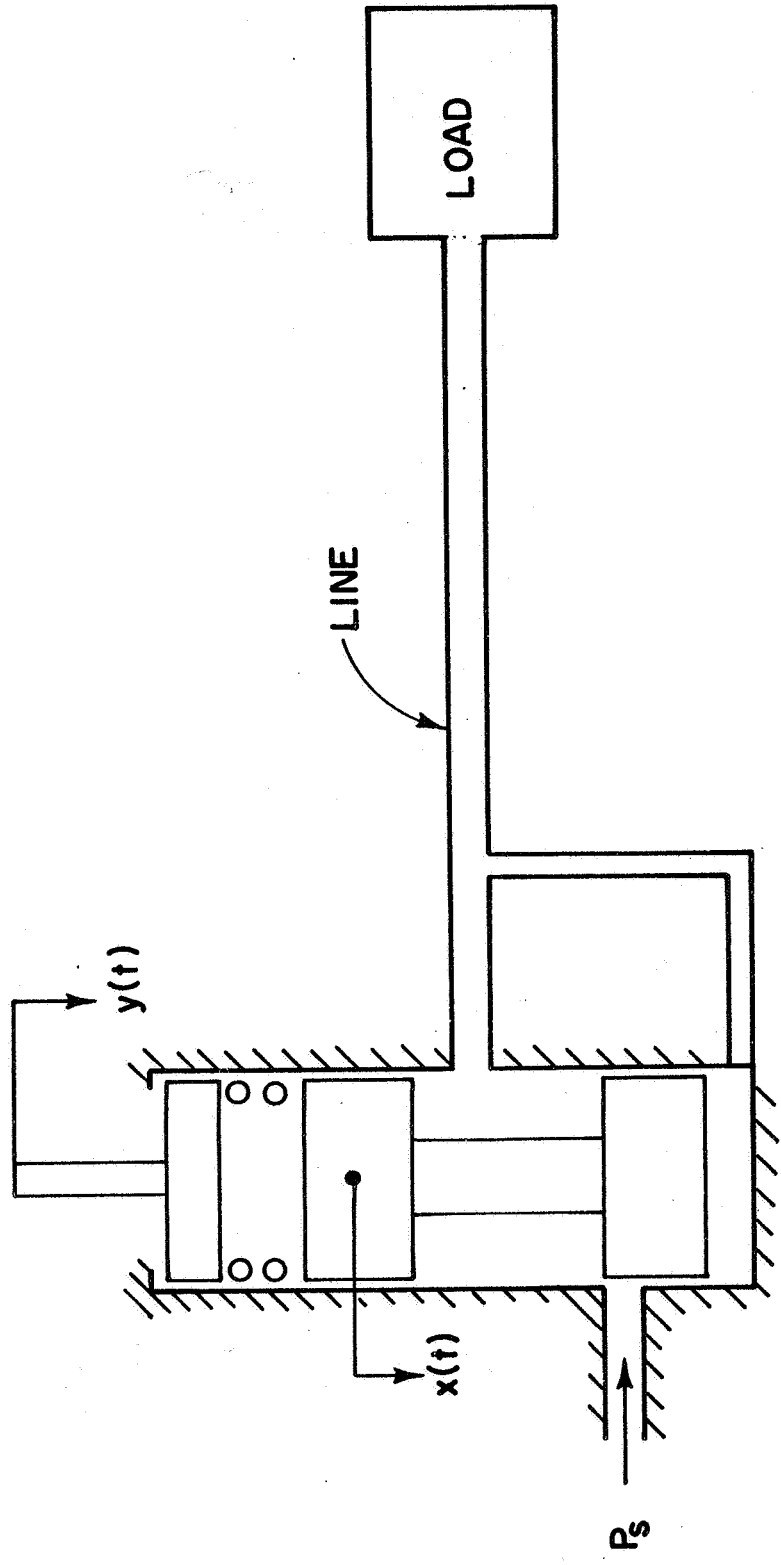


Figure 8.12. Schematic of Physical Layout for Example Problem 2

$$\begin{aligned}
 Z_1 &= 43. \text{ lb-sec/in}^5 \\
 \rho_0 &= 0.0000812 \text{ lb-sec}^2/\text{in.}^4 \\
 \Delta p &= 500 \text{ psi} \\
 L &= 10 \text{ ft} \\
 r_0 &= 0.2 \text{ in} \\
 \nu &= 10^{-4} \text{ ft}^2/\text{sec} \\
 c_0 &= 4500 \text{ ft/sec.}
 \end{aligned}$$

A frequency analysis of the valve will be made by first neglecting line effects and next by including a one-term approximation of the line. Considering first no line effects, the Laplace domain equation describing the displacement of the valve in terms of the input Y is

$$X(s) = \frac{K Y(s)}{[ms^2 + bs + (k + CZ_L \Delta p)]} \quad (8.11)$$

A plot of the amplitude and phase of $X(i\omega)/Y(i\omega)$ is shown in Figure 8.13.

It is desired now to include the line effects by modeling it with one term of the approximate model. First calculating the line axial damping number to allow the use of Figures 8.1 and 8.2 for finding the line parameters ξ_{c_0} and ω_{c_0} gives

$$D_{N2} = \frac{\nu L}{c_0 r_0^2} = 8 \times 10^{-4}$$

Thus,

$$\cosh \Gamma(s) \approx \left\{ 1 + 2\xi_{c_0} s / \omega_{c_0} + s^2 / \omega_{c_0}^2 \right\}$$

$$\sinh \Gamma(s) \approx sL / c_0$$

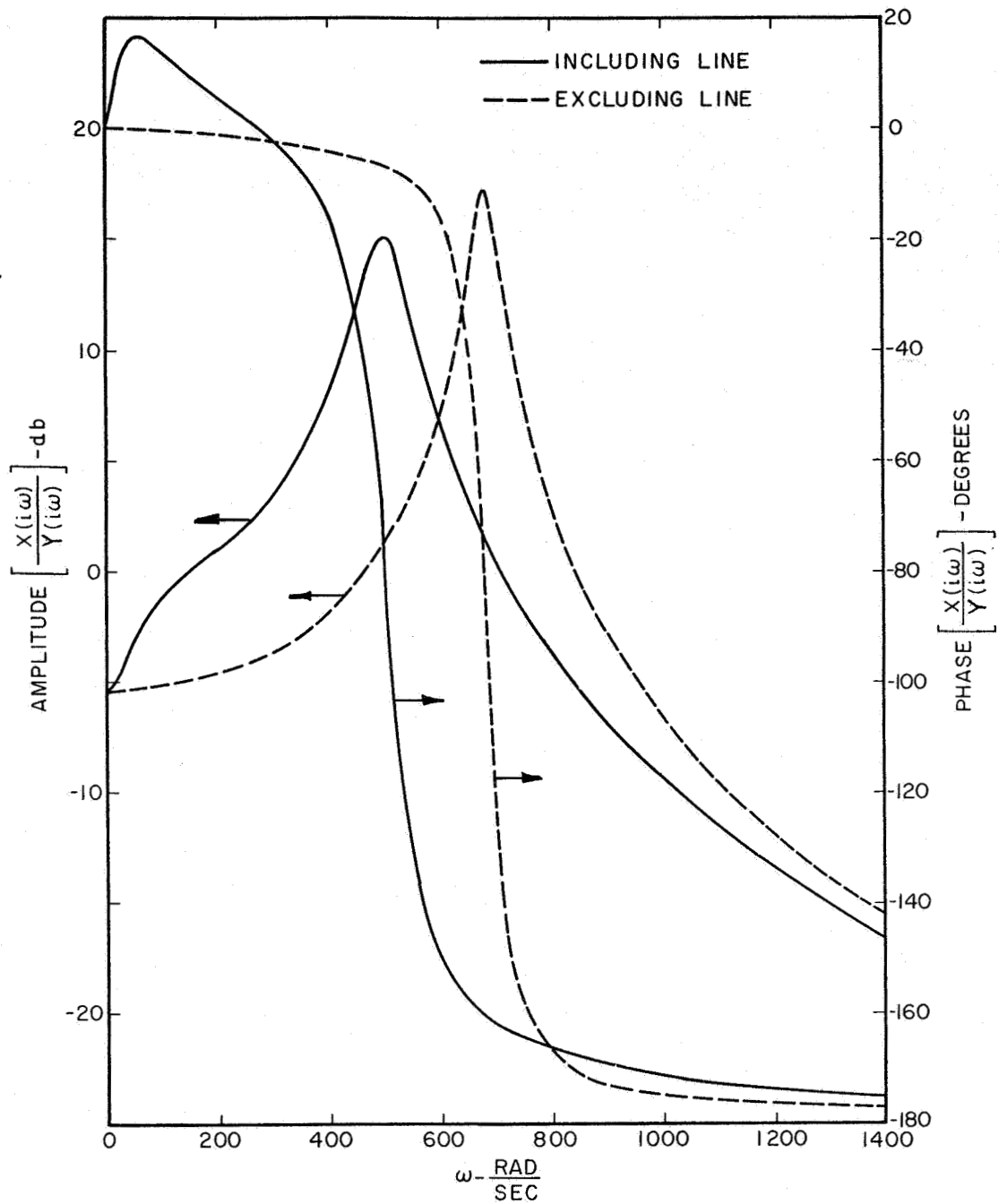


Figure 8.13. Amplitude and Phase of $X(i\omega)/Y(i\omega)$ Versus Frequency With and Without Line Effects for Example Problem 2

with

$$\xi_{co} = 0.05, \omega_{co} = 353.0.$$

This leads to

$$\begin{aligned} Q_1 &= Q_2 \cosh \Gamma + \frac{P_2}{Z_c} \sinh \Gamma \\ &\approx \frac{P_2}{Z_L} \left\{ 1 + \frac{2\xi_{co} s}{\omega_{co}} + \frac{s^2}{\omega_{co}^2} \right\} + \frac{P_2}{Z_c} \left(\frac{SL}{L_0} \right) \end{aligned} \quad (8.12)$$

and

$$\begin{aligned} P_1 &= P_2 \cosh \Gamma + Z_c Q_2 \sinh \Gamma \\ &\approx \left\{ 1 + \frac{2\xi_{co} s}{\omega_{co}} + \frac{s^2}{\omega_{co}^2} + \frac{Z_c}{Z_L} \left(\frac{SL}{L_0} \right) \right\} P_2. \end{aligned} \quad (8.13)$$

Combining Equation (8.8), (8.9), (8.10), (8.12), and (8.13) gives a response relation for $X(s)$ in terms of $Y(s)$ or

$$X(s) = \frac{K Y(s)}{[ms^2 + bs + k + C \Delta \rho G(s)]} \quad (8.14)$$

where

$$G(s) = \frac{\left[1 + \frac{2\xi_{co} s}{\omega_{co}} + \frac{s^2}{\omega_{co}^2} + \frac{Z_c}{Z_L} \left(\frac{SL}{L_0} \right) \right]}{\frac{1}{Z_L} \left[1 + \frac{2\xi_{co} s}{\omega_{co}} + \frac{s^2}{\omega_{co}^2} \right] + \frac{1}{Z_c} \left(\frac{SL}{L_0} \right)}. \quad (8.15)$$

The amplitude and phase of $X(i\omega)/Y(i\omega)$ from Equation (8.14) is plotted in Figure 8.13 in comparison with the results of Equation (8.11) which was for no line effects. There is a dramatic difference between the results of neglecting and including line effects. The simplicity of

using the approximate line model in this analysis is also apparent.

Discussion

In this chapter, an approximate engineering model of a fluid conduit, based upon infinite product expansions of the $\cosh \Gamma(s)$ and $\sinh \Gamma(s)$ operators in terms of second-order polynomials, has been presented. The basic idea for this development was obtained from a paper by Oldenberger and Goodson (12). The writer has, however, extended the method to the extent that it is now possible to obtain the necessary polynomial coefficients from the curves presented herein. Thus, the method might now be considered a handbook engineering method. The validity of the method was examined by comparing it with "exact" model results from Chapter IV and also by demonstrating its ability to predict experimental results. The results of this examination may be summarized as follows:

1. One term of the model well approximates the hyperbolic operators up to the first critical frequency.
2. Two terms improve the approximation up to the first critical point and roughly (not well) approximate the hyperbolic operators up beyond the second critical frequency. The use of more terms would improve the results near the second critical frequency.
3. The use of one term of the model gave good results in predicting the transient response representative of water hammer.
4. The model was of good utility in solving two example problems, one which had supporting experimental data.

CHAPTER IV

SUMMARY, CONCLUSIONS, AND RECOMMENDATIONS

Summary

The problem of modeling a fluid transmission line has been treated in varying degrees of exactness.

An exact solution of the first-order Navier-Stokes equation for a compressible liquid was obtained and found to demonstrate the existence of an infinite set of viscous modes of propagation. The zeroth mode was found to be predominate, with the higher modes being generated near boundaries. The extent of propagation for the higher modes depended upon the frequency since these modes had relative cutoff frequencies below which there was considerable attenuation. Through the use of a flow visualization method, the action of the higher modes near an oscillating piston was experimentally observed.

A conduit model based upon a cross-sectional average of the zeroth mode only was derived in terms of a set of transfer type equations commonly found in the literature. Experimental investigation of these equations proved their validity over a wide range of parameters, thus qualifying this as a useful engineering model.

A third model, based upon rational approximations of the zeroth mode transfer equation model was derived and the parameters were obtained and recorded. This model was demonstrated to have usefulness

where it is desired to study complex fluid systems and where the mathematics involved in using the more sophisticated models would prove unwieldy.

An analytical investigation into the effects of nonrigid walls was undertaken and demonstrated the dramatic and not-to-be-neglected effect which these walls can have. Calculations were made to determine the effect of an elastic flexible wall upon the wave phase velocity and spatial attenuation as opposed to a rigid wall. For the case presented, it was found that the spatial attenuation was increased by approximately a thousandfold and the phase velocity decreased by approximately 75 per cent in certain frequency ranges.

Conclusions

The conclusions which have been reached as a result of this study are:

1. In general, the first-order (acoustic) disturbances in a viscous fluid transmission line consist of an infinite number of modes of viscous propagation. The excitation of each mode results from the necessity of satisfying boundary conditions. The extent of spatial propagation of each mode depends upon the frequency.
2. The conduit model based upon a cross-sectional average of the zeroth mode only is valid at least for the range of damping numbers and frequency numbers

$$0.0001 < D_{nz} < 0.02$$

$$0.5 < F_{nz} < 10.0.$$

3. The conduit model based upon rational approximations of the zeroth mode transfer equation model is useful for studying the dynamic response of complex fluid systems.
4. Wall elasticity effects should be considered when modeling fluid transmission lines with increases in the spatial attenuation of the order of 1000 and decreases in the phase velocity of the order of 75 per cent demonstrated for one case in this treatise.

Recommendations for Future Study

Areas which it is felt are worthy of future study include:

1. Investigation of the effect of a net flow upon disturbance propagation. This investigation should include laminar and turbulent flow.
2. Investigate further the effects of nonrigid walls upon viscous propagation.
3. Look into the effect of discontinuities and non-uniform cross-sectional area upon viscous propagation in a fluid conduit.

SELECTED BIBLIOGRAPHY

- (1) Hunt, F. V. "Notes on the Exact Equations Governing the Propagation of Sound in Fluids," Journal of the Acoustical Society of America, Vol. 27, November, 1955, pp. 1019-1039.
- (2) Schlichting, H. Boundary Layer Theory. New York: McGraw-Hill Book Co., Inc., 1960.
- (3) Bird, R. B., W. E. Steward, and E. N. Lightfoot. Transport Phenomena. New York: John Wiley and Sons, Inc., 1960.
- (4) Joukowsky, N. "Water Hammer," Proceedings American Water Works Association, 1904, p. 341.
- (5) Allievi, Lorenzo. "Theory of Water Hammer," translated by E. E. Halmos, 1925. See "Symposium on Water Hammer," ASME publication, 1933, Second Printing, 1949.
- (6) Rich, G. R. Hydraulic Transients. New York: McGraw-Hill Book Co., Inc., 1955.
- (7) Paynter, H. M. "Section 20, Fluid Transients in Engineering Systems," from Handbook of Fluid Dynamics, by V. L. Streeter, Ed. New York: McGraw-Hill Book Co., Inc., 1961.
- (8) Bergeron, L. J. B. Water Hammer in Hydraulics and Wave Surges in Electricity, ASME Publication, 1961.
- (9) Rouleau, W. T. "Pressure Surges in Pipelines Carrying Viscous Liquids," Trans. ASME, Vol. 82, 1960, pp. 912-920.
- (10) Walker, M. L., Jr., E. T. Kirkpatrick, and W. T. Rouleau. "Viscous Dispersion in Water Hammer," Trans. ASME, Vol. 82, 1960, pp. 759-764.
- (11) Schuder, C. B., and R. C. Binder. "The Response of Pneumatic Transmission Lines to Step Inputs," Trans. ASME, Series D, Vol. 81, 1959, pp. 578-584.
- (12) Oldenburger, R., and R. E. Goodson. "Simplification of Hydraulic Line Dynamics by Use of Infinite Products," Trans. ASME, Series D, Vol. 86, 1964, pp. 1-10.

- (13) Schiesser, Boonshaft, and Fuchs, Inc. "The Frequency Response of an Actuator Supplied by Two Long Hydraulic Lines," Trans. AIChE, 1964 Joint Automatic Control Conference, Stanford University.
- (14) Sarlat, I. M., and T. L. Wilson. "Surge Pressures in Liquid Transfer Lines," Trans. ASME, Vol. 84, 1962, pp. 363-368.
- (15) Waller, E. J. "Response of Pipe Line Systems to Transient Flow Using the Generalized Impedance Method," Oklahoma State Engineering Experiment Station Publication, Oklahoma State University, January, 1960.
- (16) Brown, F. T. "The Transient Response of Fluid Lines," Trans. ASME, Series D, Vol. 84, 1962, pp. 547-553.
- (17) D'Souza, A. F., and R. Oldenburger. "Dynamic Response of Fluid Lines," Trans. ASME, September, 1964, pp. 589-598.
- (18) Watson, G. N. A Treatise on the Theory of Bessel Functions. Cambridge: Cambridge University Press, 1958, pp. 77-83, Appendix, p. 78, p. 498.
- (19) Nichols, N. B. "The Linear Properties of Pneumatic Transmission Lines," ISA Trans., Vol. 1, January, 1962, pp. 5-14.
- (20) Iberall, A. S. "Attenuation of Oscillatory Pressures in Instrument Lines," Journal of Research, National Bureau of Standards, Vol. 45, July, 1950, pp. 85-108.
- (21) Blackburn, J. F. Gerhard Reethof, and J. L. Shearer. Fluid Power Control. Cambridge, Mass.: The M.I.T. Press, 1960.
- (22) Waller, E. J., L. E. Hove, and W. D. Bernhart. "Liquidborne Noise Reduction," Volumes I, II, and III, Engineering Report, Oklahoma State University, 1963.
- (23) Pipes, L. A. "The Matrix Theory of Four-Terminal Networks," Philosophical Magazine, Vol. 30, 1940, pp. 370-395.
- (24) Technical Documentary Report No. APL TDR 64-109, "Research Investigation of Hydraulic Pulsation Concepts," October, 1964.
- (25) Paynter, H. M. U. S. Patent No. 3044703; Filed on June 24, 1954, Issued on July 17, 1962.
- (26) Lamb, H. "On the Velocity of Sound in a Tube, as Affected by the Elasticity of the Walls," Manchester Memoirs, Vol. XLII (1898) No. 9, pp. 1-16.

- (27) Jacobi, W. J. "Propagation of Sound Waves Along Liquid Cylinders," Journal of the Acoustical Society of America, Vol. 21, 1949, pp. 120-127.
- (28) Morgan, G. W., and J. P. Kiely. "Wave Propagation in Viscous Liquid Contained in a Flexible Tube," Journal of the Acoustical Society of America, Vol. 26, May, 1954, pp. 323-328.
- (29) Lin, T. C., and G. W. Morgan. "Wave Propagation Through Fluid Contained in a Cylindrical, Elastic Shell," Journal of the Acoustical Society of America, Vol. 28, November, 1956, pp. 1165-1176.
- (30) Skalak, R. "An Extension of the Theory of Water Hammer," Trans. ASME, Vol. 78, 1956, pp. 105-116.
- (31) Ingard, Uno. "On the Radiation of Sound Into a Circular Tube With an Application to Resonators," Journal of the Acoustical Society of America, Vol. 20, September, 1948, pp. 665-682.
- (32) Kaplan, W. Advanced Calculus. Reading, Penn.: Addison-Wesley Publishing Company, Inc., p. 395.
- (33) Thurston, G. B., and J. L. Schrag. "Shear Wave Propagation in a Birefringent Viscoelastic Medium," Journal of Applied Physics, Vol. 35, 1964, p. 141.
- (34) Frenkel, J. Kinetic Theory of Liquids. New York: Oxford University Press, 1946, p. 288.
- (35) Morse, P. M., and H. Feshbach. Methods of Theoretical Physics. New York: McGraw-Hill Book Company, p. 1459.
- (36) Lin, T. C., and G. W. Morgan. "A Study of Axisymmetric Vibrations and Cylindrical Shells as Affected by Rotatory Inertia and Transverse Shear," Transactions ASME, Vol. 78, 1956 pp. 255-261.

APPENDIX A

CALCULATION OF EIGENVALUES

CALCULATION OF EIGENVALUES

The purpose of this Appendix is to demonstrate the calculation procedure used to obtain the eigenvalues from the characteristic equations.

Consider Equations (3.32) and (4.3), or

$$\gamma_n^2 = k_n^2 + \frac{S}{D} = \beta_n^2 + \frac{S^2}{c_0^4 + \frac{4}{3} \nu S} \quad (\text{A.1})$$

and

$$k_n \beta_n \frac{J_1(\beta_n r_0)}{J_0(\beta_n r_0)} = \gamma_n^2 \frac{J_1(k_n r_0)}{J_0(k_n r_0)} \quad (\text{A.2})$$

which are the characteristic equations for the eigenvalues of a rigid fluid conduit. In order that the calculations can be based upon dimensionless numbers, define

$$G_n = \gamma_n r_0$$

$$B_n = \beta_n r_0$$

$$k_n = k_n r_0$$

$$FN = sr_0/c_0$$

and

$$DN = \nu/c_0 r_0$$

where each is dimensionless.

Equations (A.1) and (A.2) now become

$$G_n^2 = K_n^2 + FN = B_n^2 + \frac{FN^2}{1 + \frac{4}{3}(FN)(DN)} \quad (\text{A.3})$$

and

$$K_n B_n \frac{J_1(B_n)}{J_0(B_n)} = G_n^2 \frac{J_1(K_n)}{J_0(K_n)}. \quad (\text{A.4})$$

The actual calculation here must be a numerical trial and error procedure. Hence, define

$$E = K_n B_n \frac{J_1(B_n)}{J_0(B_n)} - G_n^2 \frac{J_1(K_n)}{J_0(K_n)} \quad (\text{A.5})$$

and start the calculation by assuming a value for B_n . This is then used to calculate K_n and G_n from Equation (A.3). Knowing B_n , G_n , and K_n (for a given value of F and D) we can calculate E . In order to know how to adjust B_n , calculate dE/dB_n and adjust B_n from the equation

$$B_{n1} = B_{n0} - \frac{E}{dE/dB_n}$$

where B_{n1} represents the new value and B_{n0} the previous value. A listing of the computer program used to perform these calculations is given on the following page. The data read in are:

DN = damping number

FNO = initial value of frequency number

DFN = increment in frequency number

FNM = maximum value of frequency number

BOX = starting value of Real (B_n)

BOY = starting value of Imaginary (B_n).

```

C      CALCULATION OF HIGHER MODE EIGENVALUES
      COMPLEX B,F,CK,CK2,RJB,RJK,CT1,CT2,E
      COMPLEX T1,T2,T3,T4,T5,DB,G2,G
20     FORMAT(7F10.8)
21     FORMAT(7F11.8)
22     FORMAT(2X,F11.8,2E15.8,2X,2E15.8)
1      READ(5,20)DN,FNO,DFN,FNM,BOX,BOY,ER
2      WRITE(6,21)DN,FNO,DFN,FNM,BOX,BOY,ER
      B=CMPLX(BOX,BOY)
      FN=FNO
10     F=CMPLX(0.,FN)
7      CK2=B**2+F**2-F/DN
      CK=CSQRT(CK2)
      IF(AIMAG(CK2))3,4,4
3      CK=-CK
4      CALL JOORJ1(CK,RJK)
      CALL JOORJ1(B,RJB)
      G2=B**2+F**2
      CT1=CK*B*RJB
      CT2=G2*RJK
      E=CT1-CT2
      R1=CABS(E)/CABS(CT1)
      IF(R1-ER)6,6,5
5      T1=RJB*(B**2/CK+CK)
      T2=B*CK*((1.,0.)-RJB/B+RJB**2)
      T3=2.*B*RJK
      T4=(B/CK)*G2*((1.,0.)-RJK/CK+RJK**2)
      T5=T1+T2-T3-T4
      DB=-E/T5
      B=B+DB
      GO TO 7
6      G=CSQRT(G2)
      IF(AIMAG(G2))8,9,9
8      G=-G
9      GX=REAL(G)
      GY=AIMAG(G)
      CCO=FN/GY
      WRITE(6,22)FN,GX,CCO,B
      FN=FN+DFN
      IF(FN-FNM)10,10,11
11     GO TO 1
12     STOP
      END

```

```

SUBROUTINE JOORJ1(Z,RJ)
C      CALCULATION OF J0Z AND J1Z
COMPLEX Z,J1,J0,TERMO,TERM1,Z1,Z2,P0,Q0,P1,Q1,PH0,PH1,FZ1,FZ2,RJ
X=REAL(Z)
Y=AIMAG(Z)
R=CABS(Z)
IF(R-18.)100,100,110
100  TERM1=Z/2.
      J1=Z/2.
      J0=(1.,0.)
      TERMO=(1.,0.)
      A=1.
      AM=7.+P.
101  TERMO=TERMO*(-(Z/2.)**2)/A**2
      J0=J0+TERMO
      TERM1=TERM1*(-(Z/2.)**2)/((A+1.)*A)
      J1=J1+TERM1
      A=A+1.
      IF(A-AM)101,101,115
110  IF(X)111,112,112
111  Z1=-Z
      GO TO 113
112  Z1=Z
113  PI=3.1415926
      Z2=8.*Z1
      IF(CABS(Z2)-5000.)120,120,121
120  P0=(1.,0.)-4.5/Z2**2+3675./(8.*Z2**4)
      Q0=-1./Z2+37.5/Z2**3-59535./(8.*Z2**5)
      P1=(1.,0.)+7.5/Z2**2-4725./(8.*Z2**4)
      Q1=3./Z2-52.5/Z2**3+6615./(8.*Z2**5)
      GO TO 122
121  P0=(1.,0.)-4.5/Z2**2
      Q0=-1./Z2
      P1=(1.,0.)+7.5/Z2**2
      Q1=3./Z2
122  PH0=Z1-PI/4.
      PH1=Z1-.75*PI
      FZ1=2./PI*Z1
      FZ2=CSQRT(FZ1)
      AZ1=AIMAG(Z1)
      IF(ABS(AZ1)-50.)116,116,117
116  J0=FZ2*(P0*CCOS(PH0)-Q0*CSIN(PH0))
      J1=FZ2*(P1*CCOS(PH1)-Q1*CSIN(PH1))
      IF(X)114,115,115
114  J1=-J1
115  RJ=J1/J0
      GO TO 119
117  RJ=((0.,1.)*P1+Q1)/(P0-(0.,1.)*Q0)
119  RETURN
      END

```


APPENDIX B

INVERSE LAPLACE TRANSFORMATION FOR
VISCOUS WATER HAMMER PROBLEM

INVERSE LAPLACE TRANSFORMATION FOR
 VISCOUS WATER HAMMER PROBLEM

In this Appendix, the method employed in the calculation of the pressure history for the viscous water hammer problem, as presented in Chapter IV, will be given.

It has been shown (Chapter IV) that the transformed pressure response output to a transformed velocity input is

$$P(s) = -Z_c(s) V(s) \tanh \Gamma(s) \quad (\text{B.1})$$

where

$$\Gamma(s) = \frac{sL}{c_0 [F(s)]^{1/2}}$$

$$Z_c(s) = \frac{\rho_0 c_0}{[F(s)]^{1/2}}$$

$$F(s) = 1 - \frac{2 J_1(kr_0)}{kr_0 J_0(kr_0)}$$

and

$$k = i \sqrt{\frac{s}{\nu}}$$

Putting $V(s) = -V_0/s$, which represents the transformed input due to sudden valve closure; V_0 being the initial fluid velocity before

closure, gives

$$P(s) = V_0 \frac{Z_c(s)}{s} \tanh \Gamma(s). \quad (\text{B.2})$$

The inverse transformation of Equation (B.2) may be written as

$$p(t) = \sum_{\text{Residues}} \left\{ V_0 \left(\frac{Z_c(s)}{s} \right) \left(\frac{\sinh \Gamma(s)}{\cosh \Gamma(s)} \right) e^{st} \right\}. \quad (\text{B.3})$$

This summation will now be evaluated.

For convenience, Equation (B.3) may be written in the form

$$\frac{p(t)}{V_0 L_0 \rho_0} = \sum_{\text{Residues}} \left\{ \frac{\sinh \Gamma(s) e^{st}}{s [F(s)]^{1/2} \cosh \Gamma(s)} \right\} \quad (\text{B.4})$$

The poles which contribute residues to the above summation are given by

$$\cosh \Gamma(s) = 0$$

or

$$\Gamma(s_n) = \pm i \left(\pi/2 + n\pi \right).$$

The corresponding residues are given by

$$\begin{aligned} R_n &= \left\{ \frac{\sinh \Gamma(s) e^{st}}{s [F(s)]^{1/2} d \cosh \Gamma / ds} \right\}_{s=s_n} \\ &= \left\{ \frac{e^{st}}{s [F(s)]^{1/2} \Gamma'(s)} \right\}_{s=s_n}. \end{aligned}$$

A listing of the computer program written to calculate and sum these residues is given on the following page.

```

C      VISCIOUS WATER HAMMER PROBLEM
      COMPLEX F(100),T1,T2,T3,T4(100),FC(100),T1C,T2C,T3C,T4C(100),SUM
      COMPLEX FN,FKNRO,FF,DIF1,FN1,E2,E3,FNN,E4,RJ
2      FORMAT(I5,5F10.7)
11     FORMAT(7X,F15.8,E15.8,E15.8)
1      READ(5,2)NM,DN,DT,TM,G,TO
      WRITE(6,2)NM,DN,DT,TM,G,TO
      DO 7 N=1,NM
      PI=3.1415926
      A=N-1
      P1=(A+.5)*PI
      E1=.0001
      FNN=CMPLX(E1,P1)
      FN=FNN
4      E2=-FN/DN
      FKNRO=CSQRT(E2)
      IF(AIMAG(E2))13,14,14
13     FKNRO=-FKNRO
14     CALL JOORJ1(FKNRO,RJ)
      FF=(1.,0.)-2.*RJ/FKNRO
      ZERO=0.
      E3=CMPLX(ZERO,P1)
      E4=CSQRT(FF)
      IF(AIMAG(FF))15,16,16
15     E4=-E4
16     FN1=E3*E4
      DIF1=(FN1-FN)/FN1
      DIF2=(CABS(FN1)-CABS(FN))/CABS(FN1)
      IF(DIF2-G)6,6,5
5      FN=FN1
      GO TO 4
6      F(N)=FN1
      T1=F(N)**2/((A+.5)*PI)**2
      T2=F(N)/(DN*T1)
      T3=.5+T2*(1.+T1)**2/8.
      T4(N)=F(N)*(1.+T3)
      FC(N)=CONJG(F(N))
      T1C=FC(N)**2/((A+.5)*PI)**2
      T2C=FC(N)/(DN*T1C)
      T3C=.5+T2C*(1.+T1C)**2/8.
7      T4C(N)=FC(N)*(1.+T3C)
      T=TO
8      SUM=(0.,0.)
      DO 10 N=1,NM
10     SUM=SUM+CEXP(F(N)*T)/T4(N)+CEXP(FC(N)*T)/T4C(N)
      WRITE(6,11)T,SUM
      T=T+DT
      IF(T-TM)8,8,12
12     GO TO 1
17     STOP

```

APPENDIX C

COMPUTER PROGRAM LISTINGS

```

C      CALCULATION OF ZC
      COMPLEX CFN,G2,FKNRO,FF,G4,Z,RJ
2      FORMAT(4F15.8)
3      FORMAT(1F15.8)
4      FORMAT(2X,1F15.4,4X,E15.8,2X,E15.8)
1      READ(5,2)DN,FNO,DFN,FNM
      WRITE(6,3)DN
      FN=FNO
      PI=3.1415926
90     CFN=CMPLX(0.,FN)
      G2=-CFN/DN
      FKNRO=CSQRT(G2)
      IF(AIMAG(G2))91,92,92
91     FKNRO=-FKNRO
92     CALL JOORJ1(FKNRO,RJ)
      FF=(1.,0.)-2.*RJ/FKNRO
      G4=CSQRT(FF)
      IF(AIMAG(FF))93,94,94
93     G4=-G4
94     Z=1./G4
      ZX=REAL(Z)
      ZY=AIMAG(Z)
      AZ=CABS(Z)
      PHZ=ATAN2(ZX,ZY)
      PHZD=(180./3.1415926)*PHZ
      WRITE(6,4)FN,AZ,PHZD
      FN=FN+DFN
      IF(FN-FNM)90,90,8
8      GO TO 1
9      STOP
      END

C      CALCULATION OF GAMMA
      COMPLEX CFN,G2,FKNRO,FF,G4,GAMA,RJ
2      FORMAT(4F15.8)
3      FORMAT(1F15.8)
4      FORMAT(2X,1F15.4,4X,E15.8,2X,E15.8)
1      READ(5,2)DN,FNO,DFN,FNM
      WRITE(6,3)DN
      FN=FNO
      PI=3.1415926
90     CFN=CMPLX(0.,FN)
      G2=-CFN/DN
      FKNRO=CSQRT(G2)
      IF(AIMAG(G2))91,92,92
91     FKNRO=-FKNRO
92     CALL JOORJ1(FKNRO,RJ)
      FF=(1.,0.)-2.*RJ/FKNRO
      G4=CSQRT(FF)
      IF(AIMAG(FF))93,94,94
93     G4=-G4
94     GAMA=CFN/G4
      GX=REAL(GAMA)
      GY=AIMAG(GAMA)
      CCO=FN/GY
      WRITE(6,4)FN,GX,CCO
      FN=FN+DFN
      IF(FN-FNM)90,90,8
8      GO TO 1
9      STOP
      END

```

```

C   FREQUENCY RESPONSE OF LINE WITH CONST. PRESS. TERMINATION
COMPLEX CFN,G2,FKNRO,FF,G4,GAMA,RJ,COSHG,SINHG,POV
2   FORMAT(4F15.8)
3   FORMAT(///,15X,1F15.8,/)
4   FORMAT(1F15.2,5X,1E15.8,5X,1E15.8)
1   READ(5,2)DN,FNO,DFN,FNM
    WRITE(6,3)DN
    FN=FNO
    PI=3.1415926
90  CFN=CMPLX(0.,FN)
    G2=-CFN/DN
    FKNRO=CSQRT(G2)
    IF(AIMAG(G2))91,92,92
91  FKNRO=-FKNRO
92  CALL JOORJ1(FKNRO,RJ)
    FF=(1.,0.)-2.*RJ/FKNRO
    G4=CSQRT(FF)
    IF(AIMAG(FF))93,94,94
93  G4=-G4
94  GAMA=CFN/G4
    COSHG=(CEXP(GAMA)+CEXP(-GAMA))/2.
    SINHG=(CEXP(GAMA)-CEXP(-GAMA))/2.
    POV=GAMA*SINHG/(CFN*COSHG)
    RPV=CABS(POV)
    RPVDB=20.*ALOG10(RPV)
    PVX=REAL(POV)
    PVY=AIMAG(POV)
    PHPV=ATAN(PVY/PVX)
    IF(PVX)6,7,7
6   PHPV=PHPV+PI
7   PHPVD=PHPV*180./PI
    WRITE(6,4)FN,RPVDB,PHPVD
    FN=FN+DFN
    IF(FN-FNM)90,90,10
10  GO TO 1
11  STOP
    END

```

```

C   CALCULATION OF ZEROES OF SINHG
COMPLEX FN,FKNRO,FF,DIF1,FN1,E2,E3,FNN,E4,RJ
2   FORMAT(F15.8,I15,F15.8)
3   FORMAT(2X,1F15.8)
8   FORMAT(7X,3F15.5)
1   READ(5,2)DN,NM,G
    WRITE(6,3)DN
11  DO 7 N=1,NM
    PI=3.1415926
    T=N
    P1=T*PI
    E1=.0001
    FNN=CMPLX(E1,P1)
    FN=FNN
4   E2=-FN/DN
    FKI;RO=CSQRT(E2)
    IF(AIMAG(E2))13,14,14
13  FKNRO=-FKNRO
    GO TO 4
6   FNx1=REAL(FN1)
    FNY1=AIMAG(FN1)
    D=1.+((FNY1/FNX1)**2)
    ZETA=SQRT(1./D)
    FUD=-FNx1/ZETA
    ALPHA=FNx1
    FND=FNY1
7   WRITE(6,8)DN,ZETA,FUD
9   GO TO 1
10  STOP
    END

```

```

C      ELASTIC WALL FLEXIBLE
      COMPLEX B,F,CK,CK2,RJB,RJK,CT1,CT2,E
      COMPLEX T1,T2,T3,T4,T5,T6,T7,DB,G2,G,EE
20     FORMAT(7F10.8,2F5.2)
21     FORMAT(7F11.8,2F6.3)
22     FORMAT(2X,F11.8,2E15.8,2X,2E15.8)
1      READ(5,20)DN,FNO,DFN,FNM,BOX,BOY,ER,P1,P2
2      WRITE(6,21)DN,FNO,DFN,FNM,BOX,BOY,ER,P1,P2
      B=CMPLX(BOX,BOY)
      FN=FNO
10     F=CMPLX(0.,FN)
7      CK2=B**2+F**2-F/DN
      CK=CSQRT(CK2)
      IF(AIMAG(CK2))3,4,4
3      CK=-CK
4      CALL JOORJ1(CK,RJK)
      CALL JOORJ1(B,RJB)
      G2=B**2+F**2
      CT1=CK*B*RJB
      CT2=G2*RJK
      E=CT1-CT2
      T6=(P1*(F**2))+P2
      EE=E-(CK*(F**2))/T6
      R1=CABS(EE)/CABS(E)
      IF(R1-ER)6,6,5
5      T1=RJB*(B**2/CK+CK)
      T2=B*CK*((1.,0.)-RJB/B+RJB**2)
      T3=2.*B*RJK
      T4=(B/CK)*G2*((1.,0.)-RJK/CK+RJK**2)
      T5=T1+T2-T3-T4
      T7=T5-(B*(F**2))/(CK*T6)
      DB=-EE/T7
      B=B+DB
      GO TO 7
6      G=CSQRT(G2)
      IF(AIMAG(G2))8,9,9
8      G=-G
9      GX=REAL(G)
      GY=AIMAG(G)
      CCO=FN/GY
      WRITE(6,22)FN,GX,CCO,B
      FN=FN+DFN
      IF(FN-FNM)10,10,11
11     GO TO 1
12     STOP
      END

```


LIST OF SYMBOLS

A	Constant at integration Conduit cross-sectional area
B	Constant of integration
c	Phase velocity
c_o	Isentropic speed of sound in fluid
c_v	Specific heat, constant volume
C_q	Conduit capacitance based on flow rate
C_v	Conduit capacitance based on velocity
C_w	Conduit capacitance based on weight flow rate
D	Conduit diameter
$\frac{D}{D_t}$	Substantial derivative
D_i	Conduit inside diameter
D_o	Conduit outside diameter
D_{nr}	Radial damping number, $v/r_o c_o$
D_{nz}	Axial damping number, $vL/c_o r_o^2$
\bar{F}	Vector body force per unit mass
F_{cn}	Axial frequency number for nth zero of $\cosh \Gamma$
F_{nr}	Radial frequency number, $\omega r_o/c_o$
F_{nz}	Axial frequency number, $\omega L/c_o$
F_{sn}	Axial frequency number for nth zero of $\sinh \Gamma$
$F_{zn}(r)$	Axial velocity profile function for the nth mode
f	Tube wall factor, defined by Equation (2.35)

g	Acceleration due to gravity
i	Imaginary unit, $\sqrt{-1}$
i_j	Electrical current at point j
I_q	Fluid inertance based on flow rate
I_v	Fluid inertance based on velocity
I_w	Fluid inertance based on weight flow rate
$J_0(x)$	Bessel function of order zero and argument x
$J_1(x)$	Bessel function of order one and argument x
k	Eigenvalue defined in Equation (3.24)
k_n	Eigenvalue for n th mode
L	Conduit length
L_e	Electrically equivalent inductance
n	Index number
$p(t)$	Fluid pressure
p_0	Zeroth order fluid pressure
p_1	First order fluid pressure
$P(s)$	Transformed pressure
$P_j(s)$	Transformed pressure at point j
\bar{P}_j	Average transformed pressure at point j
q	Fluid flow rate
\bar{q}	Vector heat flow rate
r	Radial coordinate position
r	Unit vector in radial direction
r_0	Conduit inner radius
R_1	Resistance coefficient, Equation (2.9)
s	Laplace variable
t	Time

T	Temperature
\bar{v}	Vector fluid velocity
\bar{v}_0	Zeroth order vector fluid velocity
\bar{v}_1	First order vector fluid velocity
V_{1r}	First order transformed radial velocity
V_{1z}	First order transformed axial velocity
V_{zn}	First order transformed axial velocity for the n th mode
\bar{V}_j	Average transformed axial velocity at position j
z	Axial coordinate
Z_c	Characteristic impedance
\bar{Z}_j	Average impedance at position j
β	Eigenvalue defined in Equation (3.25)
β_n	Eigenvalue for n th mode
γ	Eigenvalue defined in Equations (3.24) and (3.25)
γ_n	Eigenvalue for n th mode
γ_r	Real part of
γ_c	Imaginary part of
Γ	Propagation operator, L
Γ_r	Real part of Γ
Γ_c	Imaginary part of Γ
ζ_{cn}	Damping ratio for n th zero of $\cosh \Gamma$
ζ_{sn}	Damping ratio for n th zero of $\sinh \Gamma$
θ	Unit vector in θ direction
\mathcal{K}	Bulk modulus of elasticity of fluid
μ	Absolute shear viscosity
μ'	Absolute dilational viscosity
μ_B	Absolute bulk viscosity

ν	kinematic shear viscosity
ρ	Fluid mass density
ρ_0	Zeroth order density
ρ_1	First order density
ρ_t	Tube wall density
ϕ	Scalar field
$\hat{\phi}$	Transformed scalar field
Φ	Dissipation function
ψ	Magnitude of vector field $\vec{\psi}$
$\vec{\psi}$	Vector field
ω	Angular frequency
∇	Vector operator del